# Implementing belowground controls on nutrient uptake in ELMv2-SPRUCE improves representation of a boreal peatland ecosystem

Yaoping Wang[1], Daniel M. Ricciuto[1], Jiafu Mao[1], Sören E. Weber[2], Verity G. Salmon[1], Xiaoying Shi[1], Xiaojuan Yang[1], Natalie A. Griffiths[1], Paul J. Hanson[1], Anthony P. Walker[1], Jonathan Stelling[3], Katherine Duchesneau[4], Camille E. Defrenne[5], Jeffrey M. Warren[1], Stephen D. Sebestyen[6], Kyle J. Pearson[1], Keith Oleheiser[1], Joshua Birkebak[1], Mark Guilliams[1], Misha B. Krassovski[1], Melanie A. Mayes[1], Peter E. Thornton[1]

[1]Environmental Sciences Division, Oak Ridge National Laboratory, Oak Ridge, TN, 37830, USA
[2]Department of Biology, West Virginia University, Morgantown, WV, 26505, USA
[3]North Central Research and Outreach Center, College of Food, Agricultural, and Natural Resource Sciences, University of Minnesota, MN, 55744, USA
[4]School of Integrative Plant Science, Cornell University, NY, 14850, USA
[5]RECON environmental, Inc., San Diego, CA, 92108, USA
[6]Northern Research Station, U.S. Department of Agriculture Forest Service, Grand Rapids, MN, 55744, USA

*Correspondence to*: Yaoping Wang (wangy7@ornl.gov), Jiafu Mao (maoj@ornl.gov)

Deleted: 3
Deleted: 4
Deleted: 5
Deleted: 3
Deleted: 4
Deleted: 5

provide public access to these results of federally sponsored research in accordance with the DOE Public Access Plan (http://energy.gov/downloads/doe-public-access-plan, last access: 2025/11/14).

**Abstract.** Boreal peatlands store 13-32% of the global soil carbon (C) stock, a service dependent on plant-mycorrhizal fungi associations. In these nutrient poor systems, ectomycorrhizal and ericoid mycorrhizal fungi supply up to >80% of the nutrient requirements of their plant hosts, partly with mined nitrogen (N) and phosphorus (P) from soil organic matter that are otherwise inaccessible to plants. Despite the ecological significance, mycorrhizal associations are only represented in a few land surface or ecosystem models. We modify the peatland branch of version 2 of the Energy Exascale Earth System Land Model (ELMv2-SPRUCE) to replace the default photosynthesis-driven inorganic N and P (NP) uptake process with a more realistic representation of the process via three pathways: (1) direct inorganic NP uptake by uncolonized fine roots, (2) indirect inorganic NP acquisition and (3) indirect NP acquisition from organic sources by mycorrhizal roots. We systematically evaluated the performance of the default and modified models with field observations from a whole ecosystem warming and carbon dioxide fertilization experimental site: Spruce and Peatland Responses Under Changing Environment (SPRUCE), in northern Minnesota, USA. The modified model reduces the underestimation of the growth response of shrubs in the default model to warming from 40-80% to 17-35% and reduces the overall relative absolute error on C fluxes from 1.61 to 1.54 in calibration. Improvements on modeled shrub growths and shrub-moss community net ecosystem exchanges are also seen in validation. The improved growth response of shrubs to warming is accompanied by several-fold increase in direct inorganic NP uptake and decrease in fungal colonization rate. The modified model simulates a smaller magnitude of transition of the ecosystem from C sink to C source under warming due to alleviation of plant nutrient limitation. Equifinality analysis shows the newly added parameters in the modified model can be constrained by the observed C fluxes. Sensitivity analysis shows the newly added parameters have stronger statistical interactions than the preexisting parameters in the default model. Overall, the modified model is an improvement over the default ELMv2-SPRUCE and will be a useful tool for understanding boreal peatland change.

Deleted: weaker

## 1 Background

Boreal peatlands store an estimated 234-546 Gt carbon (C), equal to 13-32% of the global soil C stock (Friedlingstein et al., 2022; Loisel et al., 2017). The high C storage arises from slow decomposition rates driven by the cold, waterlogged, nutrient-limited, and acidic conditions of these ecosystems (Dise, 2009; Frolking et al., 2011; Salmon et al., 2021). Ongoing rapid warming in the northern high latitudes is expected to shift ecosystem C balance, but the magnitude of change remains highly uncertain due to poorly constrained temperature sensitivities of vegetation productivity and soil C decomposition (Ito et al., 2020). More accurate modeling of the mechanisms governing C cycling in boreal peatlands will improve our ability to project future changes in this ecosystem and its feedback to the Earth system.

Among the various biotic and abiotic mechanisms underlying boreal peatland C cycling, plant-mycorrhizal associations represent a key component owing to their central role in nutrient cycling (Shao et al., 2022, 2023b; Shi et al., 2015, 2021).

Mycorrhizal fungi deliver nutrients to plants in exchange for carbon, and have three broad classes: ectomycorrhizae (EcM), ericoid mycorrhizae (ErM), and arbuscular mycorrhizae (AM). Unlike AM, which are more common in low latitudes and only acquire inorganic nutrients, EcM and ErM can acquire nutrients from soil organic matter (SOM), making them suited to cold, nitrogen (N)-limited ecosystems with slow decomposition rates (Egerton-Warburton et al., 2013; Ward et al., 2022). One estimate suggests that EcM are associated with >75% of the aboveground plant biomass in the non-permafrost boreal region and ~50% in the permafrost region; ErM, which selectively colonize ericaceous shrubs, are associated with ~20% aboveground plant biomass in the permafrost region (Soudzilovskaia et al., 2019). Plants associated with EcM transfer on average ~13% (0–50% in range) of their net primary productivity (NPP) to fungal symbionts while plants associated with ErM transfer on average ~3.5% (0–14% in range) (Hawkins et al., 2023). The fraction of plant N supplied by EcM or ErM in return varies from <30% to >80%, depending on site and plant species, though less is known about the fraction of EcM- or ErM-supplied phosphorus (P) (Hilman et al., 2024; Hobbie and Hobbie, 2006; Yin et al., 2022). Beyond nutrient supply, mycorrhizal fungi regulate SOM turnover by competing with free-living saprotrophs, transporting C away from the rhizosphere, and promoting soil aggregate formation and stabilization (Fernandez and Kennedy, 2016; Hawkins et al., 2023; Smith and Wan, 2019).

To date, only a limited number of land surface models – here defined as the land component of Earth system models – simulate mycorrhizal associations (Warren et al., 2015). They generally focus on AM and EcM associations and use the return-on-investment principle, where "return" refers to gains in growth or nutrient uptake, and "investment" refers to the C costs of acquiring nutrient through different pathways (Brzostek et al., 2014). For example, the Community Land Model (CLM) and Energy Exascale Earth System Land Model (ELM) have been linked with the Fixation and Uptake of Nitrogen (FUN) model (Braghiere et al., 2022; Brzostek et al., 2014; Shi et al., 2016). Plants minimize their C expenditure on N and P (NP) uptake by optimally allocating C to satisfy their NP demands among biological fixation, retranslocation, nonmycorrhizal passive and active uptake, EcM uptake, and AM uptake, each of which has a unique C cost function (Braghiere et al., 2022; Brzostek et al., 2014; Shi et al., 2016). Simulations of ELM-FUN suggest that the EcM and AM pathways together supply ~75% of plant N and ~41% of plant P globally, and account for ~50% of the NP uptake-related C costs, but neither ELM-FUN or CLM-FUN consider organic nutrient mining (Braghiere et al., 2022; Shi et al., 2016). The Symbiotic Nitrogen Acquisition by Plants (SNAP) model, which is linked to the Geophysical Fluid Dynamics Laboratory land model LM3 (GFDL-LM3), improves FUN by dynamically simulating fungal biomass, fungal organic nutrient mining, and the resulting C cost to the plants (Sulman et al., 2019). Simulations of GFDL-LM3-SNAP show that EcM-mining of organic N explains the stronger positive response to carbon dioxide ($CO_2$) fertilization in EcM-dominated ecosystems than AM-dominated ecosystems (Sulman et al., 2019). Also, allowing plants to shift in N uptake pathways results in four times the terrestrial C sequestration relative to fixed N uptake pathways under a 100-ppm increase in atmospheric $CO_2$ concentration (Sulman et al., 2019).

Terrestrial ecosystem models not coupled to Earth system models have represented mycorrhizal associations in more detail than the return-on-investment models described above. For example, the McGill Wetland Model (MWM) focuses on interactions among moss, ericaceous shrub, and ErM in peatland ecosystems and shows that the shrub-ErM association explain the increased shrub growth and decreased moss growth in a NP fertilization experiment (Shao et al., 2022, 2023b). The MWM

Deleted: varieties

explicitly models microbial and ErM biomass dynamics and ErM mining of organic nutrients. The MWM models the shrub-ErM interactions as "excess fluxes" in which (1) shrub transfers C to ErM when shrub C reserve exceeds a set fraction of its total stem and root C, (2) ErM fungi transfers NP to the shrub when the NP contents of the ErM exceed predefined fractions of the C content of the ErM (Shao et al., 2023b). Compared to return-on-investment, the excess flux mechanism may better describe EcM and ErM exchanges with the host plant, because the reciprocity of EcM and ErM are more strongly affected by environmental, developmental, and physiological factors than AM (Bunn et al., 2024; Garcia et al., 2015). The drawback is a large number of parameters. The CoupModel has been used to compare three representations of nutrient limitation: fixed limitation, implicit EcM, and explicit EcM, across a climate and N-deposition gradient of EcM-dominated boreal forests (He et al., 2018). In the fixed limitation approach, plant growth is scaled down by a constant nutrient limitation factor throughout the year. The implicit approach omits the EcM intermediary, simulating plant acquisition of NP from organic sources as a function of soil organic nutrients content, plant demand, and optionally root distributions (He et al., 2018, 2021; Svensson et al., 2008). The explicit approach simulates EcM biomass dynamics and organic nutrient mining, with plant transfer of C to EcM determined by belowground allocation, and EcM transfer of NP to plant co-determined by plant demand and excess flux (He et al., 2018, 2021). The implicit and explicit approaches outperform the fixed N limitation approach, and both indicate declining plant dependence on organic N from the more N-limited northern Sweden to the less N-limited southern Sweden; yet the explicit parameterization is more difficult to constrain, and the implicit and explicit approaches differ in the simulated litter production, soil respiration, and the magnitude of the north-south trend (He et al., 2018).

The above reviewed modeling studies demonstrate that mycorrhizal associations are needed for more accurate simulation of nutrient limitation on productivity and the resulting feedback to Earth system and land surface models can benefit from testing alternative model structures than return-on-investment schemes and understanding the parameterization difficulty. We address this research gap by adding implicit representation of EcM and ErM associations into the NP uptake processes of a peatland branch of ELM, ELMv2-SPRUCE (Griffiths et al., 2017; Shi et al., 2015, 2021). AM is not added because it is not a key component of northern peatland ecosystems (Egerton-Warburton et al., 2013). We compare the original model, hereafter "ELM-OLD", and the modified model, hereafter "ELM-MYCI" (for mycorrhizal-implicit), against observed C fluxes, pore water NP concentrations, resin-exchange-measured plant available NP, and peat C-N-P stocks from the Spruce and Peatland Responses Under Changing Environment experiment (SPRUCE) (Griffiths et al., 2017; Griffiths and Sebestyen, 2016; Hanson et al., 2020a; Iversen et al., 2022; Salmon et al., 2021). SPRUCE is a whole ecosystem warming and $CO_2$ fertilization experiment located in a boreal peatland ecosystem (Hanson et al., 2017). The site has EcM-associated trees (black spruce [*Picea mariana*] and tamarack [*Larix laricina*]), various species of ErM-associated ericaceous shrubs, offering an array of interactions between plants, fungi, and soils under experimental treatments that have not been tested by the above-reviewed modeling studies. Warming at SPRUCE increased shrub productivity, decreased *Sphagnum* moss productivity, and increased resin-exchange nutrient availability (Hanson et al., 2020a, 2025; Iversen et al., 2022). A persistent issue in ELM-OLD has been the inability to reproduce the larger increase in shrub productivity relative to tree productivity under warming (Shi et al., 2021). Using ELM-MYCI, we test the hypothesis that the shrub responses can be explained by decreasing dependence on ErM

**Deleted:**

**Deleted:** (Bunn et al., 2024; Garcia et al., 2015)The excess flux mechanism is likely realistic at the microscopic level (Bunn et al., 2024), but requires many parameters.

**Deleted:** and

**Deleted:** The experiment observe

**Deleted:** s

**Deleted:** in

**Deleted:** declines in

**Deleted:** s

**Deleted:** in

**Deleted:** in response to warming

in response to higher nutrients availability under warming, akin to the findings or suggestions of multiple previous studies (Defrenne et al., 2021; Duchesneau et al., 2024; He et al., 2018; Shao et al., 2023b).

## 2 Data and Methods

### 2.1 Site Description

The SPRUCE experimental site is within the S1 Bog of the United States Department of Agriculture Forest Service Marcell Experimental Forest, located in northern Minnesota, USA (47°30.476'N, 93°27.162'W, 418m above mean sea level) (Hanson et al., 2017, 2020a; Kolka et al., 2011; Salmon et al., 2021). The bog is an acidic, raised-dome ombrotrophic bog with nutrient inputs only from atmospheric deposition and nitrogen (N) fixation. The open forest canopy at the site is *Picea mariana* (Mill.) B.S.P. (black spruce) with occasional *Larix laricina* (Du Roi) K. Koch (eastern tamarack). The trees were harvested in strip cuts in 1969 and 1974 and the current canopy is mostly regenerated from the 1974 strip cut (Hanson et al., 2016a). The understory is dominated by ericaceous shrubs (*Rhododendron groenlandicum* [Oeder] Kron & Judd [Labrador tea], *Chamaedaphne calyculata* [L.] Moench. [leatherleaf], *Vaccinium angustifolium* Aiton [blueberry], and *Vaccinium oxycoccos* L [cranberry]) with a small biomass pool of forbs and sedges (Hanson et al., 2025). The bryophyte layer is dominated by *Sphagnum* spp. mosses. This vegetation community is represented by the following plant functional types (PFTs) in both ELM-OLD and ELM-MYCI: boreal evergreen needleleaf for black spruce, boreal deciduous needleleaf for tamarack, boreal deciduous shrub for the ericaceous shrubs, and *Sphagnum* moss. The forbs and sedges are not modeled but comprise less than 10% understory cover according to pretreatment surveys (Iversen et al., 2017b).

The detailed whole ecosystem warming and $CO_2$ fertilization experimental setup is reported elsewhere (Hanson et al., 2017). Briefly, the experiment has two unenclosed, ambient plots (ambient temperature, ambient $CO_2$) and five pairs of enclosures that target five whole ecosystem warming levels (+0, +2.25, +4.5, +6.75, and +9°C) above ambient temperatures crossed with ambient and elevated (+500 ppm) $CO_2$. The belowground heating extends 3 m into the peat profile and began in June 2014. The aboveground warming began in August 2015. The $CO_2$ fumigation began on June 15, 2016.

### 2.2 The default ELMv2-SPRUCE model (ELM-OLD)

ELM is the land component of the Energy Exascale Earth System Model (E3SM), which consists of atmosphere, land, ocean, sea ice, and land ice components (Burrows et al., 2020; Yang et al., 2019, 2023). ELM-OLD is currently branched off ELM version 2 with improved peatland processes, including hummock-hollow hydrological interactions (Shi et al., 2015) and the *Sphagnum* moss PFT (Shi et al., 2021). ELM-OLD has been used primarily for site-level simulations, in which we represent the bog as two interacting grid cells that represent a hummock soil column and a hollow soil column (Shi et al., 2015). Each soil column has multiple PFTs that compete for water and nutrients (Shi et al., 2021). Soil decomposition uses a first-order decay model with one coarse woody debris pool, three plant litter pools (labile, cellulose, lignin), and four SOM pools (Burrows et al., 2020; Oleson et al., 2013a) (Supplementary Information [SI] Sect. 1.1.3). Belowground nutrient competition among the

Deleted: and modified

Deleted: s

Deleted: and ELM-MYCI

PFTs and the soil decomposition process is simulated with the Relative Demand approach (SI Sect. 1.1.2; Figure 1a). Plant photosynthesis creates potential NP uptake through the fixed C:N and C:P in the plant structural tissues (leaf, fine root, coarse root, stem). Soil decomposition creates potential NP immobilization due to the need for extra NP when C decomposes from an upstream pool that has higher C:N and C:P into a downstream pool that has lower C:N to C:P. The potential uptakes and immobilization are compared to the total available inorganic NP in soil, and scaled down by the same factor so that the total available inorganic NP is not exceeded (Burrows et al., 2020; Thornton and Rosenbloom, 2005). Due to this NP limitation, some photosynthesized C cannot become growth in the structural tissues; those extra C enters the nonstructural carbohydrates (NSC) pool as C reserve (Burrows et al., 2020).

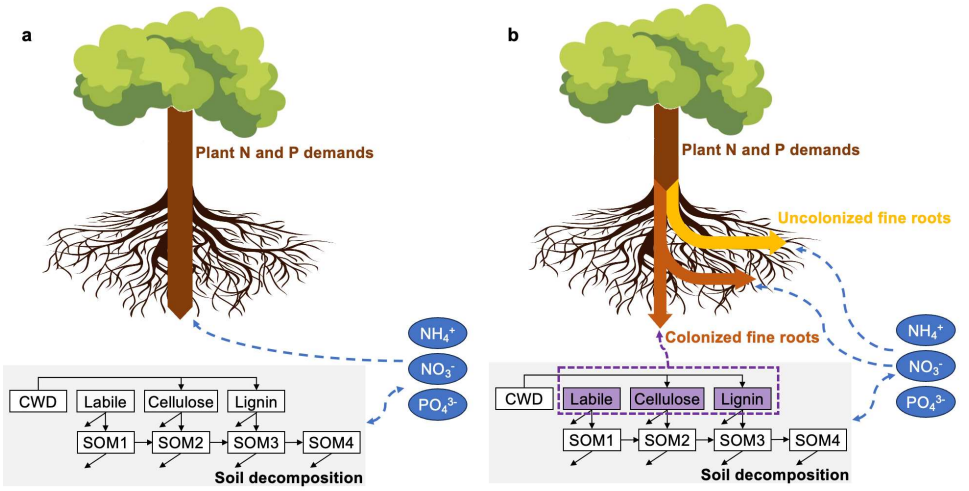


**Figure 1: Simplified illustration of the belowground nutrient competition between the vascular plant functional types and the soil decomposition processes in ELM-OLD (a) and ELM-MYCI (b).** Boxed arrows indicate potential plant uptakes. Dashed arrows indicate directions of nutrients flow, with blue for mineral nutrients and purple for nutrients locked in organic forms. Solid arrows between the decomposition pools indicate direction of carbon flow, with unattached arrow heads meaning respirational losses. CWD – coarse woody debris.

## 2.3 The modified ELMv2-SPRUCE model (ELM-MYCI)

ELM-MYCI is designed to improve the process-realism of nutrient uptake for the three vascular PFTs (spruce, tamarack, shrubs) by considering the following three pathways: (1) direct inorganic nutrient uptake by uncolonized fine roots, $PATH^{root}$, (2) indirect inorganic nutrient acquisition by mycorrhizal roots, $PATH^{myc,inorg}$, and (3) indirect nutrient acquisition from organic sources by mycorrhizal roots, $PATH^{myc,org}$ (Figure 1b). The entire set of equations and detailed descriptions are provided in SI

Deleted: 1

Formatted: Font: 9 pt, Not Bold

Formatted: Font: 9 pt, Not Bold

Formatted: Font: 9 pt

Formatted: Font: 9 pt, Not Bold

Formatted: English (UK)

Formatted: Font color: Red

Formatted: Heading 2

Moved (insertion) [1]

Deleted: 1

Deleted: more details

Sect. 1.1.4–1.1.10. The major equations and assumptions are described here. Unless otherwise noted, the equations are only shown for N, and the equations for P can be obtained simply by replacing all N with P.

Like in ELM-OLD, ELM-MYCI still calculates the NP demand implied by photosynthesis, but decouples this demand from the potential NP take, which are determined through the three pathways. ELM-MYCI uses fungi-colonization fraction to idealize the fine root into a uncolonized part, which can only use $PATH^{root}$, and a colonized part, which can only use $PATH^{myc,inorg}$ and $PATH^{myc,org}$. The colonization fraction of EcM for the two tree PFTs and ErM for the shrub PFT is a clipped linear function of annual average soil inorganic N (Eq. 1). The sensitivity to P is currently set to zero in Eq. 1, because observational constraints on this sensitivity are weak in past experimental studies (Bashian-Victoroff et al., 2025) and at the SPRUCE site (SI Sect. 1.1.5).

The potential inorganic NP uptake via $PATH^{root}$ is dependent on uncolonized fine root surface area, soil inorganic NP concentrations, soil temperature, soil moisture, and the current NP-limitation level of the plant (Eq. 2). The fine root surface area, $A_{froot,i,j}$, is calculated from modelled fine root biomass, and observed fine root radius and density at the SPRUCE site (Eq. S32). The dependence on soil inorganic NP concentrations, $\mathcal{F}_j(N_{conc,i})$, follows the conventional Michaelis-Menten form (Eq. S22) (Knox et al., 2024). The dependence on soil temperature, $\mathcal{F}(T_{soi,i})$, follows the conventional Q10 form (Eq. S13). The dependence on soil moisture, $\mathcal{F}(\Theta_{soi,i})$, follows a previous unimodal function to let both dry and excessively wet soil inhibit nutrient uptake (Eq. S14) (Frolking et al., 2002). The NP-limitation feedback term, $\mathcal{F}(F_{Nlimit,j})$, is exactly one when the PFT is not NP-limited and decreases asymptotically to zero as soil inorganic NP become more abundant (Eq. S15, Figure S3). This term prevents numerical instability in the model and is somewhat supported by experimental observations (Glass et al., 2002).

The potential inorganic NP acquisition via $PATH^{myc,inorg}$ is dependent on colonized fine root biomass, the same soil inorganic NP concentrations, soil temperature, and soil moisture multipliers as $PATH^{root}$, and NSC availability (Eq. 3). The NSC availability term reflects fungal dependence on C transfer from the host plant (Eq. S16) (Bunn et al., 2024; He et al., 2018; Shao et al., 2023b). The potential NP acquisition from organic sources via $PATH^{myc,org}$ is dependent on colonized fine root biomass, the same soil temperature and moisture multipliers as $PATH^{root}$ and $PATH^{myc,inorg}$, and the same NSC availability term as $PATH^{myc,inorg}$ (Eq. 4). $PATH^{myc,org}$ does not include a Michaelis-Menten term for organic NP concentrations, because the peatland environment is rich in organic substrates. Also, the soil decomposition pools in ELM are rate-based rather than corresponding to actual chemical compounds and do not distinguish between solid and dissolved phases (Oleson et al., 2013b), making it difficult to separate fungi-accessible from fungi-inaccessible fractions (Näsholm et al., 2009; Talbot and Treseder, 2010). The total potential mycorrhizal inorganic and organic NP acquisitions is capped by 50% of net photosynthesis per time step, scaled by a constant C-cost factor (Eq. S25). The 50% threshold was selected based on the maximum percentage of C allocated to mycorrhizal fungi in a previous meta-analysis (Hawkins et al., 2023). The cap, like the NSC availability term, reflects fungal dependence on C input from the host plants.

Deleted: T
Deleted: in Eq. 1-3
Deleted: and
Deleted: 1
Deleted: soil inorganic NP concentration, and
Deleted: 2
Deleted: ).
Deleted: (Talbot and Treseder, 2010)(Talbot and Treseder, 2010)
Deleted: s
Deleted: and
Deleted: 3

The potential rates of the three pathways are compared to soil inorganic and organic NP availability to determine actual rates. The potential inorganic NP uptake or acquisition from PATH$^{root}$, PATH$^{myc,inorg}$, and soil decomposition processes are scaled down by soil inorganic NP availability analogously to the default Relative Demand approach (Eq. S3, S4, S9, S11). The potential organic NP acquisition from PATH$^{myc,org}$ per hourly time step is capped by 0.0001 of the total organic NP in the labile, cellulose, and lignin plant litter pools (Figure 1; Eq. S19-S20). The 0.0001 multiplier is adopted from the upper bound in CoupModel (He et al., 2018), and is intentionally chosen to be a large number that prevents unrealisticaflly large uptake rate rather than serving as a true upper bound on the fungi-accessible fraction of organic NP. The restriction to only access plant litter pools is again due to structural constraint in ELM's soil decomposition pools. The plant litter pools allow variable C:N and C:P ratios, but the SOM pools do not, so that mycorrhizal acquisition of N and P from the SOM pools will require considering how much C is lost as fungal respiration, which is beyond the scope of this project (SI Sect. 1.1.7). Finally, the actual rates are compared to the implied demand by photosynthesis to determine plant structural growth. The actual rate of PATH$^{myc,org}$ is used to subtract NP from the three plant litter pools, distributing the acquisition proportional to the size of each pool.

$$M_{myc,j} = \max\left(0, \min\left(1, a_j + b_j N_{soil,annavg}\right)\right) \quad (1)$$

$$N_{froot,i,j} = v_{N,froot,j}\left(1 - M_{myc,j}\right)A_{froot,i,j}\mathcal{F}_j\left(N_{conc,i}\right)\mathcal{F}\left(T_{soi,i}\right)\mathcal{F}\left(\Theta_{soi,i}\right)\mathcal{F}\left(F_{Nlimit,j}\right) \quad (2)$$

$$N_{myc,pot,inorg,i,j} = v_{N,myc,j}M_{myc,j}C_{froot,j}F_{froot,i,j}\mathcal{F}_j\left(N_{conc,i}\right)\mathcal{F}\left(T_{soi,i}\right)\mathcal{F}\left(\Theta_{soi,i}\right)\mathcal{F}\left(F_{Nlimit,j}\right)F\left(C_{ns,j}\right) \quad (3)$$

$$N_{myc,pot,org,i,j} = u_{N,myc,j}M_{myc,j}C_{froot,j}F_{froot,i,j}\mathcal{F}\left(T_{soi,i}\right)\mathcal{F}\left(\Theta_{soi,i}\right)\mathcal{F}\left(F_{Nlimit,j}\right)F\left(C_{ns,j}\right) \quad (4)$$

$i$ – soil layer index

$j$ – PFT index

$M_{myc,j}$ – fraction of fine roots colonized by EcM (for the spruce and tamarack PFTs) or ErM (for the shrub PFT)

$N_{soil,annavg}$ – annual average soil inorganic N ($NH_4^+ + NO_3^-$) content in the rooting zone, g N m$^{-3}$

$a_j$ – intercept parameter

$b_j$ – slope parameter

$N_{froot,i,j}$ – the potential inorganic N uptake rate via PATH$^{root}$, g N m$^{-2}$ ground area s$^{-1}$

$N_{myc,pot,inorg,i,j}$ – the potential inorganic N acquisition rate via PATH$^{myc,inorg}$, g N m$^{-2}$ ground area s$^{-1}$

$N_{myc,pot,org,i,j}$ – the potential N acquisition rate from organic sources via PATH$^{myc,org}$, g N m$^{-2}$ ground area s$^{-1}$

$v_{N,froot,j}$ – the maximum inorganic N acquisition rate per unit uncolonized fine-root surface area, g N m$^{-2}$ ground area s$^{-1}$

$v_{N,myc,j}$ – the maximum inorganic N acquisition rate per unit colonized fine-root biomass, g N g C$^{-1}$ s$^{-1}$

$u_{N,myc,j}$ – the maximum organic N acquisition rate per unit colonized fine-root biomass, gN g C$^{-1}$ s$^{-1}$

$M_{myc,j}A_{froot,i,j}$ – total fine root surface area in one soil layer, cm$^2$ m$^{-2}$ ground area

$C_{froot,j}$ – total fine root biomass in one soil layer, g C m$^{-2}$ ground area

$\mathcal{F}_j\left(N_{conc,i}\right)$ – Michaelis-Menten multiplier of soil inorganic N concentration ($N_{conc,i}$, g N m$^{-3}$ soil volume)

**Moved up [3]:** The equations for P can be obtained by replacing all N with P in Eq. 1-3.

**Deleted:** All three pathways are also affected by soil temperature, soil moisture, and the current NP-limitation level of the plant (Eq. 1-3).

**Deleted:** 1

**Deleted:** , which

**Deleted:** then

**Moved up [1]:** The entire set of equations and more details are provided in SI Sect. 1.1.

**Formatted:** (Asian) Chinese (China)

**Formatted Table**

**Deleted:** 1

**Deleted:** 2

**Deleted:** 3

**Moved (insertion) [2]**

**Deleted:** ¶

**Moved up [2]:** $M_{myc,j}$ – fraction of fine roots colonized by EcM (for the spruce and tamarack PFTs) or ErM (for the shrub PFT)¶

$\mathcal{F}(T_{soi,i})$ – $Q_{10}$ multiplier of soil temperature ($T_{soi,i}$, °C)

$\mathcal{F}(F_{Nlimit,j})$ – a feedback factor to prevent infinite N uptake when inorganic N is abundant ($F_{Nlimit,j}$ is the PFT's N-limitation level in the previous time step)

$F(C_{ns,j})$ – degree of NSC saturation in the plant ($C_{ns,j}$ is the NSC biomass in the plant, g C $m^{-2}$ ground area)

### 2.4 Simulation protocol

Following previously established protocols (Griffiths et al., 2017; Hanson et al., 2020a; Shi et al., 2021), we first conducted a single-grid simulation that consists of an accelerated spin-up of 207 years, a normal spin-up of 407 years, and an 1850–2014 transient simulation, and then branched the simulations into eleven treatments corresponding to one control simulation for unenclosed plot + five pairs of enclosures (Sect. 2.1) during 2015-2023. The control simulation only uses one of the two unenclosed plots, which is labeled plot 7 in the experiment (Hanson et al., 2020a), because it has a longer water table record, which is needed to force ELMv2-SPRUCE. The accelerated and normal spin-ups were driven by cyclic ambient meteorological forcing during 2015-2023, preindustrial $CO_2$ concentration, preindustrial N deposition, and constant land cover. The transient simulation cyclically used the ambient meteorological forcing during 2015-2023, historically varying $CO_2$ concentration and N deposition, and included the 1974 strip cut event where 99% aboveground tree biomass was removed. The treatment simulations were forced by meteorological observations and water table depths in each plot during 2015-2023 (Hanson et al., 2016b, 2020b). The simulated water table depths in the two columns equilibrate with each other and observed water table depths (Shi et al., 2015). The atmospheric $CO_2$ concentrations in the elevated $CO_2$ plots were set to 500 ppm above ambient level starting from March 15th, 2016. Within the grid, the hummock soil column was set to 64% of the area and hollow 36% (Graham et al., 2020). A limitation of this version of ELM is that we do not represent multiple canopy layers. Therefore, we must specify fractional coverages for each PFT that add to 100% total. We started with the default assumption that each of the four PFT covers 25% and then adjusted for the observed distribution of the two tree types. Within each soil column, the PFT fractions were: needleleaf evergreen boreal tree 36% (for spruce), needleleaf deciduous boreal tree 14% (for larch), broadleaf boreal deciduous shrub 25% (for ericaceous shrubs), and *Sphagnum* moss 25% in the pre-treatment simulations and fractionally adjusted using the annually observed fractional coverages in the treatment simulations (Table S8). All the simulations used an hourly time step.

### 2.5 Model calibration data

For the parameter optimization experiments described in Sect. 2.7.1, we focused on the following annual C fluxes: (1) the aboveground NPP of the spruce trees ($AGNPP_{spruce}$), (2) the aboveground NPP of the tamarack trees ($AGNPP_{tamarack}$), (3) the aboveground NPP of the shrubs ($AGNPP_{shrub}$), (4) the NPP of *Sphagnum* moss ($NPP_{moss}$), (5) the belowground NPP of total tree and shrub fine roots ($BGNPP_{treeshrub}$), (6) heterotrophic respiration (HR) (Hanson et al., 2018a, b, 2020a; Norby et al., 2019). We additionally summed up (1-5) to obtain (7) an aggregated "NPP" term – note this is not true NPP because it does

Deleted: enclosure

Deleted: enclosures

Deleted: Evaluation data¶
Annual C fluxes…

Deleted: Our primary evaluation data are the following

Deleted: measurements

not contain coarse root production. There are some temporal mismatches across the datasets: $BGNPP_{treeshrub}$ observations only span 2016-2017 (Malhotra et al., 2020b); the other observations span 2016-2021, but year 2020 was excluded due to the high uncertainty associated with the limited measurements taken during the COVID era (Hanson et al., 2020a; Norby and Childs, 2018). To facilitate concise comparison, we summarized each of those variables into two mean values and two temperature sensitivities, similar to a previous approach at the site (Hanson et al., 2020a). The mean values were calculated, respectively, over all the years in the ambient $CO_2$ plots and over all the years in the elevated $CO_2$ plots. The temperature sensitivities were calculated as the slope of least squares linear regression between each C-flux variable and observed mean annual 2-m air temperatures, respectively, over all the years in the ambient $CO_2$ plots, and over all the years in the elevated $CO_2$ plots. Those means and slopes were used in parameter optimization objective function (Eq. 5).

Deleted: enclosures

Deleted: enclosures

Deleted: enclosures

Deleted: enclosures

Deleted: (Sect. 2.5)

## 2.6 Model evaluation data

Formatted: Heading 2

The datasets described in the following subsections were withheld from model calibration and used solely for evaluation.

### 2.6.1 Post-calibration annual C fluxes

Formatted: English (UK)

We reserved the following annual C fluxes for post-calibration model evaluation: $AGNPP_{spruce}$ and $AGNPP_{tamarack}$, available for year 2022 in the ten treatment enclosures; $AGNPP_{shrub}$, available for year 2023 in all eleven plots; the growing season average NEE of the shrub-moss community ($NEE_{shrubmoss}$, gC $m^{-2}$ $gs^{-1}$, "gs"), available for year 2023 in the ten treatment enclosures. The data sources of $AGNPP_{spruce}$, $AGNPP_{tamarack}$, and $AGNPP_{shrub}$ are the same as in Sect. 2.5. The growing season mean $NEE_{shrubmoss}$ was calculated from the average of gapfilled 15-minute automated chamber measurements made on the shrub-moss community (Stelling et al., 2024). Growing season is defined as May 1 to Oct 31, to match the observational period (2023-04-27 to 2023-10-27). The gapfilling method is adapted from previous work at the SPRUCE site (Walker et al., 2017) and is described in detail in SI Sect. 1.3. Note the automated chamber measurements and the gap-filling method used here are preliminary and were applied solely for the purposes of this study, pending availability of the full analysis of the automated chamber data (Stelling J., personal communication). To obtain the modelled equivalence of $NEE_{shrubmoss}$, we considered what component fluxes were included in the observed $NEE_{shrubmoss}$. The chambers only enclosed shrubs and moss aboveground. Therefore, the chamber fluxes included aboveground shrub and moss GPP and respiration. The belowground collars of the chambers did not exclude tree roots. Therefore, the chamber fluxes included belowground soil HR, tree root respiration, shrub root respiration, and belowground moss respiration. Furthermore, because the chambers have small footprints, the sampled shrub and moss growths were often not representative of the average plot conditions. Therefore, we down-scaled the modelled plot-level shrub and moss GPP and respiration to the chamber-level using each PFT's ratio of measured aboveground biomass in the chamber (gC $m^{-2}$) to the measured aboveground biomass in the corresponding plot (gC $m^{-2}$, Table S8). We assumed the soil HR and tree root respiration components of the chamber fluxes correspond to plot-level averages due to lack of prior information. In summary, the modelled equivalence of $NEE_{shrubmoss}$ is calculated as (Plot-average HR + Plot-average tree root

respiration + Scaled shrub autotrophic respiration + Scaled moss autotrophic respiration – Scaled shrub GPP – Scaled moss GPP).

### 2.6.2 Annual maximum leaf area index

To evaluate the simulated C biomass, we compared the models against the annual maximum leaf area index (LAI) of the two trees and shrub, measured using LICOR LAI 2200 device during 2015–2020 (McPartland et al., 2019). The annual C fluxes and LAI observations all have direct correspondence with modeled variables. $AGNPP_{spruce}$ and $AGNPP_{tamarack}$ have strong pre-treatment variation that impacts the interpretation of results (Hanson et al., 2025). Therefore, we fitted ordinary least squares linear regression models to remove the pre-treatment effect; because LAI is closely related to aboveground NPP, we used the same method to remove the pre-treatment variation in the LAI of the two tree species (SI Sect. 1.2). We did not compare the models against observed net C exchange or methane flux data because the net C exchange has small components of lateral outflow of organic C and dissolved inorganic C (Hanson et al., 2020a), which are not yet considered in ELMv2-SPRUCE, and the model cannot yet fully capture methane dynamics (Shi et al., In preparation).

### 2.6.3 Porewater nutrient concentrations

For nutrient cycling, we evaluated the models against several forms of observations. The first of those was porewater ammonia ($NH_4^+$), nitrate ($NO_3^-$), and inorganic P ($PO_4^{3-}$) concentrations, which characterize the pool of dissolved nutrients in soil. The porewater concentrations were measured roughly twice per month during the non-frozen months of 2015-2020 near the bottom of the rooting profile (30cm) in the hollow (Griffiths et al., 2016). The pore water nutrient concentrations were measured on a per water volume basis (mg N $L^{-1}$, mg P $L^{-1}$), but ELM can only simulate nutrient concentrations on a per soil volume basis (gN $m^{-3}$ soil, gP $m^{-3}$ soil). Therefore, we divided the simulated $NH_4^+$, $NO_3^-$, and soluble P [as defined in (Yang et al., 2019)] concentrations by the simulated volumetric soil water content to bring them to the same unit as the observations. Because the sampling interval was irregular and relatively infrequent, and nutrient concentrations in water can exhibit sharp, episodic fluctuations (Basu et al., 2010), we chose not to interpolate the observations to annual level like the annual C fluxes (Hanson et al., 2018a, b, 2020a; Norby et al., 2019). Instead, we down sampled the model outputs to only include the dates on which pore water concentrations were measured, ensuring that both observed and modeled data reflect the same seasonality. For each enclosure, we then summarized the observed and down-sampled modeled porewater nutrient concentrations into two statistics: the mean value and the temporal linear trend, to facilitate concise comparison. Here, the temporal linear trend is defined as the slope of a least-squares regression between the modeled/observed values and the elapsed days since January 1, 2015. We chose enclosure-specific temporal trends, instead of cross-enclosure temperature sensitivity (as done in Sect. 2.5), because the former metric captures well the behavior of the data when plotted as a time series, whereas scatterplots between the observed porewater nutrient concentrations and the air temperature on the corresponding dates do not show clear correlation.

Deleted: verify

Deleted: the

Deleted: compared

### 2.6.4 Resin-exchange plant available nutrients

The second form of nutrient cycling observations we used is resin-exchange $NH_4^+$ and $PO_4^{3-}$ (Iversen et al., 2017a). Those values approximately represent plant-available nutrients but previous study suggests that in shallow soil layers (10 cm), competition with roots invalidates this interpretation (Iversen et al., 2017a, 2022). Therefore, we focus on the resin-exchange nutrients measured at 30 cm in both the hummock and hollow, and at 60 cm in the hollow during 2015-2018, at which depths few roots exist in the anaerobic peatland environment (Iversen et al., 2017a). The raw measurements were cumulative absorbed weights of $NH_4^+$ or $PO_4^{3-}$ per resin capsule surface area during roughly monthly intervals; the values used in this study are the aggregated annual averages by the data collector (Iversen et al., 2017a). Following previous study, we compared the temperature sensitivities of the observed resin-exchange nutrients to the temperature sensitivities of the most comparable modeled variable, annual average net nutrient mineralization rates (NET_NMIN [gN $m^{-3}$ $s^{-1}$], NET_PMIN [gP $m^{-3}$ $s^{-1}$]) for a qualitative comparison (Iversen et al., 2022). To remove unit difference between the observed and modeled quantities, we divided the observed values and the modeled values, respectively, by the mean value of each during the observational period, separately for each nutrient species and soil depth. The resulting regression slopes against temperature represent relative (mean-scaled) changes per unit change in soil temperature. This normalization approach is commonly used in elasticity analysis for comparing effects across variables with different units (Sydsaeter and Hammond, 1995).

### 2.6.5 Pretreatment peat C, N, P stocks

The final observation of nutrient cycling we used for evaluation are pre-treatment vertical profiles of C, N, and P stocks in the peat (Griffiths et al., 2017; Salmon et al., 2021). The compared model variables are the summed C, N, and P contents of all four SOM pools (1, 2, 3, 4) in all the soil layers in the decomposition processes [SI Sect. 1.1.3, (Oleson et al., 2013a)] in the control plot.

## 2.7 Sensitivity experiments

### 2.7.1 Parameter optimization

In both ELM-OLD and ELM-MYCI, the soil decomposition process uses column-level parameters that are shared between hummock and hollow. Vegetation processes like photosynthesis, respiration, and nutrients uptake/acquisition use PFT-specific parameters that are also shared between hummock and hollow. We used observed parameter values as much as possible in ELM-OLD (SI Table S2) and ELM-MYCI (Table S4). For those unobserved, we used either optimized values obtained from 4000-member ensemble simulations that are described below (Tables S3 and Table 1) or manually set default values (Tables S2 and S4) if a parameter has relatively minor influence on the quantities of interest in this study. All the parameter optimization simulations excluded moss parameters for the purpose of consistency – because moss is not modified in this study, the newly added parameters do not cover moss.

Deleted:
Deleted: 1
Deleted: S5

We selected eleven preexisting parameters in ELM-OLD to optimize based on previous sensitivity findings (Meng et al., 2021; Ricciuto et al., 2018). Those parameters affect photosynthesis, plant respiration, plant allocation, and soil decomposition processes (Table S3). For each parameter, we generated an equal number of uniform random samples between predetermined upper and lower bounds from previous studies (Griffiths et al., 2017; Meng et al., 2021; Ricciuto et al., 2018) (Table S3). We then formed all possible combinations of these samples across the parameters to create a total of 4000 samples. We then ran the model with these 4,000 parameter sets. Finally, we ranked these parameter sets by relative absolute error (RAE) and selected the sample with the lowest RAE as the optimized parameter values. The RAE formula is shown in Eq. 5 and considers the relative errors in mean and in temperature sensitivity of annual C fluxes:

$$RAE = \frac{1}{|V|} \sum_{c\in\{\text{ambient,elevated}\}} \sum_{v\in V} \left( \left| \frac{A_{sim,v,c} - A_{obs,v,c}}{U_{obs,v,c}} \right| + \left| \frac{S_{sim,v,c} - S_{obs,v,c}}{Q_{obs,v,c}} \right| \right) \quad (5)$$

where the subscripts $sim$ means simulated, $obs$ means observed, $v$ is variable, $c$ is the $CO_2$ treatment (ambient or elevated), $V$ is the set of variables compared, $|V|$ is the number of variables, $A$ is the mean magnitude of the variable across all the treatments and years, $S$ is the linear regression slope of the variable against annual mean air temperature across all the treatments and years, $U$ is the observational uncertainty in mean, $Q$ is the observational uncertainty in slope. During calibration, the performance metric calculated on the annual C fluxes that are items 1-6 in Sect. 2.5, because those are directly comparable to model outputs. Other observations are either reserved for validation (Sect. 2.6.1-2.6.2), not directly comparable to model outputs (Sect. 2.6.3-2.6.4), or pretreatment (Sect. 2.6.5). We did not include the aggregate NPP (item 7) or annual maximum LAI because of strong overlap with items 1-6. The $U_{obs,v,c}$ values were estimated from pre-treatment standard deviation across the enclosure locations (Hanson et al., 2020a, 2025) by assuming that the relative uncertainty stays the same, i.e. the ratio of pre-treatment standard deviation to pre-treatment mean is the same as the ratio of $U_{obs,v,c}$ to $A_{obs,v,c}$. The $Q_{obs,v,c}$ values are the $1\sigma$ uncertainty in the linear regression slopes (DeGroot and Schervish, 2018). We chose normalization by uncertainty to ensure the $BGNPP_{treeshrub}$ variable, which are based on ingrowth core samples that had limited spatial representativeness and only span two years, was not overemphasized compared to the other C fluxes, which have five-year estimates (Hanson et al., 2020a; Iversen et al., 2021b). The normalization additionally ensured that all the variables are unitless, making them intercomparable.

For ELM-MYCI, the total number of preexisting and newly added parameters resulted in an extremely large search space that cannot be covered by 4000 samples. Therefore, we focus on perturbing the most sensitive half (18) of the 37 newly added parameters (Table 1). The most sensitive half was predetermined using one-at-a-time (OAT) perturbation – for each parameter, we generated 50 uniform random samples per parameter between pre-defined upper and lower bounds (Table S4, Table 1). The perturbation ranges were based on observations or previous studies when possible (Table S4). The range for $q_{10}$ of mycorrhizal acquisitions was set wider than the range of q10_hr for HR (Table S3) to explore more values (Table 1). The ranges for the rate constants ($v_{N/P,froot,j}$, $v_{N/P,fungi,j}$, $u_{N/P,fungi,j}$) always span exactly two orders of magnitudes, and were selected based on experimental measurements (Table S5) and similar rate constants in past modelling studies (He et al., 2021;

Deleted: ¶
Deleted: combinations
Deleted: combination
Deleted: 4
Deleted: name
Deleted: size of $V$
Deleted: temperature response slope
Deleted: $S$
Deleted: T
Deleted: is only based on
Deleted:
Deleted: (see Sect. 2.5, items 1-6)
Deleted: (
Deleted: )
Deleted: ) are not overemphasized
Deleted: 1
Deleted: Table S5
Deleted: -S5
Deleted: 1
Deleted: 1

Shao et al., 2023b; Wu and Blodau, 2013). The geometric centre of each range was a manually tuned value that produced acceptable performance at the site during preliminary simulations. The ranges for the half-saturation points ($k_{N/P,j}$) were set at approximately the modelled annual average soil inorganic NP levels at the SPRUCE site, because experimentally measured values (Table S6) were found to cause PFTs to die in test simulations. The ranges for the C-cost factor of mycorrhizal N acquisition ($c_N$) were selected based on past observed exchange ratios for EcM (Bogar et al., 2022), assuming ErM has similar behaviour. We did not include the high-end of the observed exchange ratios (>100) (Bogar et al., 2022) because those severely restricted mycorrhizal nutrient uptake in the modelling context, possibly due to the 50% net photosynthesis cap.

We then calculated the standard deviations of $A_{sim,v,c}$ and $S_{sim,v,c}$ over all the random samples for each variable and $CO_2$ treatment. This approach resulted in a 4th order tensor of 37 parameters x 6 variables x 2 $CO_2$ treatments x 2 coefficients [mean or temperature response slope]. We converted the standard deviation tensor to a same-dimensioned rank tensor by ranking the standard deviations high-to-low across the parameters separately for each variable, $CO_2$ treatment, and mean or slope. We show the ranks in Figure S4, with the last three dimensions of the rank tensor compressed into the form of boxplots. The selected most sensitive parameters are those with lowest median ranks in Figure S4 and are listed in Table S5. We then perturbed those most sensitive 18 parameters in a 4000-member ensemble simulation, calculated the RAE in the same way as done for ELM-OLD, and selected the sample with lowest RAE as the optimized set of parameters.

Deleted: and

It is desirable to understand whether our structural change can improve ELM-OLD beyond the capability of parameter optimization. Therefore, we conducted two sets of 4000-member ensemble simulations for ELM-MYCI: one with the preexisting parameters fixed at default levels, and one with the preexisting parameters fixed at optimized levels. Table 2 lists the final four simulations compared in this study. Comparing ELM-OLD$_{optim}$ to ELM-OLD gives the effect of parameter optimization. Comparing either ELM-MYCI to ELM-OLD, or ELM-MYCI$_{optim}$ to ELM-OLD$_{optim}$, gives the effect of structural modification. Comparing ELM-MYCI$_{optim}$ to ELM-OLD gives the combined effects of parameter optimization and structural modification.

**Table 1: Newly added parameters in ELM-MYCI that are optimized.**

| Symbol (Unit) | Equation appeared in | Plant functional type | Range | Optimized values | |
|---|---|---|---|---|---|
| | | | | ELM-MYCI | ELM-MYCI$_{optim}$ |
| $a_j$ (1) | Eq. 1 (identical to Eq. 12) | Shrub | [0.2, 0.8] | 0.9053 | 0.6868 |
| $b_j$ (1) | | Spruce | [-0.1, 0.1] | -0.07366 | -0.09000 |
| | | Tamarack | | 0.00576 | -0.06763 |
| | | Shrub | [-0.1, 0] | -0.07368 | -0.06777 |
| $q_{10}$ (1) | Eq. S13 | - | [1, 4] | 3 | 1 |
| $u_{N,fungi,j}$ (gN gC$^{-1}$ s$^{-1}$) | Eq. S17 | Spruce | [2.55*10$^{-10}$, 2.55*10$^{-8}$] | 2.4368*10$^{-8}$ | 1.9289*10$^{-8}$ |

| | | | | | |
|---|---|---|---|---|---|
| $u_{P,fungi,j}$ (gN gC$^{-1}$ s$^{-1}$) | Phosphorus counterpart of Eq. S17 | Spruce | [1.520*10$^{-12}$, 1.520*10$^{-10}$] | 6.9176*10$^{-11}$ | 2.749*10$^{-11}$ |
| | | Tamarack | [1.079*10$^{-11}$, 1.079*10$^{-9}$] | 8.1831*10$^{-10}$ | 7.782*10$^{-10}$ |
| | | Shrub | [1.127*10$^{-11}$, 1.127*10$^{-9}$] | 1.4757*10$^{-10}$ | 2.427*10$^{-11}$ |
| $k_{P,j}$ (gP m$^{-3}$) | Phosphorus counterpart of Eq. S22 | Spruce | [0.002478, 0.009911] | 0.004457 | 0.009172 |
| $v_{N,fungi,j}$ (gN gC$^{-1}$ s$^{-1}$) | Eq. S23 | Tamarack | [3.4833*10$^{-9}$, 3.4833*10$^{-7}$] | 8.7018*10$^{-9}$ | 2.7459*10$^{-7}$ |
| $v_{P,fungi,j}$ (gP gC$^{-1}$ s$^{-1}$) | Phosphorus counterpart of Eq. S23 | Spruce | [1.2229*10$^{-11}$, 1.2229*10$^{-9}$] | 1.8946*10$^{-11}$ | 8.2067*10$^{-10}$ |
| $c_N$ (gC gN$^{-1}$) | Eq. S25, S30 | - | [10, 100] | 34 | 32 |
| $v_{N,froot,j}$ (gN gC$^{-1}$ s$^{-1}$) | Eq. S33 | Tamarack | [9.6838*10$^{-12}$, 9.6838*10$^{-10}$] | 8.5323*10$^{-10}$ | 3.4772*10$^{-10}$ |
| | | Shrub | [9.6462*10$^{-13}$, 9.6462*10$^{-11}$] | 2.5154*10$^{-12}$ | 2.0811*10$^{-11}$ |
| $v_{P,froot,j}$ (gP gC$^{-1}$ s$^{-1}$) | Phosphorus counterpart of Eq. S33 | Spruce | [4.4409*10$^{-14}$, 4.4409*10$^{-12}$] | 2.8185*10$^{-12}$ | 3.7779*10$^{-12}$ |
| | | Tamarack | [3.6461*10$^{-13}$, 3.6461*10$^{-11}$] | 1.1268*10$^{-12}$ | 5.9747*10$^{-12}$ |
| | | Shrub | [5.5157*10$^{-14}$, 5.5157*10$^{-12}$] | 3.2882*10$^{-12}$ | 2.2162*10$^{-12}$ |

**Table 2: Summary of parameter perturbation experiments and the optimal runs compared in this study**

| Notation | Notation for the corresponding ensemble simulation | Model Structure | Preexisting parameters choice | New parameters choice |
|---|---|---|---|---|
| ELM-OLD | - | Default (Shi et al., 2021) | Default | - |
| ELM-OLD$_{optim}$ | ELM-OLD$_{optim}$ _ENS | Default (Shi et al., 2021) | Optimized | - |
| ELM-MYCI | ELM-MYCI_ENS | Updated (this study) | Default | Optimized |
| ELM-MYCI$_{optim}$ | ELM-MYCI$_{optim}$ _ENS | Updated (this study) | Optimized | Optimized |

### 2.7.2 Verification of parameter constraint

Eq. 5 only uses C fluxes but the optimized new parameters are mainly relevant to NP. To examine whether the selected optimal parameter values are indeed from a constrained subregion of the search space by Eq. 5, or simply perform best by chance, we used a clustering metric. This metric, though not using a formal likelihood framework, is consistent with the equifinality concept, where parameters are considered identifiable if the high-likelihood parameter values are concentrated in a small region, and non-identifiable if broadly distributed across the parameter space (Raue et al., 2009). We first normalized all the sampled parameter values to between 0 and 1 using the predefined ranges (Tables S3 and S5). Then, we calculated the Euclidean distances between the normalized parameter values of two types of ensemble member pairs. The first type was all the pairs that can be formed between the best performing 1% (i.e. 40) members. The second type was all the pairs formed between one value from the best performing 1% members, and one value from the bottom 99% (4000 – 40 = 3960) members. If the pairwise distances in the first group are systematically lower than the pairwise distances in the second group, it means the better-performing parameter sets are clustered, which we interpret as being constrained by Eq. 5.

### 2.7.3 Sobol's sensitivity analysis

While the OAT perturbation helps us to downsize the number of parameters to perturb, it offers limited insight into the full sensitivity of model outputs, because it omits potential interactions among parameters. Using the 4000-member ensembles, we therefore applied a previously established procedure on ELM to calculate Sobol's main-effect and total-effect indices between selected model outputs and all the perturbed parameters (Ricciuto et al., 2018). Sobol's sensitivity indices are based on variance decomposition, where the total variance in a model output is decomposed into fractions attributed to individual parameters and interactions among parameters (Saltelli et al., 2004). The main effect measures the relative fraction attributed to a parameter excluding all interactions. Due to the omission of interactions, the sum of main effects across all the parameters is less than 1. The total effect measures the relative fraction attributed to a parameter including itself and all higher-order interactions involving the parameter. Due to duplicated counting of interactions, the sum of total effects across all the parameters is greater than 1.

## 3 Results

### 3.1 Comparison between model and observations

#### 3.1.1 Model performance on C fluxes and leaf area index

On the calibration set of C fluxes, ELM-MYCI$_{optim}$ best captures the mean and temperature sensitivity of the C fluxes (RAE = 1.54), followed by ELM-OLD$_{optim}$ (RAE = 1.61), ELM-OLD (RAE =1.80), and lastly ELM-MYCI (RAE = 1.82) (Figure 2). Also, ELM-MYCI$_{optim}$ and ELM-OLD$_{optim}$ have the fewest number of variables falling outside the +/- one standard deviation observational uncertainty window (6 out of 28), followed by ELM-MYCI (8 out of 28), and lastly ELM-OLD (9 out of 28; the

Deleted: ¶
Formatted: Heading 3
Deleted: Based on the aggregate RAE metric
Deleted: Figure 2

number of "x's" of Figure 2). Among the individual variables, the mean $NPP_{moss}$ under elevated $CO_2$, the temperature sensitivity of $BGNPP_{TreeShrub}$ under ambient and elevated $CO_2$, and the temperature sensitivity of aggregate NPP under elevated $CO_2$ are least well-captured, with all four model setups simulating outside the observational uncertainty (Figure 2acd). ELM-MYCI captures mean HR better than the other three model setups but performs worse on several other variables (mean $AGNPP_{shrub}$, temperature sensitivity of $AGNPP_{spruce}$ under ambient $CO_2$, mean $NPP_{moss}$ under ambient $CO_2$, and temperature sensitivity of $NPP_{moss}$ under elevated $CO_2$) (Figure 2). Consistent with our hypothesis (see end of Sect. 1), structural modification improves model performance in capturing the observed large positive response of shrub growth to warming. The temperature sensitivity of $AGNPP_{shrub}$ under ambient and elevated $CO_2$ are outside the observational uncertainty in ELM-OLD (Figure 2c). Using optimized preexisting parameters, $ELM\text{-}OLD_{optim}$ simulates the temperature sensitivity of $AGNPP_{shrub}$ within the observational uncertainty range, but still underestimates it by ~50% under elevated $CO_2$ (Figure 2c). With structural modification on top of optimized preexisting parameters, $ELM\text{-}MYCI_{optim}$ best captures the temperature sensitivity of $AGNPP_{shrub}$, with only 17-35% underestimation (Figure 2c). Structural modifcation appears to negtatively influence the simulated mean $AGNPP_{spruce}$, which is more severely underestimated in ELM-MYCI and $ELM\text{-}MYCI_{optim}$ than in the other two model setups.

The results of Figure 2 show aggregated statistics for all the plots. To reveal more detailed causes of model biases, Figure S7 shows the plot-wise observed and modelled annual time series of the calibration C fluxes. The interannual and inter-plot variabilities are much larger in the observations than all four model setups, especially in 2015, suggesting spatial variability in the real world remains a source of uncertainty in the model-observation comparison (SI Sect. 1.2). Increase in $AGNPP_{shrub}$, decrease in $NPP_{moss}$, and increase in HR from the coldest to the warmest treatments are visually discernible in both the observations (Figure S7c1, d1) and the simulations (Figure S7c2-c5, d2-d5). Using root mean squared error (RMSE) as a metric on each individual C flux, one can see that $ELM\text{-}MYCI_{optim}$ best captures $AGNPP_{shrub}$ (Figure S7c2-c5) as well as the aggregate NPP (Figure S7f2-f5), ELM-MYCI best captures HR (Figure S7g2-g5), but the structural modifications did not result in clear improvements on $AGNPP_{spruce}$ or $AGNPP_{tamarack}$ (Figure S7a1-b5). These are consistent with calibration-period performance evaluated on mean and temperature sensitivity (Figure 2).

On the evaluation set of C fluxes, $ELM\text{-}MYCI_{optim}$ has the best RAE (4.65), followed by $ELM\text{-}OLD_{optim}$ (RAE = 5.03), ELM-MYCI (RAE = 7.22), and ELM-OLD (RAE = 7.31) (Figure 3). RMSE and RAE values calculated on the individual C fluxes show that $ELM\text{-}MYCI_{optim}$ outperforms the other three model setups on $AGNPP_{spruce}$, $AGNPP_{shrub}$, and $NEE_{shrubmoss}$, but not on $AGNPP_{tamarack}$. This is consistent with the better performance of $ELM\text{-}MYCI_{optim}$ on shrub than trees during the calibration period (Figure 2, Figure S7). None of the model setups correctly captures the positive temperature sensitivities of $AGNPP_{spruce}$ under both $CO_2$ treatments and of $AGNPP_{tamarack}$ under the ambient $CO_2$ treatment in 2022 (Figure 3ab). The high RAE on $NEE_{shrubmoss}$ likely arises from an underestimation of observational uncertainty for this variable, since it was estimated from the RMSE of the gapfilling algorithm (Figures S4-S5), not considering pre-treatment spatial variability or uncertainty in the chamber- and plot-level biomass measurements used to harmonize model and observations (Sect. 2.6.1). Nonetheless, such bias does not affect the within-variable ranking across the model setups based on RAE or RMSE.

Deleted: Figure 2
Deleted: Figure 2
Deleted: Figure 2
Deleted: Figure 2
Deleted: Figure 2
Deleted: Figure 2
Deleted: ¶
Formatted: Not Superscript/ Subscript
Formatted: Not Superscript/ Subscript
Formatted: Font: Not Bold
Formatted: Font: Bold

In addition to C fluxes, we used annual maximum LAI, which is not a calibration variable, as a proxy to compare modelled C biomass to observed. Based on RMSE, ELM-MYCI$_{optim}$ has lower overestimation in spruce LAI and lower underestimation in shrub LAI compared to the other three model setups, although higher overestimation in tamarack LAI (Figure S8).

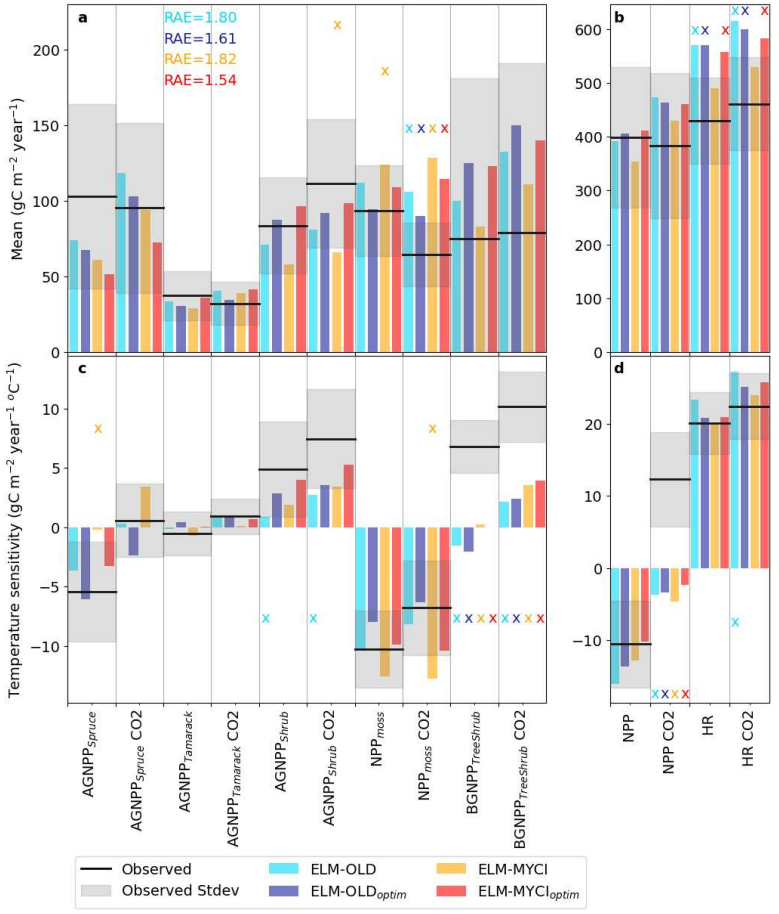


**Figure 2: Observed versus simulated mean C fluxes ($A_{obs,v,c}$, $A_{sim,v,c}$ in Eq. 5) and temperature sensitivity of C fluxes ($S_{obs,v,c}$, $S_{sim,v,c}$ in Eq. 5) on the calibration set (2015-2021). RAE is calculated from Eq. 5 for each model setup. The C fluxes names and calculation of the means and temperature sensitivities are explained in Sect. 2.5. The additional "NPP" term was summed up from C fluxes 1–6 in Sect. 2.5, to provide a measure of plot-level primary productivity, but should not be understood as standard NPP**

Deleted: ELM-MYCI reduced the

Deleted: the

Deleted: by ELM-OLD (Figure S6d-f, j-l). ELM-MYCI$_{optim}$ achieved similar error reductions compared to ELM-OLD$_{optim}$,

Deleted: increased

Deleted: the

Deleted: 6g-i, m-o

Deleted: ¶

because it does not contain coarse root production. The suffix CO2 means values for elevated $CO_2$ enclosures, and without this suffix means values for ambient $CO_2$ enclosures. The observational uncertainty intervals are estimated as described in Sect. 2.7.1. The "x" on top of each bar indicates that the simulated value is outside the observed uncertainty interval.

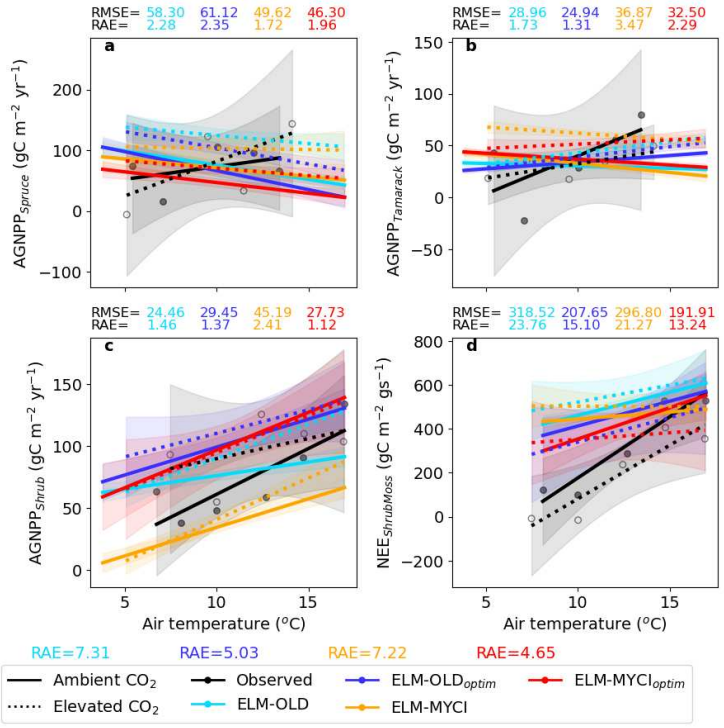


Figure 3: Observed versus simulated annual C fluxes on the evaluation set (2022-2023), showing the magnitude and temperature sensitivity. The C fluxes names are explained in Sect. 2.6 and "gs" in the unit of $NEE_{shrubmoss}$ denotes growing season. For each subplot, linear regressions relate annual mean air temperature to the C flux, separately for the ambient $CO_2$ treatment plots and the elevated $CO_2$ treatment plots. Shaded regions indicate 95% confidence bands of the regressions (DeGroot and Schervish, 2018). Scatter dots show the original data points only for the observational regressions; the simulated original data points are omitted for readability. Root mean squared errors (RMSE) were calculated between the simulated and observed annual C fluxes within each subplot. RAE were calculated from Eq. 5, for each C flux separately (subplot-level) and for all four compared C fluxes (figure-level). For RAE calculation, the uncertainty of $AGNPP_{spruce}$, $AGNPP_{tamarack}$, and $AGNPP_{shrub}$ are as documented in Sect. 2.7.1. The mean uncertainty of $NEE_{shrubmoss}$ was set equal to the combined RMSE of the gapfilling algorithm on all the observed data points (15.24 gC m$^{-2}$ gs$^{-1}$, combined from Figures S4-S5). The temperature sensitivity uncertainty of $NEE_{shrubmoss}$ was equal to the standard deviation of regression slope like the other variables documented in Sect. 2.7.1.

### 3.1.2 Model portrayal of soil nutrients

The observed resin-exchangeable nutrients increase by about two orders of magnitude with warming in all observed combinations of depth, nutrient, and hummock-hollow (Figure 4). The net mineralization rates increase only by about one order of magnitude in ELM-OLD and ELM-OLD$_{optim}$. ELM-MYCI and ELM-MYCI$_{optim}$ better capture the observed increases (yellow line in Figure 4a, yellow and red lines in Figure 4bef, red line in Figure 4c).

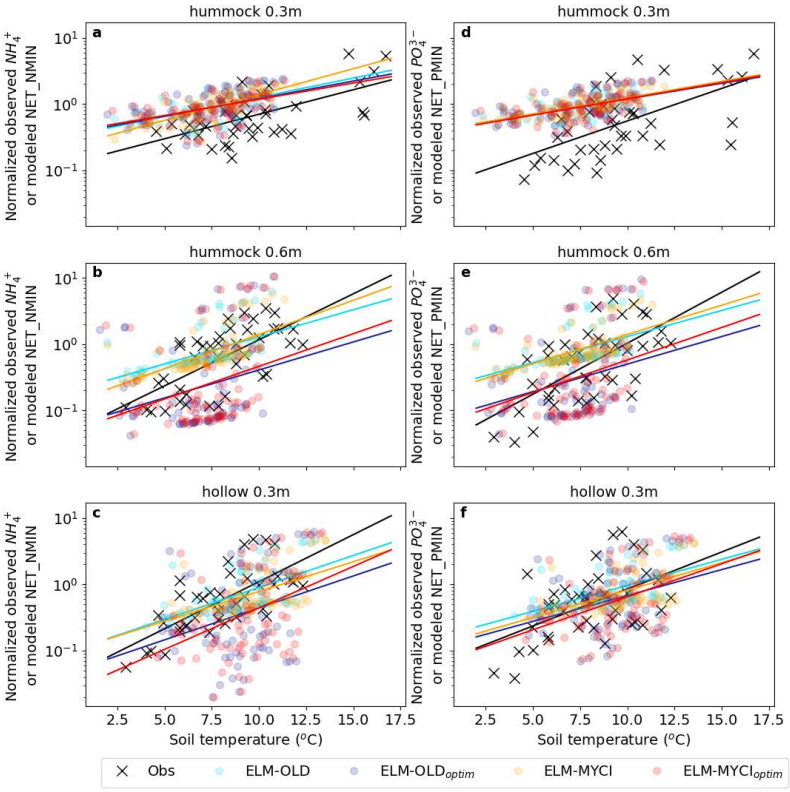


**Figure 4: Relationships between normalized plant-available nutrients and annual mean peat temperatures in the observations and models at different depths of hummock and hollow. The plant-available nutrients are represented by annual total resin-exchange nutrients ($NH_4^+$ and $PO_4^{3-}$) in observation and annual mean net mineralization rates (NET_NMIN and NET_PMIN) in the model. Annual values across all the years, enclosures, and $CO_2$ treatments are plotted together. The normalization procedure is reported in Sect. 2.6.4 and reconciles unit difference between observation and model. Lines are least-squares linear regression lines.**

Deleted: Figure 3

Deleted: Figure 3

Deleted: Figure 3

Deleted: Figure 3

Deleted: across all the enclosures

The modelled soil $NH_4^+$ and soluble P concentrations, converted to per volume soil water basis to compare with observed porewater values, show mean levels that are ELM-MYCI > ELM-OLD > ELM-MYCI$_{optim}$ > ELM-OLD$_{optim}$ (Figure S9ac). The ELM-OLD$_{optim}$ values are closest to observed $NH_4^+$ values but still about one order of magnitude higher. The ELM-MYCI values are closest to observed soluble P values but more than one order of magnitude smaller. The observed $NO_3^-$ mean concentrations are captured more accurately than $NH_4^+$ or soluble P, with ELM-OLD$_{optim}$ being closest to observations, followed by ELM-MYCI$_{optim}$, while ELM-OLD and ELM-MYCI remain within one order of magnitude of the observations (Figure S9b). These large discrepancies call into question if these observed and simulated quantities are comparable, even after the units are nominally aligned. Like the mean concentrations, the observed and simulated trends differ substantially in magnitudes. ELM-OLD and ELM-MYCI better capture the observed qualitative transition from negative to positive trends $NH_4^+$ towards the warmer enclosures than ELM-MYCI$_{optim}$; ELM-OLD$_{optim}$ did not capture this transition for the ambient $CO_2$ enclosures (Figure S9d).

All the model setups overestimate the peat C and N stock in the shallow soil layers (0-30 cm; Figure 5ab). In the deeper layers (30 cm-200 cm), ELM-OLD exhibits underestimation that is exacerbated in ELM-MYCI and remedied in ELM-OLD$_{optim}$ and ELM-MYCI$_{optim}$ (Figure 5ab). All model setups severely underestimate P stock below 30cm (Figure 5c). The total simulated soil organic C stock of all the soil layers is about 190 kg C m$^{-2}$ by ELM-OLD, 240 kg C m$^{-2}$ by ELM-OLD$_{optim}$, 140 kg C m$^{-2}$ by ELM-MYCI, and 210 kg C m$^{-2}$ by ELM-MYCI$_{optim}$. This places ELM-OLD$_{optim}$ outside the observational uncertainty of the estimated 176±40 kg C m$^{-2}$ of the S1 bog (McFarlane et al., 2018), probably due to the overestimation in the shallow layers (Figure 5a).

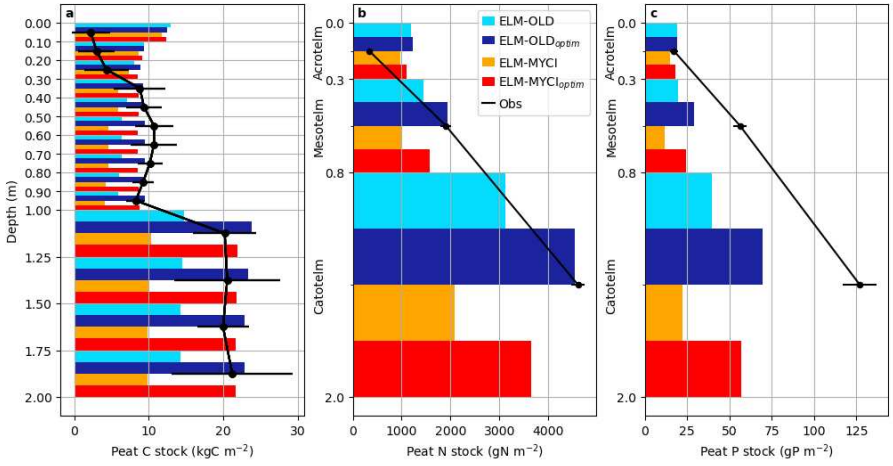


Deleted: Figure S7

Deleted: 7

Deleted: 7

Deleted: Figure 4

Deleted: Figure 4

Deleted: Figure 4

Deleted: Figure 4

**Figure 5: Observed pre-treatment peat carbon, nitrogen, and phosphorus stocks and the modelled values in the ambient control plot. Error bars on the observations are the +/- standard errors reported in the original studies (Griffiths et al., 2017; Salmon et al., 2021). The definitions of acrotelm, mesotelm, and catotelm are in (Salmon et al., 2021).**

### 3.2 Behaviour diagnostics of the modified model

#### 3.2.1 Plant nutrient acquisition response to warming and soil inorganic nutrients levels

Simulation results from ELM-MYCI and ELM-MYCI$_{optim}$ show that the total N acquisition from organic sources by PATH$^{myc,org}$ across the three vascular PFTs are about 2.5 gN m$^{-2}$ year$^{-1}$, and the total P acquisition by PATH$^{myc,org}$ about 0.07 gP m$^{-2}$ year$^{-1}$, in the unenclosed ambient plot (TAMB; Figure 6). The PFT-total N acquisition by PATH$^{myc,org}$ is mainly accounted by spruce (about 50% of the total spruce N uptake, Figure 6a) and shrub (30-50% of the total shrub N uptake in TAMB, lower in the warmed enclosures, Figure 6c). The total organic P acquisition mainly comes from tamarack (>50% of the total tamarack P uptake; Figure 6e). Those numbers and percentages are comparable to the coarse pretreatment estimates for the SPRUCE site, which suggests organic N sources account for about 30% of total plants N acquisition (2.4 gN m$^{-2}$ year$^{-1}$ out of 7.6 gN m$^{-2}$ year$^{-1}$), and organic P sources account for a negligible fraction of total plants P acquisition (0.7 gP m$^{-2}$ year$^{-1}$) (Salmon et al., 2021).

ELM-MYCI and ELM-MYCI$_{optim}$ simulates higher total spruce N acquisition through all three pathways, and greater warming-induced increases in total tamarack and shrub NP acquisitions across all three pathways, than ELM-OLD and ELM-OLD$_{optim}$ (Figure 6). The low spruce P acquisition simulated by ELM-MYCI$_{optim}$, especially under elevated $CO_2$, can explain the underestimation of AGNPP$_{spruce}$ by this model setup (Figure 2a). The large increases in shrub NP acquisition are driven by PATH$^{root}$ (Figure 6cf), consistent with declining fungal colonization rates and rising soil inorganic nutrients under warming (Figure S9a-c, Figure S10c).

In addition to changing the responses of plants nutrient acquisition to warming (Figure 6), ELM-MYCI and ELM-MYCI$_{optim}$ simulate more flexible responses of plants nutrient acquisition to soil inorganic nutrient contents (Figure S11). In ELM-OLD and ELM-OLD$_{optim}$, the uptake always displays a logistic shape where they first increase with soil inorganic N or P and then plateaus. In ELM-MYCI and ELM-MYCI$_{optim}$, the total acquisition across all three pathways can show linear relationships (e.g. Figure S11bef, ELM-MYCI$_{optim}$) or logistic shapes that saturate at higher or lower levels (e.g. Figure S11ab, ELM-MYCI).

Deleted: enclosure
Deleted: Figure 5
Deleted: Figure 5
Deleted: Figure 5
Deleted: Figure 5
Deleted: Figure 5
Deleted: Figure 2
Deleted: Figure 5
Deleted: 7
Deleted: 9
Deleted: Figure 5
Deleted: 0
Deleted: 0
Deleted: 0

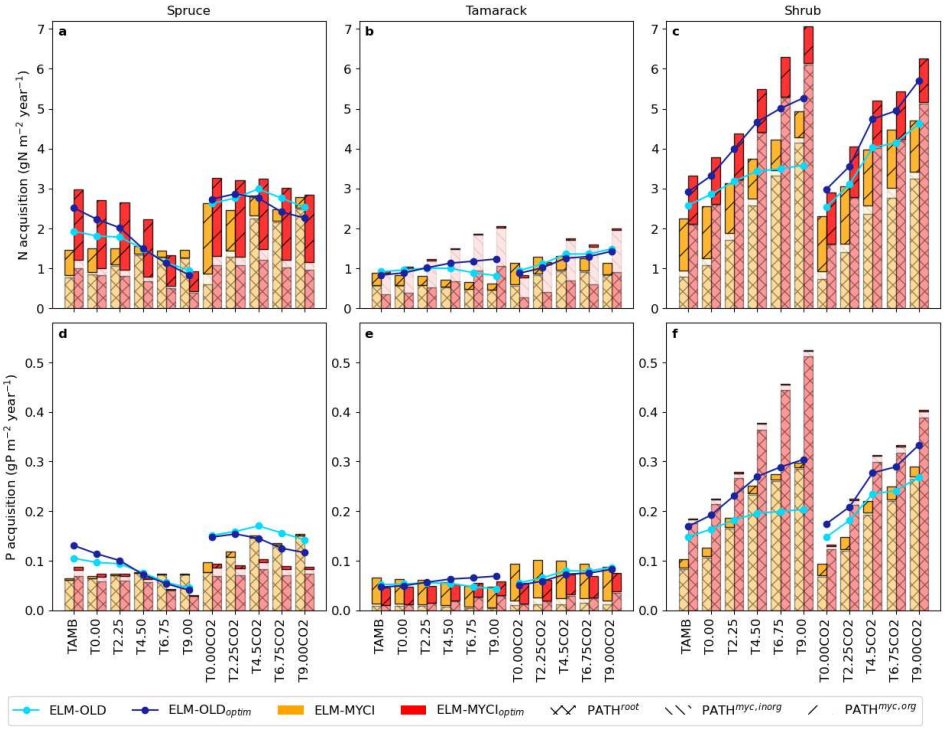


**Figure 6: Simulated annual mean nitrogen (N) and phosphorus (P) acquisition by the vascular PFTs in each treatment plot during 2015-2021. The acquisition is equal to inorganic nutrient uptake in ELM-OLD and ELM-OLD$_{optim}$, and equal to the sum of all three pathways (inorganic nutrient uptake by uncolonized fine roots [PATH$^{root}$], inorganic nutrient acquisition via mycorrhizal roots [PATH$^{myc,inorg}$], and nutrient acquisition from organic sources via mycorrhizal roots [PATH$^{myc,org}$]) in ELM-MYCI and ELM-MYCI$_{optim}$.**

Deleted: enclosure

### 3.2.2 Net ecosystem exchange responses to warming

All model setups simulate a transition from C sink to C source, that is, negative to positive net ecosystem exchange (NEE), with warming (Figure 7a). Except for the +0.00°C elevated $CO_2$ treatment, the C source strength is ELM-OLD > ELM-OLD$_{optim}$ > ELM-MYCI > ELM-MYCI$_{optim}$. NEE is mainly driven by the balance between gross primary productivity (GPP), heterotrophic respiration (HR), and autotrophic respiration (AR), i.e. NEE ≈ – (GPP – AR – HR). The low NEE of ELM-MYCI$_{optim}$ is because it has the lowest fraction of GPP lost to AR, especially in the warmest enclosures, among all the model setups (Figure 7c). Like ELM-MYCI$_{optim}$, ELM-MYCI has a low AR-to-GPP ratio, but its low NEE is likely driven by the low

Deleted: i.e.

Deleted: Figure 6

Deleted: Figure 6

GPP per se (Figure 7bc). In contrast, ELM-OLD$_{optim}$ has lower NEE than ELM-OLD is because of a high GPP (Figure 7b) and a smaller fraction of GPP lost as HR (Figure 7d). Structural modification has little effect on HR to GPP ratios (ELM-OLD v.s. ELM-MYCI, ELM-OLD$_{optim}$ v.s. ELM-MYCI$_{optim}$, Figure 7d). The temperature sensitivities of NEE, GPP, AR and HR are generally insignificant within individual enclosures, but exhibit consistent increasing, decreasing, or bell-shaped patterns across the enclosure warming levels in all the model setups (Figure 7e-l).

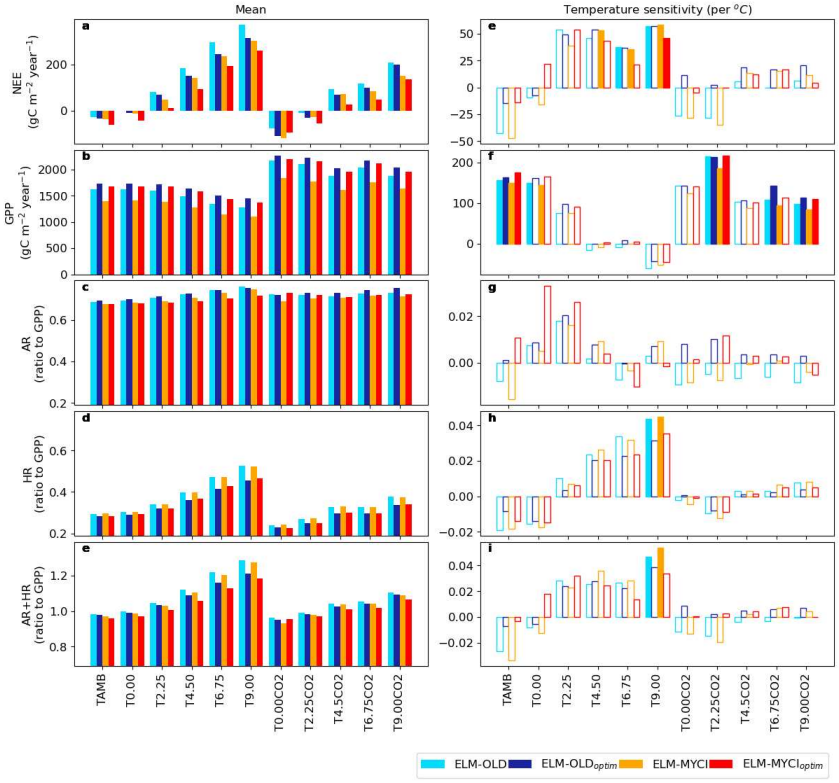


**Figure 7: Modelled plot-wise mean and temperature sensitivity of the net ecosystem exchange (NEE) and its balance terms: gross primary productivity (GPP), autotrophic respiration (AR), heterotrophic respiration (HR). AR and HR are displayed as ratios to GPP. The temperature sensitivities are calculated as linear regression slopes between the annual mean NEE, GPP, AR-to-GPP ratio, HR-to-GPP, or (AR+HR)-to-GPP ratio values against the annual mean air temperatures during 2015-2021 in each plot. The temperature sensitivities have solid bars when they are significantly different from zero at p≤0.05 (two-sided t-test), and otherwise hollow bars.**

Deleted: Figure 6
Deleted: Figure 6
Deleted: Figure 6
Deleted: Figure 6
Deleted: Figure 6
Deleted: enclosure
Deleted: enclosure

### 3.2.3 Nutrient limitations on plant growth

The difference between structural modification and parameter optimization on AR-to-GPP ratios can be better understood by examining the individual components of AR (Figure 7). In ELM, AR is the sum of excess, maintenance, and growth respiration (AR = XR + MR + GR). XR represents respiration loss due to nutrient limitation, and is calculated as an nonlinearly increasing function of the percentage of plant biomass existing as NSC (SI Sect. 1.1.2); MR represents respiration for maintaining regular plant metabolism and is approximately proportional to total living biomass; GR is a small and constant fraction of structural growth and therefore of low interest here (Oleson et al., 2013a).

At grid level, the lower fraction of GPP lost as AR in the structurally modified model setups than their unmodified counterparts (Figure 7c) is mainly driven by lower XR-to-GPP ratios, especially under warming (ELM-MYCI$_{optim}$ v.s. ELM-OLD$_{optim}$, ELM-MYCI v.s. ELM-OLD) (Figure 8a). Interestingly, parameter optimization induces large decreases in the MR-to-GPP ratio that are offset by large increases in the XR-to-GPP ratio (ELM-OLD and ELM-MYCI v.s. ELM-OLD$_{optim}$ and ELM-MYCI$_{optim}$), resulting in small net changes (Figure 8a). This "trade-off" between XR and MR can be explained by their implicit relationship. At a higher XR-to-GPP ratio, the higher nutrient limitation prevents GPP from being assimilated into structural growth, leading to lower biomass-to-GPP ratio and therefore lower MR-to-GPP ratio. By the same logic, lower XR-to-GPP ratio implies a higher biomass-to-GPP ratio, and therefore higher MR-to-GPP ratio.

Compared to the grid-level ratios, structural modification has strong effects on the ratios calculated between PFT-specific XR, MR, and GPP. For spruce, ELM-MYCI and ELM-MYCI$_{optim}$ have much higher XR-to-GPP ratio and lower MR-to-GPP ratio than ELM-OLD and ELM-OLD$_{optim}$, especially in the colder enclosures (Figure 8b), which indicates a XR-MR trade-off similar to observed at grid level. For tamarack, ELM-MYCI$_{optim}$ has much lower XR-to-GPP ratio than ELM-OLD$_{optim}$ in all the enclosures (Figure 8c). For shrub, ELM-MYCI and ELM-MYCI$_{optim}$ have much lower XR-to-GPP ratio than ELM-OLD and ELM-OLD$_{optim}$ in the warmest enclosures (Figure 8d). As such, spruce and shrub are likely the main drivers behind the more rapid decline of the grid-level XR-to-GPP ratio in the structurally modified models than ELM-OLD or ELM-OLD$_{optim}$ (Figure 8a). The weaker XR–MR trade-off in tamarack and shrub likely reflects the lower importance of MR in the two PFTs compared to spruce.

Deleted: Figure 6

Deleted: Figure 6

Deleted: Figure 7

Deleted: Figure 7

Deleted: Figure 7

Deleted: Figure 7

Deleted: Figure 7

Deleted: Figure 7

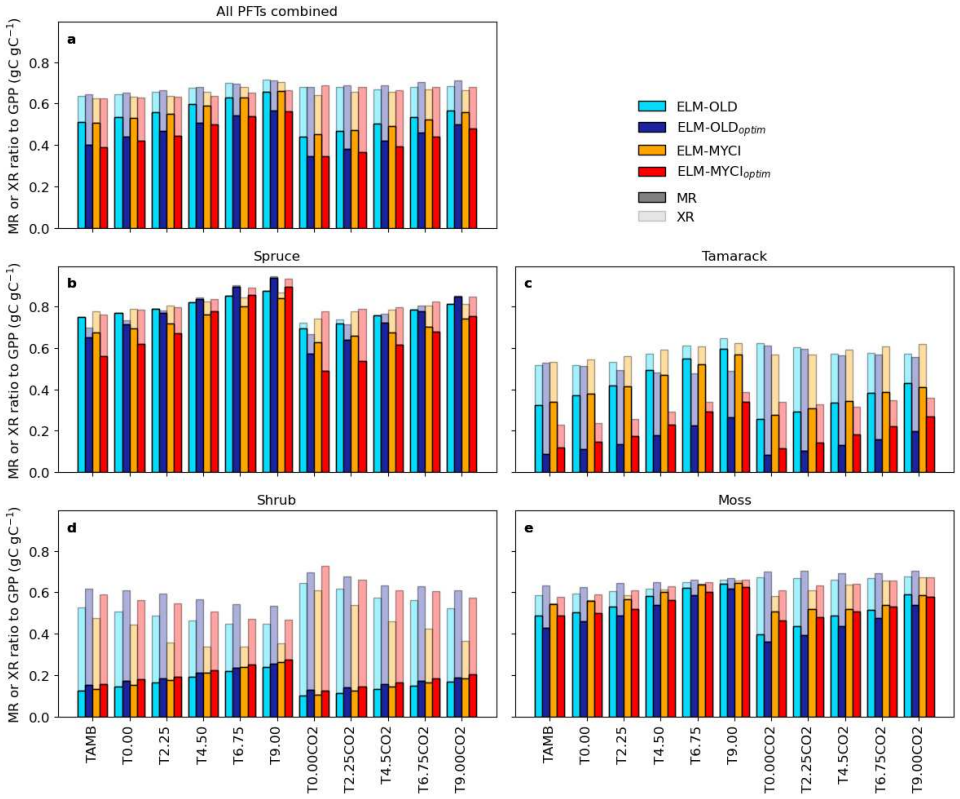


**Figure 8: Partitioning of excess respiration (XR) and maintenance respiration (MR) parts of autotrophic respiration relative to gross primary productivity (GPP) for all PFTs combined or individual PFTs. The ratios are calculated by dividing the 2015-2021 averages of the PFT-total or PFT-specific terms. XR contributions are stacked on top of MR contributions, so the total bar height reflect how much of the GPP flux is offset by total XR+MR.**

### 3.2.4 Nutrient limitations on heterotrophic respiration

Nutrient limitation of HR occurs in the default and modified models when the available soil inorganic N or P cannot satisfy the total demand of the plants and immobilization demand from soil litter and organic matter decomposition (Eq. S4, SI Sect. 1.1.3). The immobilization demand arises mainly in the decomposition step from plant litter to SOM (Oleson et al., 2013a; Schimel and Bennett, 2004). The C:N and C:P in the plant litter pool depend on litter inputs and are usually higher than the C:N and C:P of the downstream SOM pools, which are fixed parameters (Oleson et al., 2013a). As a result, the process

immobilizes additional soil inorganic NP to meet the C:N and C:P of the SOM pools. Because ELM-MYCI and ELM-MYCI$_{optim}$ allow plants to access the NP in plant litter pools via mycorrhizal roots (Sect. 2.2), the C:N and C:P the litter pools increase, resulting in greater immobilization demand per unit decomposition, which is proportional to HR. Consistent with this expectation, for each unit of HR, the corresponding actual immobilized inorganic N in ELM-MYCI and ELM-MYCI$_{optim}$ are higher than in ELM-OLD$_{optim}$ and ELM-OLD at the same level of HR (Figure S12a). The same effect is not seen in P (Figure S12b). Instead, ELM-OLD$_{optim}$ exhibits considerably higher P-immobilization per unit HR than the other three model setups. All the model setups exhibit sensitivity to warming, which suggests P-limitation on HR is more affected by litter quality changes created by relative changes in primary productivity among the PFTs than N-limitation on HR (Figure 2).

### 3.3 Parameter sensitivity analysis

#### 3.3.1 Constraint of model parameters

The distance metric (Sect. 2.7.2) shows the top-performing 1% parameter values are statistically significantly closer to each other (smaller distances) than to the remaining 99% parameter values (larger distances) in all three ensemble simulations (Table 2, Figure 9). The significant separation means the C fluxes can constrain the preexisting and newly added parameters. The distances are least well-separated for ELM-MYCI_ENS (Figure 9b), which uses the same un-optimized parameters as ELM-OLD for the unchanged model processes. Those suboptimal parameter values may have caused biases that the new model processes cannot compensate for, leading to unstable optimized values in the new parameters in the ELM-MYCI_ENS simulations.

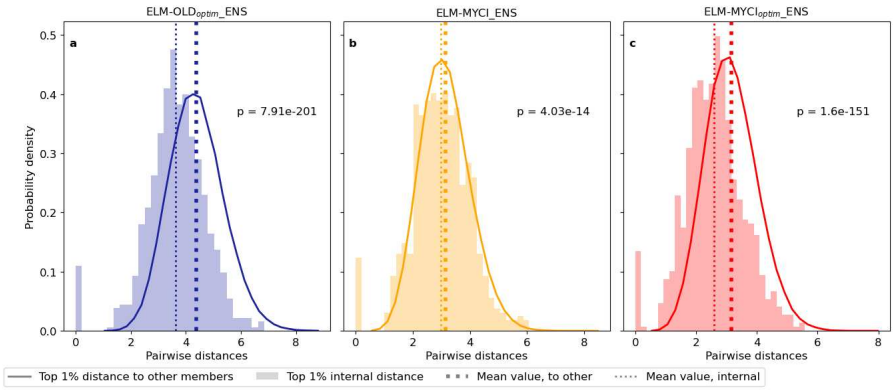


**Figure 9: Probability density distributions of the Euclidean distances between the parameter values of two groups of pairs of ensemble members: between the best-performing 1% members (shaded bars), and between the best-performing 1% members and the other 99% members (solid line). Displayed probability densities are pooled from all pairs in each group. The p-values in each**



Deleted: i

Deleted: Figure 2

Deleted: ¶

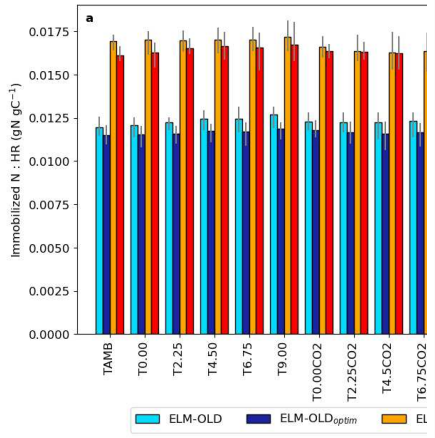


**Figure 7. Ratio of annual mean actual immobilized NP to annual mean heterotrophic respiration (HR) in the soil decomposition process, across the enclosures. The bars show the mean values during 2015-2021 and errorbars show the ranges.** ¶

…

Deleted: Figure 8

Deleted: Figure 8

Deleted: Comparing

**panel indicate whether the two groups are significantly different, using two-sided t-test for the mean values of two independent samples.**

### 3.3.2 Sensitivity of model outputs to parameter values

We show the parameter sensitivities of ELM-MYCI$_{optim}$_ENS in the main text (Figure 10), since the finding of Sect. 3.3.1 suggests this may be a more reliable perturbed parameter ensemble than ELM-MYCI_ENS (Figure S11), and the sensitivities of preexisting parameters (Figure S12) are similar to the well-reported findings of past studies (Meng et al., 2021; Ricciuto et al., 2018).

The relative sensitivity of model outputs to each parameter is approximately the same whether assessed using total effects or main effects (compare the rows in Figure 10). The grid total GPP is sensitive to the parameters of all three vascular plants and grid-level parameters (topmost bar in each panel of Figure 10). The grid total NEE and vegetation C (TOTVEGC) are most sensitive to spruce parameters, especially the sensitivity of fungal colonization rate to soil inorganic N ($b_j$, Eq. S12) and maximum rate of inorganic N acquisition via mycorrhizal association ($v_{N,myc,j}$, Eq. S23). The grid total HR and total soil organic C (TOTSOMC) are most sensitive to shrub parameters, especially the maximum rate of N uptake via fine root ($v_{N,froot,j}$, Eq. S33). The C variables in any vascular PFT are mainly determined by the parameters specific to that PFT, especially the maximum uptake/acquisition rates of NP ($u_{N,myc,j}$ and $u_{P,myc,j}$ for spruce [Eq. S17], $v_{P,froot,j}$ for tamarack [Eq. S33], and $v_{N,froot,j}$ for shrub [Eq. S33]). Moss C variables are sensitive to the parameters of all three vascular plants and grid-level parameters.

Compared to ELM-MYCI$_{optim}$_ENS, the sensitivities derived from ELM-MYCI_ENS are similar for tamarack and shrub parameters (Figure 10bcfg, Figure S11bcfg). For spruce parameters, the model outputs of ELM-MYCI_ENS are more sensitive to the fungal colonization rate to soil inorganic N ($b_j$, Eq. S12 and Figure S11ae), whereas ELM-MYCI$_{optim}$_ENS are more sensitive to the maximum organic NP acquisition rates via mycorrhizal association ($u_{N,myc,j}$ and $u_{P,myc,j}$ for spruce, (Eq. S17; Figure 10ae). Still, the two sets of parameters fulfil similar functions, with the former controlling all the nutrient uptake/acquisition pathways (see $M_{myc,j}$ in Eq. S17, S23, and S33) and the latter only controlling the organic pathway (Eq. S17). For column level parameters, ELM-MYCI_ENS is mainly sensitive to the $Q_{10}$ of NP acquisition rates ($q_{10}$, Eq. S13) and has little sensitivity to the C cost of mycorrhizal nutrients acquisition to the plant ($c_N$, Eq. S25, S30) (Figure S11dh). ELM-MYCI$_{optim}$_ENS exhibits the same contrast, albeit less strongly (Figure 10dh).

Comparing between the newly added (Figure 10, Figure S11) and preexisting parameters (Figure S12), one can see the newly added parameters exhibit more inter-PFT interactions. That is, the C variables of each PFT are even more strongly determined by the parameters specific to that PFT in ELM-OLD$_{optim}$_ENS (Figure S12abcefg) than in ELM-MYCI$_{optim}$_ENS (Figure 10abcefg) or ELM-MYCI_ENS (Figure S11abcefg). Additionally, the grid-level C variables are mainly responsive to spruce parameters in ELM-OLD$_{optim}$_ENS (Figure S12ae), compared to both spruce and shrub parameters in ELM-MYCI$_{optim}$_ENS (Figure 10aceg) and ELM-MYCI_ENS (Figure S11aceg). Moss C variables are more responsive to spruce parameters in ELM-OLD$_{optim}$_ENS (Figure S12ae), compared to shrub parameters in ELM-MYCI$_{optim}$_ENS (Figure 10cg) and ELM-MYCI_ENS

Deleted: Figure 9
Deleted: Figure 9
Deleted: Figure 9
Deleted: Figure 9
Deleted: Figure 9
Deleted: Figure 9
Deleted: Figure 9
Deleted: Figure 9
Deleted: Figure 9
Deleted: Figure 9

(Figure S11cg). The main and total effects of ELM-OLD$_{optim}$_ENS are close to 1 when summed over all the parameters (Figure S12 grey lines), while the main effects of ELM-MYCI_ENS and ELM-MYCI$_{optim}$-ENS are much smaller than 1 and the total effect much greater than 1 (Figure 10, Figure S11, grey lines). The larger difference between total and main effects in the modified models means the newly added parameters have stronger statistical interactions than the preexisting parameters in the default model.

Deleted: Figure 9

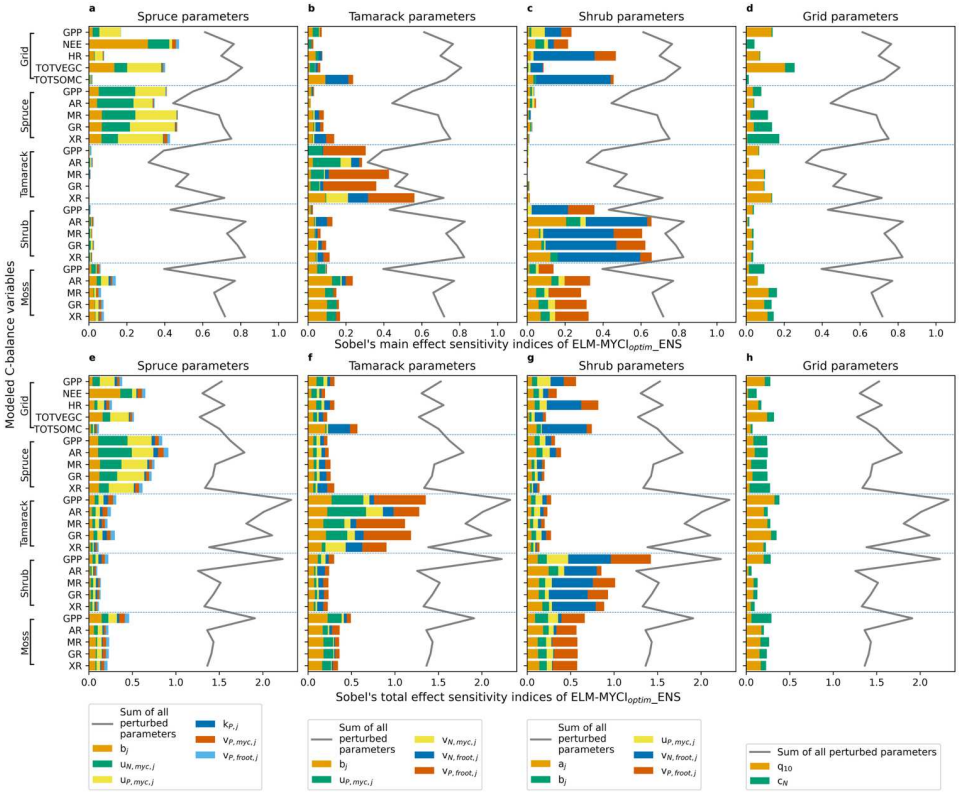


**Figure 10: Sobol's main-effect and total-effect sensitivity indices of selected C-balance variables to the newly added model parameters, calculated from ELM-MYCI$_{optim}$_ENS. For better display, the indices are partitioned into subpanels according to whether it is a PFT-specific or column-level parameter. Stacking the bars across the four panels in each row gives the sum of the main or total effects over all the perturbed parameters, which are also displayed as a grey line for reference in each panel. The C-balance variables in each panel are grouped according to whether it is a column-level, spruce, tamarack, shrub, or moss variable. Parameter definitions can be found in Table S5 and equations referred therein.**

## 4 Discussion

### 4.1 Summary of evaluation performance and remaining gaps

We present a development of the ELMv2-SPRUCE model to replace the photosynthesis-driven, inorganic-only plant nutrient uptake with three pathways that consider influences from fine root biomass, fungi-colonization level, and plant access to organic nutrients through fungi-colonized roots (SI Sect. 1.1). Although EcM and ErM are only implicitly represented and simplifications are made in the treatment of the C cost of mycorrhizal acquisition and the organic NP sources (Sect. 2.2; SI Sect. 1.1.8 and 1.1.9), the modified model shows improved performance. Compared to parameter optimization only (ELM-OLD$_{optim}$), structural modification (ELM-MYCI$_{optim}$) leads to lower RAE and RMSE on vegetation C fluxes, especially in the shrub-moss community (Figure 2, Figure 3), improved LAI in two out of the three modified PFTs (Figure S8), improved qualitative similarity to resin-exchange nutrients (Figure 4), and similar performance on soil total C-N-P stocks (Figure 5). Interestingly, structural modification imposed on un-optimized preexisting parameters (ELM-MYCI) does not improve RAE (Figure 2) and the new parameters appear ill-constrained (Figure 9b). These findings indicate the biases in ELM-OLD arise from both incorrect parameter values and inadequate process representation (Bastrikov et al., 2018). The strong performance of ELM-MYCI$_{optim}$, after optimizing newly-added parameters on top of pre-optimized preexisting parameters, supports stepwise calibration as a viable strategy for land surface models when the parameter search space is large (Ma et al., 2024).

One notable finding is that ELM-MYCI$_{optim}$ captures the observed large positive warming response of AGNPP$_{shrub}$ better than the parameter-optimized default model (ELM-OLD$_{optim}$; Figure 2b, Figure 3c). This increasing growth is accompanied by rising NP uptake via PATH$^{root}$ and unchanging NP acquisition from organic sources via PATH$^{myc,org}$ (Figure 6c), consistent with our initial hypothesis and previous finding at the Mer Bleue peatland site (Shao et al., 2023b), that declining dependence on ErM drives shrub growth under warming. Recent analysis of minirhizotron data at the SPRUCE site shows increasing specific root length for the shrubs with deeper water tables as a consequence of warming (Weber et al., 2025). This shift towards more acquisitive fine root trait (Bergmann et al., 2020; Weber et al., 2025) is not yet considered in the current study and might partially explain the remaining underestimation in the temperature sensitivity of AGNPP$_{shrub}$. The simulated high importance of direct fine root uptake in shrubs at the SPRUCE site differs from the simulated >90% dependence on fungi-mined organic N for shrubs at Mer Bleue (Shao et al., 2023b). This wide range is comparable to past observations (Hilman et al., 2024; Hobbie and Hobbie, 2006; Yin et al., 2022) and might reflect inter-site difference, wherein SPRUCE is a more southern site with lower shrub fractional cover and higher porewater inorganic N compared to Mer Bleue (Kennedy et al., 2018; Shao et al., 2023b).

ELM-MYCI$_{optim}$ more severely underestimates mean AGNPP$_{spruce}$ than the other model setups (Figure 2a), likely because it simulates stronger P limitation on spruce (Figure 6d). The stronger P limitation, in turn, may be because the modelled peat P stock and soil inorganic P levels are generally too low (Figure 5c, Figure S7c). With the enhanced shrub growth in ELM-MYCI$_{optim}$, the remaining inorganic P becomes insufficient to support spruce growth (Figure 2a). All model setups underestimate mean AGNPP$_{spruce}$ in the ambient $CO_2$ plots, fail to capture the reversal from negative to positive response to

Deleted: Figure 2
Deleted: 6
Deleted: Figure 3
Deleted: Figure 4
Deleted: Figure 2
Deleted: Figure 8
Deleted: Figure 2
Deleted: Figure 5
Deleted: Figure 2
Deleted: Figure 5
Deleted: Figure 4
Deleted: Figure 2
Deleted: enclosures
Deleted: and

warming over time (Figure 3a), and fail to capture the observed lack of response to elevated $CO_2$ (Figure 2a). Those biases might be related to seasonal variations and acclimation in spruce photosynthetic parameters (Dusenge et al., 2024; Jensen et al., 2019), gradual acclimation in tree respiration or hydraulics (Hanson et al., 2025), delayed response to elevated $CO_2$ or increased C allocation belowground (e.g. to roots, mycorrhizal fungi, or exudates) (Duchesneau et al., 2024; Norby et al., 2010, 2024; Palmroth et al., 2006). Addressing them will require future process developments.

The severe underestimation of the temperature sensitivity of $BGNPP_{treeshrub}$ in all model setups (Figure 2b) may be due to high uncertainty in the ingrowth core observations or the presence of dynamic above-to-belowground allocation in response to warming (Drewniak, 2019; Rehschuh et al., 2022). Dynamic allocation is not yet in the model processes of ELM-OLD or ELM-MYCI. Note the ingrowth core observations used in Figure 2 only span 2016-2017, while the other evaluation variables span 2016-2019 and 2021 (Hanson et al., 2020a). The uncertainty problem will be remedied as additional years of ingrowth core and minirhizotron observations are completed for the SPRUCE site. The initial ingrowth core observations do suggest the fine root biomass of the trees and shrub are more sensitive to warming than their aboveground NPP (compare the fine root biomass reported in Fig. S1 of Malhotra et al. (2020a) to the observed aboveground NPP values this paper Figure S7).

The persistent bias in $NPP_{moss}$ and its temperature sensitivity is unsurprising. ELMv2-SPRUCE cannot yet simulate the decline of moss growth with warming (Norby et al., 2019), instead depending on assigned observed fractional covers (Sect. 2.4). Missing processes may include shading from shrub, inaccurate photosynthesis-water relations, and microbial relationships (Carrell et al., 2019; Norby et al., 2019; Petro et al., 2023; Shi et al., 2021). The persistent bias in vertical distribution of peat C and N may be due to insufficient vertical mixing of the soil decomposition pools (Oleson et al., 2013a). The persistent bias in HR and peat P stock might be due to inaccurate C:P in the SOM pools (Figure 2b, Figure 5), and the current lack of consideration of fungal respiration (SI Sect. 1.1.7). Because the HR-to-GPP ratio is remarkably invariant to our current structural modification (Figure 7), focused parameter investigation and structural modification on the soil decomposition model may be needed to address the HR bias.

The discrepancy between observed and modelled porewater concentrations (Figure S9) suggests the values are not directly comparable, which may be due to missing process representation of the adsorption of $NH_4^+$ to inorganic and organic matter surfaces (Eick et al., 1999; Matschonat and Matzner, 1996), inaccurate partitioning between labile P and soluble P (Yang et al., 2023), and underestimation of peat P stock (Figure 5). Better matches between the temperature sensitivities of normalized model NP mineralization and normalized resin-available $NH_4^+$ and $PO_4^{3-}$ (Figure 4) suggest the model is better at capturing relative changes in plant nutrient availability than absolute sizes.

### 4.2 Impact on ecosystem productivity

We found that parameter optimization reduces the strength of NEE increase under warming (Figure 7a) via higher GPP and lower HR (Figure 7b). The GPP effect is likely explained by the dominant control of the photosynthetic parameter "flnr" (fraction of leaf N in in Rubisco enzyme) on grid- and PFT-level C balances in $ELM\text{-}OLD_{optim}\_ENS$, and the HR effect likely by the parameter "q10_hr" ($Q_{10}$ for heterotrophic respiration; Figure S14). Interestingly, the overall NEE balance is most

Deleted: Figure 2
Deleted: .
Deleted: Figure 2
Deleted: Figure 2
Deleted: 5
Deleted: Figure 2
Deleted: Figure 4
Deleted: Figure 6
Deleted: 7
Deleted: Figure 4
Deleted: Figure 3
Deleted: Figure 6
Deleted: Figure 6
Deleted: 2

strongly affected by the $Q_{10}$ parameter of spruce MR (Figure S14), despite this parameter having little effect on the other C-balance terms (Figure S14) – this might be a case of emergent phenomena (Brient, 2020; Wang et al., 2022) and worth future modelling and empirical investigations.

Structural modification reduces the extent of NEE increases under warming (Figure 7a) via lower AR (Figure 7c), which is driven by decreases in XR with warming (Figure 8a), especially in spruce and shrub (Figure 8bd). The XR-MR trade-off at grid-level and in spruce (Sect. 3.2.3) mitigates the XR-driven decreases in AR, demonstrating a case of nonlinear feedback. The greater declines in XR in ELM-MYCI and ELM-MYCI$_{optim}$ compared to ELM-OLD and ELM-OLD$_{optim}$ are directly due to declines in NSC (SI Sect. 1.1.2), which is in turn likely due to reduced nutrient limitation (Figure 6acdf) under warming. Although NSC is additionally affected by the C cost of the mycorrhizal pathways (SI Sect. 1.1.8), the C cost should decrease with warming as the importance of the mycorrhizal pathways decline (Figure 6acdf). Therefore, this mechanism cannot explain the simulated NSC decline with warming. The lower nutrient limitation under warming implies greater increase of plant carbon use efficiency (CUE), especially for the shrub PFT where most of AR is due to XR (Figure 8d). This modelling result is consistent with empirical evidence that EcM-tree association is key to explaining the negative correlation between CUE and latitude in northern boreal regions (Mäkelä et al., 2022). This consistency supports the effectiveness of our implicit approach as a parameter-efficient framework. Biologically, the CUE-latitude correlation is driven by complex interactions between plant C flow to mycorrhizal colonization level, and nutrient availability (Mäkelä et al., 2022; Shao et al., 2023b).

In the structurally modified model setups, SOM decomposition becomes more N-limited because of the acquisition of N from plant litter pools via PATH$^{myc,org}$ (Figure S12, SI Sect. 1.1.9). Surprisingly, the higher N-immobilization per unit HR only corresponds to slightly lower mean HR in ELM-MYCI and ELM-MYCI$_{optim}$ (Figure 2bd, Figure 7dh), meaning the lower availability of organic N in plant litter pools are offset by higher inorganic N uptake. This pattern suggests that decomposition suppression through nutrient competition – classically termed the Gadgil effect when mediated by EcM fungi (Fernandez and Kennedy, 2016) – may be limited in strength under our simulated conditions. Although our model does not explicitly represent fungal guild interactions, the modest reduction in decomposition is consistent with studies showing that such effects are highly context-dependent and often confounded by litter quality, niche partitioning among EcM, ErM, and saprotrophs, and priming processes (Fanin et al., 2022; Mielke, 2022; Shao et al., 2023a). P-limitation on immobilization appears to be controlled by more complex factors than N-limitation (FigureS12b) and may be affected by current model bias in peat P stock (Figure 5). Additionally, soil decomposition process in ELMv2-SPRUCE do not explicitly simulate microbial biomass and guilds, and therefore might misrepresent the partitioning of immobilization demand between the external nutrient uptake and the cycled nutrient between dead and live microbial biomass, which is especially important for P (Duchesneau et al., 2024; Schmidt et al., 1997). Given this limitation in the ELMv2-SPRUCE soil decomposition model and current model limitation in treating organic NP sources (SI Sect. 1.1.9), the HR results should be interpreted with caution.

Deleted: 2
Deleted: 2
Deleted: Figure 6
Deleted: Figure 6
Deleted: Figure 7
Deleted: Figure 7
Deleted: , Figure S8ac
Deleted: Figure 5
Deleted: Figure 5
Deleted: observed
Deleted: Figure 7
Deleted: Figure 2
Deleted: Figure 6
Deleted: Figure 4

## 4.3 Limitations, Uncertainties, and Future directions

### 4.3.1 Limitations of the ELM-MYCI equations

In ELM-MYCI, the partitioning of plant nutrient demand between non-mycorrhizal and mycorrhizal pathways is a linear function of soil inorganic N concentration (Eq. 1). The focus on N is likely acceptable for northern boreal regions, where plant growth is N limited or co-limited by N and P, but extending the model into temperate or tropical regions will require considering P limitation (Du et al., 2020). A second question is whether the covariate, soil inorganic nutrient concentration (Eq. 1), is simplistic and should be replaced with plant nutrient status. Plant exudates and phytohormones play a large role in the early establishment of EcM and AM, making plant nutrient status a mechanistically defensible choice (Garcia et al., 2015). But, EcM colonization may also respond to soil inorganic N directly, because assimilating inorganic N is more C-expensive than assimilating organic N (Garcia et al., 2015). Therefore, the relative appropriateness of the two covariates will be best determined via multi-site, multi-PFT simulations across N and P gradients. The current ELM-MYCI equations already have two terms related to plant nutrient status: the N-limitation and NSC availability multipliers (Eq. 3–4). Therefore, to implicitly encode an effect on colonization rate, one can simply let the parameter value in the N-limitation multiplier (Eq. S15) differ between $PATH^{root}$ and the two mycorrhizal pathways.

The current formulation for $PATH^{myc,org}$ makes a few significant simplifications that do not conform to real world processes (Sect. 2.3). The restriction of mycorrhizal organic NP acquisition to plant litter pools may underestimate total mycorrhizal organic NP acquisition. This, in turn, could lead to underestimation of mineral NP limitation on HR and overestimation of the NP limitation on plant growth, contributing to the biases shown in Figure 2. The acquisition rate does not vary with soil organic NP content or the recalcitrance of the accessed plant litter pools (Eq. 4), and the upper bound (0.0001 * total plant litter pool size per hourly time step) is more a sanity constraint rather than a realistic upper bound on fungi-accessible organic matter. This may result in underestimation of the changes in acquisition rates across environmental gradients. In reality, mycorrhizal nutrient acquisition involves two sequential steps: depolymerization followed by uptake of small organic molecules for N (Talbot and Treseder, 2010), and enzymatic hydrolysis and uptake of released phosphate for P (Plassard et al., 2011). Each step is describable by Michaelis-Menten kinetics (Näsholm et al., 2009; Plassard et al., 2011). In the organic matter-rich peatland environment, the first step would be much more limited by fungal enzyme availability than substrate availability, making a colonization-proportional formulation (Eq. 4) acceptable. Extending the model to mineral soil environments will require revisiting the formulation. Although the rate of the first step may be higher for labile than recalcitrant organic matter (Talbot and Treseder, 2010), current understanding of mycorrhizal enzyme activity is largely from a biochemical perspective, i.e. characterizing individual compounds, rather than from an ecological perspective, i.e. classifying numerous compounds into measurable fractions that significantly differ in rates (Lavallee et al., 2020; Oleson et al., 2013b). Therefore, the current even distribution of organic NP acquisition across the plant litter pools, proportional only to pool sizes, serves as a starting point that can be refined as ecological-scale data become available. Modelling the second step in Michaelis-Menten form

Deleted: (Du et al., 2020).(Talbot and Treseder, 2010)(Talbot and Treseder, 2010)(Lavallee et al., 2020; Oleson et al., 2013b)

Formatted: Heading 3

would require explicit representation of the turnover of mono- and oligomeric fractions of organic N pools, or of soluble P pools in microsites, which are beyond the scope of this study.

The total mycorrhizal acquisition of inorganic and organic NP is capped by 50% of net photosynthesis per time step (Sect. 2.3). In the real world, belowground C allocation to mycorrhizal fungi peaks later in the growing season than aboveground photosynthesis (Högberg et al., 2010). Therefore, the current model formulation may underestimate mycorrhizal NP acquisition later in the growing season. In principle, this could lead to underestimated NP limitation on the heterotrophic microbes later in the growing season and overestimated NP limitation during leaf expansion in the following spring and. The practical effect in the current ELMv2-SPRUCE, however, may be minor. The model also does not yet separate heterotrophic microbes and mycorrhizal fungi in soil decomposition. The model also uses fixed C:N:P ratios for plant structural tissues, and always evaluates nutrient limitation based on concurrent soil nutrient availability rather than nonstructural nutrient storage pool sizes.

#### 4.3.2 Uncertainty of the ELM-MYCI parameters and potential constraints

The new equations in ELM-MYCI introduces a fairly large number of new parameters (in total 37 in Table S4 and Table 1) compared to ELM-OLD. Although the annual C fluxes demonstrated ability to constrain these parameters (Figure 9), the ability may have benefited from the temperature gradient, with implied inorganic nutrient gradient, across the SPRUCE treatments. Extending ELM-MYCI to other sites will therefore require more direct constraints.

The highest priority should be given to uptake rate constants ($v_{N/P,froot,j}$, $v_{N/P,fungi,j}$, $u_{N/P,fungi,j}$) and half-saturation points ($k_{N/P,j}$) because of the high sensitivity of model outputs to these parameters (Sect. 3.3.2). Many experimental measurements of these parameter exist, but the data points are concentrated in temperate regions and crop species, and exhibit high cross-species uncertainty (Craig et al., 2025; Griffiths and York, 2020) (Table S5-S6). Therefore, these data points are likely useful for large-scale simulations, but less so for site-scale simulations involving only a few species or simulations targeting underrepresented ecosystems like peatlands. In those cases, total plant NP uptakes, estimated from paired NPP and whole-plant C:N and C:P measurements, provide a reasonable nutrient-centred constraint. The efficiency of the parameter search can be increased in future studies by constraining the search space with well-validated qualitative findings in experimental data – for example, mycorrhizal roots generally have higher rate constants for inorganic NP on a per unit fine root biomass basis than uncolonized roots (Craig et al., 2025; Plassard and Dell, 2010).

Other large sources of uncertainty in the modified model include the fungal colonization fractions (Figure S10), relative contributions of different pathways to total plant NP acquisition (Figure 8), and the transfer of plant C to mycorrhizal fungi (SI Sect. 1.1.8). EcM colonization is known to respond to large temperature, water, and nutrient gradients and covary with fine root traits (Ostonen et al., 2011, 2017; Xie et al., 2021). Stable isotope fractionation studies ($\delta^{15}N$, $\delta^{13}C$) provide the most direct constraint on mycorrhizal contribution to plant demand and plant C allocation to mycorrhizal fungi (Hawkins et al., 2023; Hilman et al., 2024; Hobbie and Hobbie, 2006; Yin et al., 2022). Observations of all these quantities vary between 0-

**Formatted:** Heading 3

**Deleted:** Given

**Deleted:** acquisition rate

**Deleted:** and high uncertainty in current experimental observations (Table S6)

**Deleted:** , one priority of future model-data integration should be to better constrain these parameters.

**Deleted:** 9

**Deleted:** Figure 7

**Deleted:** –

**Deleted:** o

100% (Hawkins et al., 2023; Hilman et al., 2024; Hobbie and Hobbie, 2006; Ostonen et al., 2011, 2017; Xie et al., 2021; Yin et al., 2022) and root tip counts at SPRUCE corroborate the high uncertainty (Figure S10). Therefore, multi-site model-data integration will be needed to capture the broad pattern and prevent overfitting.

Root morphology parameters come from measurements in this study (root diameter - $r_j$ and root tissue density - $\rho_j$ in Table S5). These two traits belong to, respectively, the collaboration and conservation gradients in the root economics space, and both are correlated with other traits (Bergmann et al., 2020; Craig et al., 2025). Thinner roots tend to depend less on fungal partners and have higher uptake rate constants. Lower root density tends to be associated with higher root N content, turnover rates, uptake rate constants, yet higher half-saturation points. These qualitative understandings, along with global root trait observations from, e.g. the Fine-Root Ecology Databases (Iversen et al., 2021a), provide good constraints for ELM-MYCI in future multi-site or regional extensions.

### 4.3.3 Other potential future work

Several process developments in ELM are being carried out during the same time as this work, including division of fine root biomass into transport, absorption, and mycorrhizal pools (Wang et al., 2023), nutrient-responsive dynamic above-belowground allocation (Knox et al., 2024), and explicit microbial biomass pools and dissolved organic matter dynamics (Ricciuto et al., 2021). These developments can be merged with this work to relax many of the assumptions listed in Sect. 4.3.1 and improve the model results. Explicit simulation of fungal and heterotrophic microbial biomass will enable separating mycorrhizal fungal from non-mycorrhizal respiration and the modelling of fungal necromass, which has different decomposability from saprotrophic residues due to higher melanin content, particularly in ErM fungi (Fernandez et al., 2019). Other efforts of interest may include separating the behaviours of EcM and ErM, spruce photosynthesis and MR, *Sphagnum* growth, and considering direct plant uptake of small organic N molecules (Näsholm et al., 2009). Nonetheless, process-development should consider the limited constraint available from empirical observations (Figure 9) and ensure the complexity is commensurate with our ability to check model accuracy and interpret cause and effect in model responses.

The modified ELMv2-SPRUCE has extended capabilities compared to the default model, e.g. fine tune nutrients competition relationships between PFTs using the maximum uptake/acquisition rates and half-saturation parameters (SI Tables S4-S5), assimilating nutrient uptake kinetics data, and testing the ecosystem impacts of changing fine root traits. Those improvements will enable new hypothesis testing and more accurate modelling of peatland C, N, and P cycling. It will also be interesting to compare the modified ELMv2-SPRUCE with other models that use similar fine root-based uptake rules (Knox et al., 2024; Zhu et al., 2019) and/or have mycorrhizal representations (He et al., 2018; Shao et al., 2023b; Sulman et al., 2019), and to test the performance of the model at multi-site to regional scale and its implications for carbon cycle feedbacks to the climate system.

Deleted: , suggesting
Deleted: may better
Formatted: Font color: Text 1
Formatted: Font: Not Bold
Deleted: (Iversen et al., 2021a)
Formatted: Heading 3
Deleted: On the
Deleted: side
Deleted: and
Deleted: are being carried out on ELM,
Deleted: and
Deleted: realism and
Deleted: Another useful endeavour will be to explicitly
Deleted: simulate
Deleted: in ELMv2-SPRUCE, to
Deleted: separate
Deleted: and
Deleted: and allowing the fungi to access other pools beside the litter pools
Deleted: Figure 8

## 5 Conclusions

We present a development on the ELMv2-SPRUCE model to replace default, photosynthesis-driven nutrient uptake processes with fine root and implicit mycorrhizal pathways, allowing more realistic processes like the access to organic nutrients by mycorrhizal roots and the dependence of plant nutrient uptake on fine root biomass, fungi colonization level, and environmental conditions. The modified ELMv2-SPRUCE model better captures the observed large increase in shrub growth under whole ecosystem warming than the default model, as well as overall measured C fluxes and resin-exchange nutrients response to warming. The modelled increase in shrub growth is accompanied by stable fungi-mediated nutrient acquisition from organic matter, and several fold increase in direct fine root inorganic uptake, supporting our initial hypothesis that the observed increase in shrub growth is driven by a shift from mycorrhizal outsourcing to direct fine root uptake strategy. Non-validated comparisons to the default model show the modified model simulates less nutrient limitation on plant growth under warming, resulting in weaker C-sink to C-source transition, and more flexible relationships between plant nutrient acquisition and soil inorganic nutrient concentrations. Outstanding model biases and caveats indicate needs to improve non-mycorrhizal processes for spruce and *Sphagnum* moss growth, and above-to-belowground allocation. Other future developments may add or refine representation fine root trait responses to warming, more realistic organic nutrient access, shifts in allocation, and mycorrhizal fungal biomass turnover. Overall, the new model is a useful tool for model-data integration, hypothesis testing in ecosystem carbon-nitrogen-phosphorus cycling, and investigating boreal peatland responses to environmental change.

## 6 Code and data availability

The ELM-OLD and ELM-MYCI source codes used to conduct all simulations in this study are available at https://zenodo.org/records/17582789. The main branch of the E3SM model is at https://github.com/E3SM-Project/E3SM. ELM simulations must be conducted as land-only simulations in the E3SM framework, and the documentation for conducting such simulations are available at https://docs.e3sm.org/E3SM/ELM/user-guide. All the accelerated spin-up simulations in this study used the ICB1850CNRDCTCBC compset. All the normal spin-up simulations in this study used the ICB20TRCNPRDCTCBC compset. All the transient and treatment simulations in this study used the ICB20TRCNPRDCTCBC compset. The analysis and plotting codes are available at https://zenodo.org/records/17584836. The list of input and evaluation data used by this study is as follows:

- Environmental forcings:
  - Hanson, P.J., J.S. Riggs, W.R. Nettles, M.B. Krassovski, and L.A. Hook. 2016. **SPRUCE Whole Ecosystems Warming (WEW) Environmental Data Beginning August 2015**. Oak Ridge National Laboratory, TES SFA, U.S. Department of Energy, Oak Ridge, Tennessee, U.S.A. https://doi.org/10.3334/CDIAC/spruce.032
- Water table depth:
  - Hanson, P.J., Phillips, J.R., Nettles, W.R., Pearson, K.J., Hook, L.A. 2020. **SPRUCE Plot-Level Water Table Data Assessments for Absolute Elevations and Height with Respect to Mean Hollows**

**Beginning in 2015.** Oak Ridge National Laboratory, TES SFA, U.S. Department of Energy, Oak Ridge, Tennessee, U.S.A. https://doi.org/10.25581/spruce.079/1608615

- Carbon fluxes:
  - Hanson, P.J., J.R. Phillips, D.J. Brice and L.A. Hook. 2018. **SPRUCE Shrub-Layer Growth Assessments in S1-Bog Plots and SPRUCE Experimental Plots beginning in 2010.** Oak Ridge National Laboratory, TES SFA, U.S. Department of Energy, Oak Ridge, Tennessee, U.S.A. https://doi.org/10.25581/spruce.052/1433837
  - Hanson, Paul J, Jana R Phillips, Stan D Wullschleger, W Robert Nettles, Jeffrey M Warren, Eric J Ward, Jake D Graham, and Thomas A Ruggles. 2018. **SPRUCE Tree Growth Assessments of *Picea* and *Larix* in S1-Bog Plots and SPRUCE Experimental Plots beginning in 2011.** Oak Ridge National Laboratory, TES SFA, U.S. Department of Energy, Oak Ridge, Tennessee, U.S.A. https://doi.org/10.25581/spruce.051/1433836
  - Malhotra, A., D.J. Brice, J. Childs, H.M. Vander Stel, S.E. Bellaire, E. Kraeske, S.M. Letourneau, L. Owens, L.M. Rasnake, C.M. Iversen. 2020. **SPRUCE Production and Chemistry of Newly-Grown Fine Roots Assessed Using Root Ingrowth Cores in SPRUCE Experimental Plots beginning in 2014**. Oak Ridge National Laboratory, TES SFA, U.S. Department of Energy, Oak Ridge, Tennessee, U.S.A. https://doi.org/10.25581/spruce.077/1607860
  - Norby RJ, Childs J. 2018. **SPRUCE: *Sphagnum* Productivity and Community Composition in the SPRUCE Experimental Plots.** Oak Ridge National Laboratory, TES SFA, U.S. Department of Energy, Oak Ridge, Tennessee, U.S.A. https://doi.org/10.25581/spruce.049/1426474
  - Stelling, JM, MA Mayes, PJ Hanson, and M Krassovski. 2024. **SPRUCE: Carbon Dioxide and Methane Soil Flux Measurements at High Temporal Resolution, Beginning in 2022**. 2024. Oak Ridge National Laboratory, TES SFA, U.S. Department of Energy, Oak Ridge, Tennessee, U.S.A. https://doi.org/10.25581/spruce.104/1922635
- Pore-water chemistry:
  - Griffiths, N. A., S.D. Sebestyen, K.C. Oleheiser, J.M. Stelling, C.E. Pierce, E.A. Nater, B.M. Toner, & R.K. Kolka. 2016. **SPRUCE Porewater Chemistry Data for Experimental Plots, Beginning in 2013, Version 4**. Oak Ridge National Laboratory, TES SFA, US Department of Energy, Oak Ridge, Tennessee, USA. https://doi.org/10.3334/CDIAC/spruce.028
- Resin-exchange measurements:
  - Iversen CM, Latimer J, Burnham A, Brice DJ, Childs J, Vander Stel HM, Schwaner GW, Weber SE. 2017. **SPRUCE Plant-Available Nutrients Assessed with Ion-Exchange Resins in Experimental Plots, Beginning in 2013.** Oak Ridge National Laboratory, TES SFA, U.S. Department of Energy, Oak Ridge, Tennessee, U.S.A. http://dx.doi.org/10.3334/CDIAC/spruce.036
- Ectomycorrhizal colonization of tree root tips:
  - Duchesneau, K, CE Defrenne, C Petro, A Malhotra, JAM Moore, J Childs, PJ Hanson, CM Iversen, and JE Kostka. 2024. **SPRUCE Root Tip and Ectomycorrhizal Fungi Colonization Measurements from Ingrowth Cores, 2017**. Oak Ridge National Laboratory, TES SFA, U.S. Department of Energy, Oak Ridge, Tennessee, U.S.A. https://doi.org/10.25581/spruce.119/2476173

## 7 Author contribution

Y.W., D.M.R., and J. M. co-conceived the research. Y.W. performed model development, simulations, and analysis. D. M. R. helped with model simulations and sensitivity analysis. S.E.W., V.S., X. Y., N. A. G., P. J. H., A. P. W., J. S., K. D., C. E. D., J. M. W., S. D. S., K.J. P., K. O., J. B., M. G., and M. B. K. provided observational data and helped with their correct usage

Deleted: Ingrowth cores:

Formatted: Font: Bold

Deleted: Moss NPP data:

Formatted: Font: Bold

Deleted: and

and interpretation. J. M., D. M. R., P. H., M. A. M., and P. T. obtained funding. All authors contributed to results interpretation and manuscript writing.

## 8 Competing interests

There is no competing interest.

## 9 Acknowledgements

This study was conducted as a part of the Oak Ridge National Laboratory (ORNL) Terrestrial Ecosystem Sciences Scientific Focus Area which is funded by the U.S. Department of Energy (DOE) Office of Biological and Environmental Research, Environmental Systems Science program. ORNL is managed by UT-Battelle, LLC, for the U.S. DOE under contract DE-AC05-1008 00OR22725. The simulations and data analysis were conducted using the cades-baseline supercomputer, which is part of the Oak Ridge Leadership Facility. The contributions of S. D. S. were funded by the U.S. Department of Agriculture Forest Service Northern Research Station. The corresponding authors thank Colleen M. Iversen for providing the resin-exchange dataset and for facilitating connections with some of the coauthors. ChatGPT was used to improve language.

## 10 References

Bashian-Victoroff, C., Yanai, R. D., Horton, T. R., and Lamit, L. J.: Nitrogen and phosphorus additions affect fruiting of ectomycorrhizal fungi in a temperate hardwood forest, Fungal Ecol., 73, 101388, https://doi.org/10.1016/j.funeco.2024.101388, 2025.

Bastrikov, V., MacBean, N., Bacour, C., Santaren, D., Kuppel, S., and Peylin, P.: Land surface model parameter optimisation using in situ flux data: comparison of gradient-based versus random search algorithms (a case study using ORCHIDEE v1.9.5.2), Geosci. Model Dev., 11, 4739–4754, https://doi.org/10.5194/gmd-11-4739-2018, 2018.

Basu, N. B., Destouni, G., Jawitz, J. W., Thompson, S. E., Loukinova, N. V., Darracq, A., Zanardo, S., Yaeger, M., Sivapalan, M., Rinaldo, A., and Rao, P. S. C.: Nutrient loads exported from managed catchments reveal emergent biogeochemical stationarity, Geophys. Res. Lett., 37, https://doi.org/10.1029/2010GL045168, 2010.

Bergmann, J., Weigelt, A., van der Plas, F., Laughlin, D. C., Kuyper, T. W., Guerrero-Ramirez, N., Valverde-Barrantes, O. J., Bruelheide, H., Freschet, G. T., Iversen, C. M., Kattge, J., McCormack, M. L., Meier, I. C., Rillig, M. C., Roumet, C., Semchenko, M., Sweeney, C. J., van Ruijven, J., York, L. M., and Mommer, L.: The fungal collaboration gradient dominates the root economics space in plants, Sci. Adv., 6, eaba3756, https://doi.org/10.1126/sciadv.aba3756, 2020.

Bogar, L. M., Tavasieff, O. S., Raab, T. K., and Peay, K. G.: Does resource exchange in ectomycorrhizal symbiosis vary with competitive context and nitrogen addition?, New Phytol., 233, 1331–1344, https://doi.org/10.1111/nph.17871, 2022.

Braghiere, R. K., Fisher, J. B., Allen, K., Brzostek, E., Shi, M., Yang, X., Ricciuto, D. M., Fisher, R. A., Zhu, Q., and Phillips, R. P.: Modeling Global Carbon Costs of Plant Nitrogen and Phosphorus Acquisition, J. Adv. Model. Earth Syst., 14, e2022MS003204, https://doi.org/10.1029/2022MS003204, 2022.

Brient, F.: Reducing uncertainties in climate projections with emergent constraints: concepts, examples and prospects, Adv. Atmospheric Sci., 37, 1–15, https://doi.org/10.1007/s00376-019-9140-8, 2020.

Brzostek, E. R., Fisher, J. B., and Phillips, R. P.: Modeling the carbon cost of plant nitrogen acquisition: Mycorrhizal trade-offs and multipath resistance uptake improve predictions of retranslocation, J. Geophys. Res. Biogeosciences, 119, 1684–1697, https://doi.org/10.1002/2014JG002660, 2014.

Bunn, R. A., Corrêa, A., Joshi, J., Kaiser, C., Lekberg, Y., Prescott, C. E., Sala, A., and Karst, J.: What determines transfer of carbon from plants to mycorrhizal fungi?, New Phytol., 244, 1199–1215, https://doi.org/10.1111/nph.20145, 2024.

Burrows, S. M., Maltrud, M., Yang, X., Zhu, Q., Jeffery, N., Shi, X., Ricciuto, D., Wang, S., Bisht, G., Tang, J., Wolfe, J., Harrop, B. E., Singh, B., Brent, L., Baldwin, S., Zhou, T., Cameron-Smith, P., Keen, N., Collier, N., Xu, M., Hunke, E. C., Elliott, S. M., Turner, A. K., Li, H., Wang, H., Golaz, J. -C., Bond-Lamberty, B., Hoffman, F. M., Riley, W. J., Thornton, P. E., Calvin, K., and Leung, L. R.: The DOE E3SM v1.1 biogeochemistry configuration: Description and simulated ecosystem-climate responses to historical changes in forcing, J. Adv. Model. Earth Syst., 12, https://doi.org/10.1029/2019MS001766, 2020.

Carrell, A. A., Kolton, M., Glass, J. B., Pelletier, D. A., Warren, M. J., Kostka, J. E., Iversen, C. M., Hanson, P. J., and Weston, D. J.: Experimental warming alters the community composition, diversity, and N2 fixation activity of peat moss (Sphagnum fallax) microbiomes, Glob. Change Biol., 25, 2993–3004, https://doi.org/10.1111/gcb.14715, 2019.

Craig, M. E., Walker, A. P., Iversen, C. M., Knox, R. G., Yaffar, D., and York, L. M.: Tree root nutrient uptake kinetics vary with nutrient availability, environmental conditions, and root traits: a global analysis, New Phytol., 246, 2495–2505, https://doi.org/10.1111/nph.70140, 2025.

Defrenne, C. E., Childs, J., Fernandez, C. W., Taggart, M., Nettles, W. R., Allen, M. F., Hanson, P. J., and Iversen, C. M.: High-resolution minirhizotrons advance our understanding of root-fungal dynamics in an experimentally warmed peatland, Plants People Planet, 3, 640–652, https://doi.org/10.1002/ppp3.10172, 2021.

DeGroot, M. and Schervish, M.: Probability and statistics, 4th ed., Pearson, 912 pp., 2018.

Dise, N. B.: Peatland Response to Global Change, Science, 326, 810–811, https://doi.org/10.1126/science.1174268, 2009.

Drewniak, B. A.: Simulating dynamic roots in the Energy Exascale Earth System Land Model, J. Adv. Model. Earth Syst., 11, 338–359, https://doi.org/10.1029/2018MS001334, 2019.

Du, E., Terrer, C., Pellegrini, A. F. A., Ahlström, A., van Lissa, C. J., Zhao, X., Xia, N., Wu, X., and Jackson, R. B.: Global patterns of terrestrial nitrogen and phosphorus limitation, Nat. Geosci., 13, 221–226, https://doi.org/10.1038/s41561-019-0530-4, 2020.

Duchesneau, K., Defrenne, C. E., Petro, C., Malhotra, A., Moore, J. A. M., Childs, J., Hanson, P. J., Iversen, C. M., and Kostka, J. E.: Responses of vascular plant fine roots and associated microbial communities to whole-ecosystem warming and elevated CO2 in northern peatlands, New Phytol., 242, 1333–1347, https://doi.org/10.1111/nph.19690, 2024.

Dusenge, M. E., Warren, J. M., Reich, P. B., Ward, E. J., Murphy, B. K., Stefanski, A., Bermudez, R., Cruz, M., McLennan, D. A., King, A. W., Montgomery, R. A., Hanson, P. J., and Way, D. A.: Photosynthetic capacity in middle-aged larch and spruce acclimates independently to experimental warming and elevated CO2, Plant Cell Environ., 47, 4886–4902, https://doi.org/10.1111/pce.15068, 2024.

Egerton-Warburton, L. M., Querejeta, J. I., Allen, M. F., and Finkelman, S. L.: Mycorrhizal Fungi, in: Reference Module in Earth Systems and Environmental Sciences, Elsevier, B978012409548905226X, https://doi.org/10.1016/B978-0-12-409548-9.05226-X, 2013.

Eick, M. J., Brady, W. D., and Lynch, C. K.: Charge Properties and Nitrate Adsorption of Some Acid Southeastern Soils, J. Environ. Qual., 28, 138–144, https://doi.org/10.2134/jeq1999.00472425002800010016x, 1999.

Fanin, N., Clemmensen, K. E., Lindahl, B. D., Farrell, M., Nilsson, M.-C., Gundale, M. J., Kardol, P., and Wardle, D. A.: Ericoid shrubs shape fungal communities and suppress organic matter decomposition in boreal forests, New Phytol., 236, 684–697, https://doi.org/10.1111/nph.18353, 2022.

Fernandez, C. W. and Kennedy, P. G.: Revisiting the 'Gadgil effect': do interguild fungal interactions control carbon cycling in forest soils?, New Phytol., 209, 1382–1394, https://doi.org/10.1111/nph.13648, 2016.

Fernandez, C. W., Heckman, K., Kolka, R., and Kennedy, P. G.: Melanin mitigates the accelerated decay of mycorrhizal necromass with peatland warming, Ecol. Lett., 22, 498–505, https://doi.org/10.1111/ele.13209, 2019.

Friedlingstein, P., O'Sullivan, M., Jones, M. W., Andrew, R. M., Gregor, L., Hauck, J., Le Quéré, C., Luijkx, I. T., Olsen, A., Peters, G. P., Peters, W., Pongratz, J., Schwingshackl, C., Sitch, S., Canadell, J. G., Ciais, P., Jackson, R. B., Alin, S. R., Alkama, R., Arneth, A., Arora, V. K., Bates, N. R., Becker, M., Bellouin, N., Bittig, H. C., Bopp, L., Chevallier, F., Chini, L. P., Cronin, M., Evans, W., Falk, S., Feely, R. A., Gasser, T., Gehlen, M., Gkritzalis, T., Gloege, L., Grassi, G., Gruber, N., Gürses, Ö., Harris, I., Hefner, M., Houghton, R. A., Hurtt, G. C., Iida, Y., Ilyina, T., Jain, A. K., Jersild, A., Kadono, K., Kato, E., Kennedy, D., Klein Goldewijk, K., Knauer, J., Korsbakken, J. I., Landschützer, P., Lefèvre, N., Lindsay, K., Liu, J., Liu, Z., Marland, G., Mayot, N., McGrath, M. J., Metzl, N., Monacci, N. M., Munro, D. R., Nakaoka, S.-I., Niwa, Y., O'Brien, K., Ono, T., Palmer, P. I., Pan, N., Pierrot, D., Pocock, K., Poulter, B., Resplandy, L., Robertson, E., Rödenbeck, C., Rodriguez, C., Rosan, T. M., Schwinger, J., Séférian, R., Shutler, J. D., Skjelvan, I., Steinhoff, T., Sun, Q., Sutton, A. J., Sweeney, C., Takao, S., Tanhua, T., Tans, P. P., Tian, X., Tian, H., Tilbrook, B., Tsujino, H., Tubiello, F., Van Der Werf, G. R., Walker, A. P., Wanninkhof, R., Whitehead, C., Willstrand Wranne, A., et al.: Global Carbon Budget 2022, Earth Syst. Sci. Data, 14, 4811–4900, https://doi.org/10.5194/essd-14-4811-2022, 2022.

Frolking, S., Roulet, N. T., Moore, T. R., Lafleur, P. M., Bubier, J. L., and Crill, P. M.: Modeling seasonal to annual carbon balance of Mer Bleue Bog, Ontario, Canada, Glob. Biogeochem. Cycles, 16, 4-1-4–21, https://doi.org/10.1029/2001GB001457, 2002.

Frolking, S., Talbot, J., Jones, M. C., Treat, C. C., Kauffman, J. B., Tuittila, E.-S., and Roulet, N.: Peatlands in the Earth's 21st century climate system, Environ. Rev., 19, 371–396, https://doi.org/10.1139/a11-014, 2011.

Garcia, K., Delaux, P.-M., Cope, K. R., and Ané, J.-M.: Molecular signals required for the establishment and maintenance of ectomycorrhizal symbioses, New Phytol., 208, 79–87, https://doi.org/10.1111/nph.13423, 2015.

Glass, A. D. M., Britto, D. T., Kaiser, B. N., Kinghorn, J. R., Kronzucker, H. J., Kumar, A., Okamoto, M., Rawat, S., Siddiqi, M. Y., Unkles, S. E., and Vidmar, J. J.: The regulation of nitrate and ammonium transport systems in plants, J. Exp. Bot., 53, 855–864, https://doi.org/10.1093/jexbot/53.370.855, 2002.

Graham, J. D., Glenn, N. F., Spaete, L. P., and Hanson, P. J.: Characterizing Peatland Microtopography Using Gradient and Microform-Based Approaches, Ecosystems, 23, 1464–1480, https://doi.org/10.1007/s10021-020-00481-z, 2020.

Griffiths, M. and York, L. M.: Targeting Root Ion Uptake Kinetics to Increase Plant Productivity and Nutrient Use Efficiency, Plant Physiol., 182, 1854–1868, https://doi.org/10.1104/pp.19.01496, 2020.

Griffiths, N. A. and Sebestyen, S. D.: Dynamic Vertical Profiles of Peat Porewater Chemistry in a Northern Peatland, Wetlands, 36, 1119–1130, https://doi.org/10.1007/s13157-016-0829-5, 2016.

Griffiths, N. A., Sebestyen, S. D., Oleheiser, K. C., Stelling, J. M., Pierce, C. E., Nater, E. A., Toner, B. M., and Kolka, R. K.: SPRUCE porewater chemistry data for experimental plots, beginning in 2013, version 4, Oak Ridge National Laboratory, TES SFA, US Department of Energy, Oak Ridge, Tennessee, USA, https://doi.org/10.3334/CDIAC/spruce.028, 2016.

Griffiths, N. A., Hanson, P. J., Ricciuto, D. M., Iversen, C. M., Jensen, A. M., Malhotra, A., McFarlane, K. J., Norby, R. J., Sargsyan, K., Sebestyen, S. D., Shi, X., Walker, A. P., Ward, E. J., Warren, J. M., and Weston, D. J.: Temporal and Spatial Variation in Peatland Carbon Cycling and Implications for Interpreting Responses of an Ecosystem-Scale Warming Experiment, Soil Sci. Soc. Am. J., 81, 1668–1688, https://doi.org/10.2136/sssaj2016.12.0422, 2017.

Hanson, P. J., Gill, A. L., Xu, X., Phillips, J. R., Weston, D. J., Kolka, R. K., Riggs, J. S., and Hook, L. A.: Intermediate-scale community-level flux of CO2 and CH4 in a Minnesota peatland: putting the SPRUCE project in a global context, Biogeochemistry, 129, 255–272, https://doi.org/10.1007/s10533-016-0230-8, 2016a.

Hanson, P. J., Riggs, J. S., Nettles, W. R., Krassovski, M. B., and Hook, L. A.: SPRUCE whole ecosystems warming (WEW) environmental data beginning august 2015, Oak Ridge National Laboratory, TES SFA, U.S. Department of Energy, Oak Ridge, Tennessee, U.S.A., https://doi.org/10.3334/CDIAC/spruce.032, 2016b.

Hanson, P. J., Riggs, J. S., Nettles, W. R., Phillips, J. R., Krassovski, M. B., Hook, L. A., Gu, L., Richardson, A. D., Aubrecht, D. M., Ricciuto, D. M., Warren, J. M., and Barbier, C.: Attaining whole-ecosystem warming using air and deep-soil heating methods with an elevated $CO_2$ atmosphere, Biogeosciences, 14, 861–883, https://doi.org/10.5194/bg-14-861-2017, 2017.

Hanson, P. J., Phillips, J. R., Brice, D. J., and Hook, L. A.: SPRUCE shrub-layer growth assessments in S1-bog plots and SPRUCE experimental plots beginning in 2010, Oak Ridge National Laboratory, TES SFA, U.S. Department of Energy, Oak Ridge, Tennessee, U.S.A., https://doi.org/10.25581/spruce.052/1433837, 2018a.

Hanson, P. J., Phillips, J. R., Wullschleger, S. D., Nettles, W. R., Warren, J. M., Ward, E. J., Graham, J. D., and Ruggles, T. A.: SPRUCE tree growth assessments of *Picea* and *Larix* in S1-bog plots and SPRUCE experimental plots beginning in 2011, Oak Ridge National Laboratory, TES SFA, U.S. Department of Energy, Oak Ridge, Tennessee, U.S.A., https://doi.org/10.25581/spruce.051/1433836, 2018b.

Hanson, P. J., Griffiths, N. A., Iversen, C. M., Norby, R. J., Sebestyen, S. D., Phillips, J. R., Chanton, J. P., Kolka, R. K., Malhotra, A., Oleheiser, K. C., Warren, J. M., Shi, X., Yang, X., Mao, J., and Ricciuto, D. M.: Rapid net carbon loss from a whole-ecosystem warmed peatland, AGU Adv., 1, https://doi.org/10.1029/2020AV000163, 2020a.

Hanson, P. J., Phillips, J. R., Nettles, W. R., Pearson, K. J., and Hook, L. A.: SPRUCE plot-level water table data assessments for absolute elevations and height with respect to mean hollows beginning in 2015, Oak Ridge National Laboratory, TES SFA, U.S. Department of Energy, Oak Ridge, Tennessee, U.S.A., https://doi.org/10.25581/spruce.079/1608615, 2020b.

Hanson, P. J., Griffiths, N. A., Salmon, V. G., Birkebak, J. M., Warren, J. M., Phillips, J. R., Guilliams, M. P., Oleheiser, K. C., Jones, M. W., Jones, N. J., Enterkine, J., Glenn, N. F., and Pearson, K. J.: Peatland Plant Community Changes in Annual Production and Composition Through 8 Years of Warming Manipulations Under Ambient and Elevated $CO_2$ Atmospheres, J. Geophys. Res. Biogeosciences, 130, e2024JG008511, https://doi.org/10.1029/2024JG008511, 2025.

Hawkins, H.-J., Cargill, R. I. M., Van Nuland, M. E., Hagen, S. C., Field, K. J., Sheldrake, M., Soudzilovskaia, N. A., and Kiers, E. T.: Mycorrhizal mycelium as a global carbon pool, Curr. Biol., 33, R560–R573, https://doi.org/10.1016/j.cub.2023.02.027, 2023.

He, H., Meyer, A., Jansson, P.-E., Svensson, M., Rütting, T., and Klemedtsson, L.: Simulating ectomycorrhiza in boreal forests: implementing ectomycorrhizal fungi model MYCOFON in CoupModel (v5), Geosci. Model Dev., 11, 725–751, https://doi.org/10.5194/gmd-11-725-2018, 2018.

He, H., Jansson, P.-E., and Gärdenäs, A. I.: CoupModel (v6.0): an ecosystem model for coupled phosphorus, nitrogen, and carbon dynamics – evaluated against empirical data from a climatic and fertility gradient in Sweden, Geosci. Model Dev., 14, 735–761, https://doi.org/10.5194/gmd-14-735-2021, 2021.

Hilman, B., Solly, E. F., Kuhlmann, I., Brunner, I., and Hagedorn, F.: Species-specific reliance of trees on ectomycorrhizal fungi for nitrogen supply at an alpine treeline, Fungal Ecol., 71, 101361, https://doi.org/10.1016/j.funeco.2024.101361, 2024.

Hobbie, J. E. and Hobbie, E. A.: $^{15}$N in Symbiotic Fungi and Plants Estimates Nitrogen and Carbon Flux Rates in Arctic Tundra, Ecology, 87, 816–822, https://doi.org/10.1890/0012-9658(2006)87%5B816:NISFAP%5D2.0.CO;2, 2006.

Högberg, M. N., Briones, M. J. I., Keel, S. G., Metcalfe, D. B., Campbell, C., Midwood, A. J., Thornton, B., Hurry, V., Linder, S., Näsholm, T., and Högberg, P.: Quantification of effects of season and nitrogen supply on tree below-ground carbon transfer to ectomycorrhizal fungi and other soil organisms in a boreal pine forest, New Phytol., 187, 485–493, https://doi.org/10.1111/j.1469-8137.2010.03274.x, 2010.

Ito, A., Reyer, C. P. O., Gädeke, A., Ciais, P., Chang, J., Chen, M., François, L., Forrest, M., Hickler, T., Ostberg, S., Shi, H., Thiery, W., and Tian, H.: Pronounced and unavoidable impacts of low-end global warming on northern high-latitude land ecosystems, Environ. Res. Lett., 15, 044006, https://doi.org/10.1088/1748-9326/ab702b, 2020.

Iversen, C. M., Latimer, J., Burnham, A., Brice, D. J., Childs, J., Vander Stel, H. M., Schwaner, G. W., and Weber, S. E.: SPRUCE plant-available nutrients assessed with ion-exchange resins in experimental plots, beginning in 2013, Oak Ridge National Laboratory, TES SFA, U.S. Department of Energy, Oak Ridge, Tennessee, U.S.A., https://doi.org/10.3334/CDIAC/spruce.036, 2017a.

Iversen, C. M., Garrett, A., Martin, A., Turetsky, M. R., Norby, R. J., Childs, J., and Ontl, T. A.: SPRUCE S1 Bog Tree Basal Area and Understory Community Composition Assessed in the Southern and Northern Ends of the S1 Bog, Carbon Dioxide Information Analysis Center, Oak Ridge National Laboratory, U.S. Department of Energy, Oak Ridge, Tennessee, U.S.A., https://doi.org/10.3334/CDIAC/spruce.024, 2017b.

Iversen, C. M., McCormack, M. L., Baer, J. K., Powell, A. S., Chen, W., Collins, C., Fan, Y., Fanin, N., Freschet, G. T., Guo, D., Hogan, J. A., Kou, L., Laughlin, D. C., Lavely, E., Liese, R., Lin, D., Meier, I. C., Montagnoli, A., Roumet, C., See, C. R., Soper, F., Terzaghi, M., Valverde-Barrantes, O. J., Wang, C., Wright, S. J., Wurzburger, N., and Zadworny, M.: Fine-root ecology database (FRED): a global collection of root trait data with coincident site, vegetation, edaphic, and climatic data, version 3, 2021a.

Iversen, C. M., Brice, D. J., Childs, J., Vander Stel, H. M., and Salmon, V. G.: SPRUCE S1 bog production of newly-grown fine roots assessed using root ingrowth cores in 2013, , https://doi.org/10.25581/spruce.091/1782483, 2021b.

Iversen, C. M., Latimer, J., Brice, D. J., Childs, J., Vander Stel, H. M., Defrenne, C. E., Graham, J., Griffiths, N. A., Malhotra, A., Norby, R. J., Oleheiser, K. C., Phillips, J. R., Salmon, V. G., Sebestyen, S. D., Yang, X., and Hanson, P. J.: Whole-ecosystem warming increases plant-available nitrogen and phosphorus in an ombrotrophic bog, Ecosystems, https://doi.org/10.1007/s10021-022-00744-x, 2022.

Jensen, A. M., Warren, J. M., King, A. W., Ricciuto, D. M., Hanson, P. J., and Wullschleger, S. D.: Simulated projections of boreal forest peatland ecosystem productivity are sensitive to observed seasonality in leaf physiology†, Tree Physiol., 39, 556–572, https://doi.org/10.1093/treephys/tpy140, 2019.

Kennedy, P. G., Mielke, L. A., and Nguyen, N. H.: Ecological responses to forest age, habitat, and host vary by mycorrhizal type in boreal peatlands, Mycorrhiza, 28, 315–328, https://doi.org/10.1007/s00572-018-0821-4, 2018.

Knox, R. G., Koven, C. D., Riley, W. J., Walker, A. P., Wright, S. J., Holm, J. A., Wei, X., Fisher, R. A., Zhu, Q., Tang, J., Ricciuto, D. M., Shuman, J. K., Yang, X., Kueppers, L. M., and Chambers, J. Q.: Nutrient Dynamics in a Coupled Terrestrial Biosphere and Land Model (ELM-FATES-CNP), J. Adv. Model. Earth Syst., 16, e2023MS003689, https://doi.org/10.1029/2023MS003689, 2024.

Kolka, R., Sebestyen, S., Verry, E. S., and Brooks, K. (Eds.): SPRUCE S1 Bog Tree Basal Area and Understory Community Composition Assessed in the Southern and Northern Ends of the S1 BogSPRUCE S1 Bog Tree Basal Area and Understory Community Composition Assessed in the Southern and Northern Ends of the S1 BogPeatland Biogeochemistry and Watershed Hydrology at the Marcell Experimental Forest, CRC Press, Boca Raton, FL, 512 pp., 2011.

Lavallee, J. M., Soong, J. L., and Cotrufo, M. F.: Conceptualizing soil organic matter into particulate and mineral-associated forms to address global change in the 21st century, Glob. Change Biol., 26, 261–273, https://doi.org/10.1111/gcb.14859, 2020.

Loisel, J., Van Bellen, S., Pelletier, L., Talbot, J., Hugelius, G., Karran, D., Yu, Z., Nichols, J., and Holmquist, J.: Insights and issues with estimating northern peatland carbon stocks and fluxes since the Last Glacial Maximum, Earth-Sci. Rev., 165, 59–80, https://doi.org/10.1016/j.earscirev.2016.12.001, 2017.

Ma, R., Zhang, Y., Ciais, P., Xiao, J., Xu, Y., Goll, D., and Liang, S.: Stepwise Calibration of Age-Dependent Biomass in the Integrated Biosphere Simulator (IBIS) Model, J. Adv. Model. Earth Syst., 16, e2023MS004048, https://doi.org/10.1029/2023MS004048, 2024.

Mäkelä, A., Tian, X., Repo, A., Ilvesniemi, H., Marshall, J., Minunno, F., Näsholm, T., Schiestl-Aalto, P., and Lehtonen, A.: Do mycorrhizal symbionts drive latitudinal trends in photosynthetic carbon use efficiency and carbon sequestration in boreal forests?, For. Ecol. Manag., 520, 120355, https://doi.org/10.1016/j.foreco.2022.120355, 2022.

Malhotra, A., Brice, D. J., Childs, J., Graham, J. D., Hobbie, E. A., Vander Stel, H., Feron, S. C., Hanson, P. J., and Iversen, C. M.: Peatland warming strongly increases fine-root growth, Proc. Natl. Acad. Sci., 117, 17627–17634, https://doi.org/10.1073/pnas.2003361117, 2020a.

Malhotra, A., Brice, D. J., Childs, J., Vander Stel, H. M., Bellaire, S. E., Kraeske, E., Letourneau, S. M., Owens, L., Rasnake, L. M., and Iversen, C. M.: SPRUCE Production and Chemistry of Newly-Grown Fine Roots Assessed Using Root Ingrowth Cores in SPRUCE Experimental Plots beginning in 2014, Oak Ridge National Laboratory, TES SFA, U.S. Department of Energy, Oak Ridge, Tennessee, U.S.A., https://doi.org/10.25581/spruce.077/1607860, 2020b.

Matschonat, G. and Matzner, E.: Soil chemical properties affecting NH4+ sorption in forest soils, Z. Für Pflanzenernähr. Bodenkd., 159, 505–511, https://doi.org/10.1002/jpln.1996.3581590514, 1996.

McFarlane, K. J., Hanson, P. J., Iversen, C. M., Phillips, J. R., and Brice, D. J.: Local Spatial Heterogeneity of Holocene Carbon Accumulation throughout the Peat Profile of an Ombrotrophic Northern Minnesota Bog, Radiocarbon, 60, 941–962, https://doi.org/10.1017/RDC.2018.37, 2018.

McPartland, M. Y., Kane, E. S., Falkowski, M. J., Kolka, R., Turetsky, M. R., Palik, B., and Montgomery, R. A.: SPRUCE: LAI data from SPRUCE experimental plots, 2017-2019, Oak Ridge National Laboratory, TES SFA, U.S. Department of Energy, Oak Ridge, Tennessee, U.S.A., https://doi.org/10.25581/spruce.058/1491566, 2019.

Meng, L., Mao, J., Ricciuto, D. M., Shi, X., Richardson, A. D., Hanson, P. J., Warren, J. M., Zhou, Y., Li, X., Zhang, L., and Schädel, C.: Evaluation and modification of ELM seasonal deciduous phenology against observations in a southern boreal peatland forest, Agric. For. Meteorol., 308–309, 108556, https://doi.org/10.1016/j.agrformet.2021.108556, 2021.

Mielke, L. A.: Mycorrhizal guild functions and conservational values in boreal forests, Swedish University of Agricultural Sciences, Uppsala, Sweden, 107 pp., https://doi.org/10.54612/a.75ms1inoet, 2022.

Näsholm, T., Kielland, K., and Ganeteg, U.: Uptake of organic nitrogen by plants, New Phytol., 182, 31–48, https://doi.org/10.1111/j.1469-8137.2008.02751.x, 2009.

Norby, R. J. and Childs, J.: SPRUCE: Sphagnum Productivity and Community Composition in the SPRUCE Experimental Plots, , https://doi.org/10.25581/spruce.049/1426474, 2018.

Norby, R. J., Warren, J. M., Iversen, C. M., Medlyn, B. E., and McMurtrie, R. E.: CO2 enhancement of forest productivity constrained by limited nitrogen availability, Proc. Natl. Acad. Sci., 107, 19368–19373, https://doi.org/10.1073/pnas.1006463107, 2010.

Norby, R. J., Childs, J., Hanson, P. J., and Warren, J. M.: Rapid loss of an ecosystem engineer: *Sphagnum* decline in an experimentally warmed bog, Ecol. Evol., 9, 12571–12585, https://doi.org/10.1002/ece3.5722, 2019.

Norby, R. J., Loader, N. J., Mayoral, C., Ullah, S., Curioni, G., Smith, A. R., Reay, M. K., van Wijngaarden, K., Amjad, M. S., Brettle, D., Crockatt, M. E., Denny, G., Grzesik, R. T., Hamilton, R. L., Hart, K. M., Hartley, I. P., Jones, A. G., Kourmouli, A., Larsen, J. R., Shi, Z., Thomas, R. M., and MacKenzie, A. R.: Enhanced woody biomass production in a mature temperate forest under elevated CO2, Nat. Clim. Change, 14, 983–988, https://doi.org/10.1038/s41558-024-02090-3, 2024.

Oleson, K. W., Lawrence, D. M., Bonan, G. B., Drewniak, B., Huang, M., Levis, S., Li, F., Riley, W. J., Swenson, S. C., Thornton, P. E., Bozbiyik, A., Fisher, R., Heald, C. L., Kluzek, E., Lamarque, F., Lawrence, P. J., Leung, L. R., Muszala, S., Ricciuto, D. M., Sacks, W., Sun, Y., Tang, J., and Yang, Z.-L.: Technical Description of version 4.5 of the Community Land Model (CLM), National Center for Atmospheric Research, Boulder, CO, USA, 2013a.

Oleson, K. W., Lawrence, D. M., Bonan, G. B., Drewniak, B., Huang, M., Levis, S., Li, F., Riley, W. J., Swenson, S. C., Thornton, P. E., Bozbiyik, A., Fisher, R., Heald, C. L., Kluzek, E., Lamarque, F., Lawrence, P. J., Leung, L. R., Muszala, S., Ricciuto, D. M., Sacks, W., Sun, Y., Tang, J., and Yang, Z.-L.: Technical Description of version 4.5 of the Community Land Model (CLM), National Center for Atmospheric Research, Boulder, CO, USA, 2013b.

Ostonen, I., Helmisaari, H., Borken, W., Tedersoo, L., Kukumägi, M., Bahram, M., Lindroos, A., Nöjd, P., Uri, V., Merilä, P., Asi, E., and Lõhmus, K.: Fine root foraging strategies in Norway spruce forests across a European climate gradient, Glob. Change Biol., 17, 3620–3632, https://doi.org/10.1111/j.1365-2486.2011.02501.x, 2011.

Ostonen, I., Truu, M., Helmisaari, H., Lukac, M., Borken, W., Vanguelova, E., Godbold, D. L., Lõhmus, K., Zang, U., Tedersoo, L., Preem, J., Rosenvald, K., Aosaar, J., Armolaitis, K., Frey, J., Kabral, N., Kukumägi, M., Leppälammi-Kujansuu, J., Lindroos, A., Merilä, P., Napa, Ü., Nöjd, P., Parts, K., Uri, V., Varik, M., and Truu, J.: Adaptive root foraging strategies along a boreal–temperate forest gradient, New Phytol., 215, 977–991, https://doi.org/10.1111/nph.14643, 2017.

Palmroth, S., Oren, R., McCarthy, H. R., Johnsen, K. H., Finzi, A. C., Butnor, J. R., Ryan, M. G., and Schlesinger, W. H.: Aboveground sink strength in forests controls the allocation of carbon below ground and its [CO2]-induced enhancement, Proc. Natl. Acad. Sci., 103, 19362–19367, https://doi.org/10.1073/pnas.0609492103, 2006.

Petro, C., Carrell, A. A., Wilson, R. M., Duchesneau, K., Noble-Kuchera, S., Song, T., Iversen, C. M., Childs, J., Schwaner, G., Chanton, J. P., Norby, R. J., Hanson, P. J., Glass, J. B., Weston, D. J., and Kostka, J. E.: Climate drivers alter nitrogen

availability in surface peat and decouple N2 fixation from CH4 oxidation in the Sphagnum moss microbiome, Glob. Change Biol., 29, 3159–3176, https://doi.org/10.1111/gcb.16651, 2023.

Plassard, C. and Dell, B.: Phosphorus nutrition of mycorrhizal trees, Tree Physiol., 30, 1129–1139, https://doi.org/10.1093/treephys/tpq063, 2010.

Plassard, C., Louche, J., Ali, M. A., Duchemin, M., Legname, E., and Cloutier-Hurteau, B.: Diversity in phosphorus mobilisation and uptake in ectomycorrhizal fungi, Ann. For. Sci., 68, 33–43, https://doi.org/10.1007/s13595-010-0005-7, 2011.

Raue, A., Kreutz, C., Maiwald, T., Bachmann, J., Schilling, M., Klingmüller, U., and Timmer, J.: Structural and practical identifiability analysis of partially observed dynamical models by exploiting the profile likelihood, Bioinformatics, 25, 1923–1929, https://doi.org/10.1093/bioinformatics/btp358, 2009.

Rehschuh, R., Rehschuh, S., Gast, A., Jakab, A.-L., Lehmann, M. M., Saurer, M., Gessler, A., and Ruehr, N. K.: Tree allocation dynamics beyond heat and hot drought stress reveal changes in carbon storage, belowground translocation and growth, New Phytol., 233, 687–704, https://doi.org/10.1111/nph.17815, 2022.

Ricciuto, D., Sargsyan, K., and Thornton, P.: The impact of parametric uncertainties on biogeochemistry in the E3SM Land Model, J. Adv. Model. Earth Syst., 10, 297–319, https://doi.org/10.1002/2017MS000962, 2018.

Ricciuto, D. M., Xu, X., Shi, X., Wang, Y., Song, X., Schadt, C. W., Griffiths, N. A., Mao, J., Warren, J. M., Thornton, P. E., Chanton, J., Keller, J. K., Bridgham, S. D., Gutknecht, J., Sebestyen, S. D., Finzi, A., Kolka, R., and Hanson, P. J.: An Integrative Model for Soil Biogeochemistry and Methane Processes: I. Model Structure and Sensitivity Analysis, J. Geophys. Res. Biogeosciences, 126, e2019JG005468, https://doi.org/10.1029/2019JG005468, 2021.

Salmon, V. G., Brice, D. J., Bridgham, S., Childs, J., Graham, J., Griffiths, N. A., Hofmockel, K., Iversen, C. M., Jicha, T. M., Kolka, R. K., Kostka, J. E., Malhotra, A., Norby, R. J., Phillips, J. R., Ricciuto, D., Schadt, C. W., Sebestyen, S. D., Shi, X., Walker, A. P., Warren, J. M., Weston, D. J., Yang, X., and Hanson, P. J.: Nitrogen and phosphorus cycling in an ombrotrophic peatland: a benchmark for assessing change, Plant Soil, 466, 649–674, https://doi.org/10.1007/s11104-021-05065-x, 2021.

Saltelli, A., Tarantola, S., Campolongo, F., and Ratto, M.: Sensitivity Analysis in Practice: A Guide to Assessing Scientific Models, John Wiley & Sons, 2004.

Schimel, J. P. and Bennett, J.: Nitrogen Mineralization: Challenges of a Changing Paradigm, Ecology, 85, 591–602, https://doi.org/10.1890/03-8002, 2004.

Schmidt, I. K., Michelsen, A., and Jonasson, S.: Effects of labile soil carbon on nutrient partitioning between an arctic graminoid and microbes, Oecologia, 112, 557–565, https://doi.org/10.1007/s004420050345, 1997.

Shao, S., Wu, J., He, H., and Roulet, N.: Integrating McGill Wetland Model (MWM) with peat cohort tracking and microbial controls, Sci. Total Environ., 806, 151223, https://doi.org/10.1016/j.scitotenv.2021.151223, 2022.

Shao, S., Wurzburger, N., Sulman, B., and Hicks Pries, C.: Ectomycorrhizal effects on decomposition are highly dependent on fungal traits, climate, and litter properties: A model-based assessment, Soil Biol. Biochem., 184, 109073, https://doi.org/10.1016/j.soilbio.2023.109073, 2023a.

Shao, S., Wu, J., He, H., Moore, T. R., Bubier, J., Larmola, T., Juutinen, S., and Roulet, N. T.: Ericoid mycorrhizal fungi mediate the response of ombrotrophic peatlands to fertilization: a modeling study, New Phytol., 238, 80–95, https://doi.org/10.1111/nph.18555, 2023b.

Shi, M., Fisher, J. B., Brzostek, E. R., and Phillips, R. P.: Carbon cost of plant nitrogen acquisition: global carbon cycle impact from an improved plant nitrogen cycle in the Community Land Model, Glob. Change Biol., 22, 1299–1314, https://doi.org/10.1111/gcb.13131, 2016.

Shi, X., Thornton, P. E., Ricciuto, D. M., Hanson, P. J., Mao, J., Sebestyen, S. D., Griffiths, N. A., and Bisht, G.: Representing northern peatland microtopography and hydrology within the Community Land Model, Biogeosciences, 12, 6463–6477, https://doi.org/10.5194/bg-12-6463-2015, 2015.

Shi, X., Ricciuto, D. M., Thornton, P. E., Xu, X., Yuan, F., Norby, R. J., Walker, A. P., Warren, J. M., Mao, J., Hanson, P. J., Meng, L., Weston, D., and Griffiths, N. A.: Extending a land-surface model with Sphagnum moss to simulate responses of a northern temperate bog to whole ecosystem warming and elevated $CO_2$, Biogeosciences, 18, 467–486, https://doi.org/10.5194/bg-18-467-2021, 2021.

Shi, X. D., Ricciuto, D. M., Wang, Y., Melton, J., Hui, D., Shao, S., Luo, Y., Zhuang, Q., Yuan, Y., Zhou, J., Xu, X., He, H., Wu, M., Qiu, C., Akihiko, Sun, Q., Joos, F., Hussain, A., Lu, X., Dai, Y., Hao, Y., Hanson, P., Mao, J., Griffiths, N., Mayes, M., Salmon, V., and Thornton, P.: SPRUCE-MIP: A multi-model intercomparison of the carbon cycle in a northern peatland ecosystem, In preparation.

Smith, G. R. and Wan, J.: Resource-ratio theory predicts mycorrhizal control of litter decomposition, New Phytol., 223, 1595–1606, https://doi.org/10.1111/nph.15884, 2019.

Stelling, J. M., Mayes, M. A., Hanson, P. J., and Krassovski, M.: SPRUCE: Carbon Dioxide and Methane Soil Flux Measurements at High Temporal Resolution, Beginning in 2022, , https://doi.org/10.25581/spruce.104/1922635, 2024.

Sulman, B. N., Shevliakova, E., Brzostek, E. R., Kivlin, S. N., Malyshev, S., Menge, D. N. L., and Zhang, X.: Diverse Mycorrhizal Associations Enhance Terrestrial C Storage in a Global Model, Glob. Biogeochem. Cycles, 33, 501–523, https://doi.org/10.1029/2018GB005973, 2019.

Svensson, M., Jansson, P.-E., and Berggren Kleja, D.: Modelling soil C sequestration in spruce forest ecosystems along a Swedish transect based on current conditions, Biogeochemistry, 89, 95–119, https://doi.org/10.1007/s10533-007-9134-y, 2008.

Sydsaeter, K. and Hammond, P.: Mathematics for Economic Analysis, Prentice Hall, Englewood Cliffs, NJ, 173–175 pp., 1995.

Talbot, J. M. and Treseder, K. K.: Controls over mycorrhizal uptake of organic nitrogen, Pedobiologia, 53, 169–179, https://doi.org/10.1016/j.pedobi.2009.12.001, 2010.

Thornton, P. E. and Rosenbloom, N. A.: Ecosystem model spin-up: Estimating steady state conditions in a coupled terrestrial carbon and nitrogen cycle model, Ecol. Model., 189, 25–48, https://doi.org/10.1016/j.ecolmodel.2005.04.008, 2005.

Walker, A. P., Carter, K. R., Gu, L., Hanson, P. J., Malhotra, A., Norby, R. J., Sebestyen, S. D., Wullschleger, S. D., and Weston, D. J.: Biophysical drivers of seasonal variability in *Sphagnum* gross primary production in a northern temperate bog, J. Geophys. Res. Biogeosciences, 122, 1078–1097, https://doi.org/10.1002/2016JG003711, 2017.

Wang, B., McCormack, M. L., Ricciuto, D. M., Yang, X., and Iversen, C. M.: Embracing fine-root system complexity in terrestrial ecosystem modeling, Glob. Change Biol., 29, 2871–2885, https://doi.org/10.1111/gcb.16659, 2023.

Wang, Y., Mao, J., Hoffman, F. M., Bonfils, C. J. W., Douville, H., Jin, M., Thornton, P. E., Ricciuto, D. M., Shi, X., Chen, H., Wullschleger, S. D., Piao, S., and Dai, Y.: Quantification of human contribution to soil moisture–based terrestrial aridity, Nat. Commun., 13, 6848, https://doi.org/10.1038/s41467-022-34071-5, 2022.

Ward, E. B., Duguid, M. C., Kuebbing, S. E., Lendemer, J. C., and Bradford, M. A.: The functional role of ericoid mycorrhizal plants and fungi on carbon and nitrogen dynamics in forests, New Phytol., 235, 1701–1718, https://doi.org/10.1111/nph.18307, 2022.

Warren, J. M., Hanson, P. J., Iversen, C. M., Kumar, J., Walker, A. P., and Wullschleger, S. D.: Root structural and functional dynamics in terrestrial biosphere models – evaluation and recommendations, New Phytol., 205, 59–78, https://doi.org/10.1111/nph.13034, 2015.

Weber, S. E., Childs, J., Latimer, J., Hanson, P. J., Salmon, V. G., Schwaner, G., and Iversen, C. M.: Warming and elevated CO2 cause greater and deeper root growth by shrubs in a boreal bog, https://doi.org/10.1101/2025.06.26.661811, 30 June 2025.

Wu, Y. and Blodau, C.: PEATBOG: a biogeochemical model for analyzing coupled carbon and nitrogen dynamics in northern peatlands, Geosci. Model Dev., 6, 1173–1207, https://doi.org/10.5194/gmd-6-1173-2013, 2013.

Xie, L., Zhou, X., Liu, Q., Zhao, C., and Yin, C.: Inorganic nitrogen uptake rate of *Picea asperata* curtailed by fine root acclimation to water and nitrogen supply and further by ectomycorrhizae, Physiol. Plant., 173, 2130–2141, https://doi.org/10.1111/ppl.13562, 2021.

Yang, X., Ricciuto, D. M., Thornton, P. E., Shi, X., Xu, M., Hoffman, F., and Norby, R. J.: The effects of phosphorus cycle dynamics on carbon sources and sinks in the Amazon region: A modeling study using ELM V1, J. Geophys. Res. Biogeosciences, 124, 3686–3698, https://doi.org/10.1029/2019JG005082, 2019.

Yang, X., Thornton, P., Ricciuto, D., Wang, Y., and Hoffman, F.: Global evaluation of terrestrial biogeochemistry in the Energy Exascale Earth System Model (E3SM) and the role of the phosphorus cycle in the historical terrestrial carbon balance, Biogeosciences, 20, 2813–2836, https://doi.org/10.5194/bg-20-2813-2023, 2023.

Yin, H., Adamczyk, B., Wang, Q., Zhu, B., Guo, W., Zhu, X., Liu, Q., and Zhang, Z.: How do nitrogen-limited alpine coniferous forests acquire nitrogen? A rhizosphere perspective, For. Ecosyst., 9, 100071, https://doi.org/10.1016/j.fecs.2022.100071, 2022.

Zhu, Q., Riley, W. J., Tang, J., Collier, N., Hoffman, F. M., Yang, X., and Bisht, G.: Representing nitrogen, phosphorus, and carbon interactions in the E3SM land model: Development and global benchmarking, J. Adv. Model. Earth Syst., 11, 2238–2258, https://doi.org/10.1029/2018MS001571, 2019.

# Implementing belowground controls on nutrient uptake in ELMv2-SPRUCE improves representation of a boreal peatland ecosystem

Yaoping Wang[1], Daniel M. Ricciuto[1], Jiafu Mao[1], Sören E. Weber[2], Verity G. Salmon[1], Xiaoying Shi[1], Xiaojuan Yang[1], Natalie A. Griffiths[1], Paul J. Hanson[1], Anthony P. Walker[1], Jonathan Stelling[3], Katherine Duchesneau[4], Camille E. Defrenne[5], Jeffrey M. Warren[1], Stephen D. Sebestyen[6], Kyle J. Pearson[1], Keith Oleheiser[1], Joshua Birkebak[1], Mark Guilliams[1], Misha B. Krassovski[1], Melanie A. Mayes[1], Peter E. Thornton[1]

[1]Environmental Sciences Division, Oak Ridge National Laboratory, Oak Ridge, TN, 37830, USA
[2]Department of Biology, West Virginia University, Morgantown, WV, 26505, USA
[3]North Central Research and Outreach Center, College of Food, Agricultural, and Natural Resource Sciences, University of Minnesota, MN, 55744, USA
[4]School of Integrative Plant Science, Cornell University, NY, 14850, USA
[5]RECON environmental, Inc., San Diego, CA, 92108, USA
[6]Northern Research Station, U.S. Department of Agriculture Forest Service, Grand Rapids, MN, 55744, USA

*Correspondence to*: Yaoping Wang (wangy7@ornl.gov), Jiafu Mao (maoj@ornl.gov)

Deleted: a land surface model

Deleted: 3

Deleted: 4

Deleted: 5

Deleted: 3

Deleted: 4

Deleted: 5

Deleted: *14*

Deleted: *21*

Deleted: *29*

# 1 Supplementary Text

## 1.1 Nutrient uptake modifications

### 1.1.1 Preliminary notes

The same processes apply to nitrogen (N) and phosphorus (P). The description below (Sect. 1.1.2 to 1.1.10) focuses on N. The description for P can be obtained by substituting out all N by P in the text and equations, except when specifically pointed out. The capitalized letters in all the equations are modelled variables and will be explained as they appear. The meanings of subscripts are consistent throughout and are as follows:

$i$ – soil layer

$j$ – plant functional type (PFT), $j \in \{\text{spruce}, \text{tamarack}, \text{shrub}, \text{moss}\}$, or, when describing the new equations in ELM-MYCI, $j \in \{\text{spruce}, \text{tamarack}, \text{shrub}\}$, since moss is not modified

$m$ – means the term is for soil decomposition

$h$ - plant litter pool, $h \in \{lab, cel, lig\}$, lab – labile, cel – cellulose, lig – lignin

The model time step is $\Delta t$ = 3600 seconds (1 hour). The lower-case letters that are not $\Delta t$ or in the subscript are model parameters and will be explained as they appear. Parameter values are summarized in Table S2-.

### 1.1.2 Nutrient uptake and plant C balance in ELM-OLD

Black + blue colours in Figure S1 show the calculations used to determine nutrient uptake in the default ELMv2-SPRUCE (ELM-OLD). Net photosynthesis is divided by the whole plant's C:N ratio to calculate the corresponding necessary N to support structural growth in leaf, stem, coarse root, and fine root C (Burrows et al., 2020). This growth demand for N is first met by retranslocation, and the remaining part becomes plant's demand for inorganic N, see Eq. (S1). Within a soil column, all the plant functional types (PFTs) and the soil decomposition processes compete for the same pool of soil inorganic N following the "Relative Demand" scheme (Burrows et al., 2020; Thornton and Rosenbloom, 2005). That is, the model first calculates a total potential N uptake by all the PFTs and soil decomposition (Eq. (S2)-(S3); also see Sect. 1.1.3). If the total potential N uptake is greater than the available soil inorganic N, the individual potential uptakes are all scaled down by the same column-level limitation factor, $F_{Nlimit}$, to obtain the actual uptakes, $N_{upt,act,j}$ (Eq. (S4)-(S6)). Under soil inorganic N or P limitation, plant structural growth is constrained to the lower of the two growth levels permitted by total N and P availability, i.e., the total of retranslocation and actual NP uptake, see Eq. (S7).

The calculation of each PFT's C balance is interwoven with the nutrient uptake calculations (Figure S2). At the centre is the nonstructural carbohydrates (NSC) pool, which receives new C from gross primary productivity (GPP), and supplies C to maintenance respiration (MR), excess respiration (XR), growth respiration (GR), structural C growth, and recovery of a virtual "XSMR" pool. MR reflects the metabolic energy spent to maintain a plant's regular functions, and increases approximately linearly with total living biomass. XR reflects the wasted energy due to nutrient limitation and increases exponentially up to a constant with the percentage of plant biomass existing as NSC. Both MR and XR also increase exponentially with temperature. GR reflects the energy spent to synthesize new biomaterials for structural growth and is a small and constant fraction of structural growth. The "XSMR" pool is a virtual pool,

Deleted: (S1)

Deleted: (S2)

Deleted: (S3)

Deleted: (S4)

Deleted: (S6)

Deleted: (S7)

defined for numerical purposes, to prevent the NSC pool from going negative when MR exceeds GPP for prolonged periods (e.g., in winter). Whenever MR > GPP, the unmet MR demand is subtracted from the XSMR pool instead of the NSC pool. This often causes the XSMR pool to go negative. To replenish the XSMR pool, when GPP > MR, some C is taken out of the NSC pool to slowly replenish it according to fixed rules. In this way, the XSMR pool has a small impact on net primary productivity (NPP), but it is not a physical pool or part of the plants' biomass.

$$N_{demand,inorg,j} = \max\left(\frac{C_{net}}{CN_j} - N_{retrans,j}, 0\right) \quad \forall j \tag{S1}$$

$$N_{upt,pot,j} = N_{demand,inorg,j} \quad \forall j \tag{S2}$$

$$N_{upt,pot} = N_{upt,pot,m} + \sum_j N_{upt,pot,j} \tag{S3}$$

$$F_{Nlimit} = \min\left(N_{soil}/(N_{upt,pot} \cdot \Delta t), 1\right) \tag{S4}$$

$$N_{upt,act,j} = F_{Nlimit} N_{upt,pot,j} \quad \forall j \tag{S5}$$

$$N_{upt,act,m} = F_{Nlimit} N_{upt,pot,m} \tag{S6}$$

$$\Delta C_{structural,j} = \begin{cases} C_{net} \cdot \Delta t & \text{if } \min(F_{Nlimit}, F_{Plimit}) = 1 \\ \min\left(\dfrac{CN_j \cdot \Delta t}{N_{upt,act,j} + N_{retrans,j}}, \dfrac{CP_j \cdot \Delta t}{P_{upt,act,j} + P_{retrans,j}}\right) & \text{if } \min(F_{Nlimit}, F_{Plimit}) < 1 \end{cases} \tag{S7}$$

$C_{net,j}$ – incoming net photosynthesis, g C $m^{-2}$ $s^{-1}$

$CN_j$ – the whole plant's C:N ratio, unitless

$N_{retrans,j}$ – N supply from retranslocation, g N $m^{-2}$ $s^{-1}$

$N_{demand,inorg,j}$ – plant demand for inorganic N, g N $m^{-2}$ $s^{-1}$

$N_{upt,pot,j}$ – potential plant inorganic N uptake, g N $m^{-2}$ $s^{-1}$

$N_{upt,pot,m}$ – potential soil decomposition inorganic N uptake, g N $m^{-2}$ $s^{-1}$

$N_{upt,pot}$ – total potential plant and soil decomposition inorganic N uptake, g N $m^{-2}$ $s^{-1}$

$N_{soil}$ – size of the column-level inorganic N pool (the sum of $NH_4^+$, $NO_3^-$, and biological N fixation; for P, this is soluble P [$PO_4^{3-}$]), g N $m^{-2}$

$F_{Nlimit}$ – column-level N-limitation factor, unitless

$N_{upt,act,j}$ – actual plant inorganic N uptake, g N $m^{-2}$ $s^{-1}$

$N_{upt,act,m}$ – actual soil decomposition inorganic N uptake, g N $m^{-2}$ $s^{-1}$

$\Delta C_{structural,j}$ – structural growth of the plant in the time step, g C $m^{-2}$

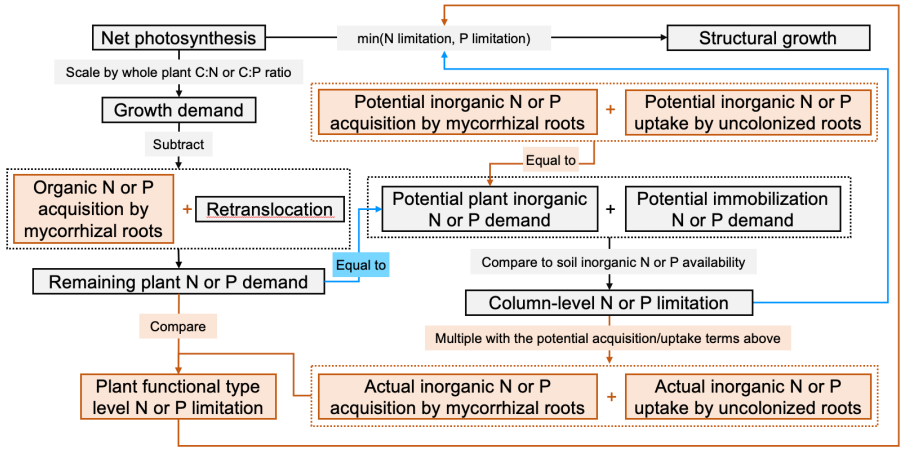


**Figure S1. Nutrient uptake processes by the vascular plant functional types in ELM-OLD and ELM-MYCI. Boxes with edge are modelled quantities, lines and boxes without edge are calculations. Black boxes and lines are shared processes, blue ones exist only in ELM-OLD, and orange ones exist only in ELM-MYCI.**

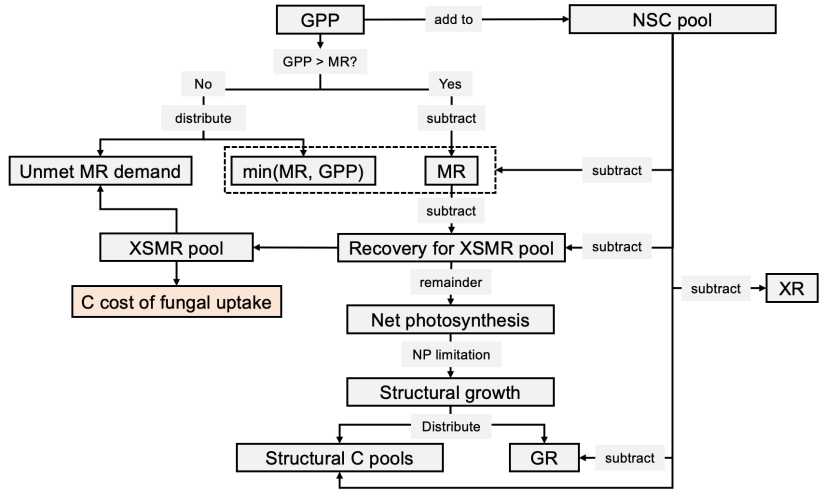


**Figure S2. Relationship between the terms involved in the N and P uptake calculations (net photosynthesis and structural growth) and the terms involved in C-balance calculations (the other terms in this figure). Black boxes are terms shared by ELM-OLD and ELM-MYCI. The orange box is a new flux out of the XSMR pool in ELM-MYCI. Abbreviations: GPP – gross primary productivity, MR – maintenance respiration, XR – excess respiration, GR – growth respiration, NSC – nonstructural carbohydrates.**

### 1.1.3 Nutrient limitation of the soil-decomposition process in ELM-OLD and ELM-MYCI

Although soil decomposition processes are not modified in this study, and the full scheme is described elsewhere (Burrows et al., 2020; Oleson et al., 2013), a brief overview is provided here to contextualize heterotrophic respiration (HR) and its dependence on nutrient availability. ELMv2-SPRUCE uses the Converging Trophic Cascade scheme, which has one coarse woody debris pool, three plant litter pools (conceptualized as labile, cellulose, and lignin), and four soil organic matter (SOM) pools (Burrows et al., 2020; Oleson et al., 2013). C flows from upstream to downstream pools, in the approximate order of woody debris → plant litter → faster-turnover SOM → slower-turnover SOM, following first-order exponential decay. The C:N and C:P ratios of the coarse woody debris and plant litter pools are flexible and determined by the input plant materials. The C:N and C:P ratios of the SOM pools are fixed parameters (Table S2).

During each transformation, a fraction of the upstream carbon is released as $CO_2$, in proportion to the pool size and the transformation rate. HR is calculated as the sum of these $CO_2$ fluxes across all transformations and soil layers. Each transformation also generates N and P demands ($N_{upt,pot,m}$ in Eq. (S3), immobilization demand in Figure S1), because the upstream pools generally have higher C:N and C:P ratios than the downstream pools. To satisfy these stoichiometric requirements, additional N and P must be obtained from the soil inorganic pool. Nutrient limitation of the transformation rate, and thus HR, occurs when the available soil inorganic N or P is insufficient to meet the combined demands of plants and decomposition (Eq. (S4)).

Deleted: (S3)

Deleted: (S4)

### 1.1.4 Overview of the nutrient uptake and plant C balance in ELM-MYCI

In the modified ELMv2-SPRUCE (ELM-MYCI), we split the nutrient uptake processes of the vascular PFTs (spruce, tamarack, and shrubs) into three pathways: (1) direct inorganic nutrient uptake by uncolonized fine roots ($PATH^{root}$), (2) indirect inorganic nutrient acquisition by mycorrhizal roots ($PATH^{myc,inorg}$), and (3) indirect nutrient acquisition from organic sources by mycorrhizal roots ($PATH^{myc,org}$). This split is based on the idea that EcM fungal mantle can prevent fine roots from accessing the soil solution (He et al., 2018). The uncolonized fine roots can only use $PATH^{root}$, whereas the fungi-colonized fine roots can only use $PATH^{myc,inorg}$ and $PATH^{myc,org}$. Pathways (2) and (3) are mycorrhizal-implicit. They do not consider fungal biomass dynamics or explicit exchanges of C-N-P between the plant host and fungi. Instead, they treat the fungal uptake of inorganic nutrient, or mining of organic nutrient, and subsequent transfer to the plant host via the colonized fine roots as a lumped process. The plant host pays a C cost for the fungi-mediated nutrient acquisitions from the XSMR pool (Figure S2 orange box), but this cost is not allocated to fungal biomass or soil respiration because doing so appropriately would require modifying the soil decomposition scheme (Sect. 1.1.3). Nutrient uptake and the C balance for the non-vascular *Sphagnum* moss remains the same as in ELM-OLD. The competition between all PFTs and soil decomposition also remains the same as in ELM-OLD, Eq. (S3)-(S7).

Deleted: (S3)

Deleted: (S7)

We embed the three pathways into the broader model as shown in Figure S1 (orange boxes). We first modify Eq. (S1) to let the growth demand for N be first met by retranslocation and $PATH^{myc,org}$, Eq. (S8). The remainder becomes the plant's demand for inorganic N. This order of subtraction gives the plant a preference of organic N over inorganic N, which we deem acceptable for the boreal peatland ecosystem because it has abundant organic matter. Under the

Deleted: (S1)

Deleted: (S8)

current code structure of ELMv2-SPRUCE, removing this assumption will require revising both the nutrient competition and soil decomposition calculations, which is beyond the scope of this study. We then replace Eq. (S2) with Eq. (S9), where the new potential inorganic N uptake is the sum of two potential uptake terms, one via $PATH^{root}$ and one via $PATH^{myc,inorg}$. After scaling down the potential inorganic N uptake by soil N availability, Eq. (S4)-(S6), we obtain the actual inorganic N uptake via $PATH^{root}$ and $PATH^{myc,inorg}$. The sum of retranslocation, the actual inorganic N uptake via fine roots, the actual inorganic N acquisition via mycorrhizal roots, and the organic N acquisition via mycorrhizal roots becomes the total N supplied to the plants for structural growth, Eq. (S10). With those modifications, we obtain PFT-specific nutrient-limitation factors, Eq. (S11), as opposed to only the column level one in Eq. (S4) in ELM-OLD.

$$N_{demand,inorg,j} = \max\left(\frac{C_{net}}{CN_j} - N_{retrans,j} - N_{myc,org,j}, 0\right) \quad \forall j \tag{S8}$$

$$N_{upt,pot,j} = N_{froot,j} + N_{myc,inorg,j} \tag{S9}$$

$$\Delta C_{structural,j} = \begin{cases} C_{net} \cdot \Delta t & \text{if } F_{Nlimit} = 1 \\ \dfrac{CN_j \cdot \Delta t}{N_{upt,act,j} + N_{retrans,j} + N_{myc,org,j}} & \text{if } F_{Nlimit} < 1 \end{cases} \tag{S10}$$

$$F_{Nlimit,j} = \begin{cases} 1 & \text{if } N_{demand,inorg,j} = 0 \\ \dfrac{N_{upt,act,j}}{N_{demand,inorg,j}} & \text{if } N_{demand,inorg,j} > 0 \end{cases} \tag{S11}$$

$N_{myc,org,j}$ – N acquisition from organic sources through mycorrhizal roots, g N $m^{-2}$ $s^{-1}$

$N_{myc,inorg,j}$ – potential inorganic N acquisition through mycorrhizal roots, g N $m^{-2}$ $s^{-1}$

$N_{froot,j}$ – potential uptake of inorganic N through uncolonized fine roots, g N $m^{-2}$ $s^{-1}$

$F_{Nlimit,j}$ – PFT-specific N limitation factor, unitless

### 1.1.5 Colonization rates by ectomycorrhizal and ericoid fungi

Operationalizing Eq. (S8)-(S11) requires modelling the fraction of roots that are uncolonized, i.e. using $PATH^{root}$, and colonized, i.e. using $PATH^{myc,inorg}$ and $PATH^{myc,org}$. At the SPRUCE site, observations found that the total abundance of dark fungal hyphae, which could be ErM in origin and from *Cenococcum geophilum*, declined by 75-100% from the unheated to the warmest chamber (Defrenne et al., 2021). SPRUCE observations also found shrub roots to vastly increase in total and specific root length in the warmer enclosures, indicating a shift towards the do-it-yourself strategy (Malhotra et al., 2020; Weber et al., 2025). Other past experiments found peatland ericaceous shrubs to uptake less N via ErM fungi under inorganic N addition (Vesala et al., 2021). Based on these studies, we have relatively high confidence that ErM colonization of shrub roots decreases towards the warmer enclosures. Observed root-tip colonization rates for the EcM trees are very noisy and do not show clear trends across warming treatments (Figure S10). Also, past experiments found both increases and decreases in EcM colonization under N additions, possibly related to the amount of added N and water conditions (Table S1).

Based on the above information, we initially tested two ways to model fungal colonization rates: a linear function of annual average water table depth, or a linear function of annual average soil inorganic N content. The first approach turned out to be inviable because it induced little gradient across the treatment chambers. Therefore, we chose the

Deleted: (S2)
Deleted: (S9)
Deleted: (S4)
Deleted: (S6)
Deleted: (S10)
Deleted: (S11)
Deleted: (S4)
Deleted: (S8)
Deleted: (S11)
Deleted: Figure S8

second approach, see Eq. (S12). We use the average soil inorganic N content over 0-30 cm because it is the rooting zone at the SPRUCE site (Iversen et al., 2018). For parameter optimization, we constrain the slope of response to be $b_j < 0$ for ErM colonization of shrubs but does not impose such constraint for the trees (). We choose not to include a soil P content control on mycorrhizal colonization in this study, because the study site's dependence on P is less well-understood and fewer prior studies have focused on P (Table S1) (Bashian-Victoroff et al., 2025), but we put a zero-coefficient into the code as placeholder for potential addition of P control in the future.

$$M_{myc,j} = \max\left(0, \min\left(1, a_j + b_j N_{soil,annavg}\right)\right) \quad \text{(S12)}$$

$M_{myc,j}$ – fraction of fine roots colonized by mycorrhizal fungi, unitless

$N_{soil,annavg}$ – annual average soil inorganic N ($NH_4^+ + NO_3^-$) content in the rooting zone, g N $m^{-3}$

$a_j$ – intercept parameter

$b_j$ – slope parameter

**Table S1. Review of previous studies on the influences of moisture and nutrients to EcM colonization of boreal trees.**

| Plant type | Treatment | Outcome | Study |
|---|---|---|---|
| *Pinus sylvestris* | N addition, 3-50 kg N $ha^{-1}$ $yr^{-1}$ | No change in colonization | (Forsmark et al., 2021) |
| Forest stands including sugar maple, beech, yellow birch, black spruce, moss and ErM shrub understory | N addition, 9-85 kg N $ha^{-1}$ $yr^{-1}$ | Small increase in abundance, possibly driven by tree growth | (Renaudin et al., 2023) |
| *Picea mariana* | N addition, 9-30 kg N $ha^{-1}$ $yr^{-1}$ | Small increase in fraction of colonized root tips | (Rossi et al., 2012) |
| *Picea asperata* | Watering gradient (40-100% field capacity) x N addition gradient (0-400 kg N $ha^{-1}$ $yr^{-1}$) | Higher EcM colonization rates in drier treatments. Lower colonization rates under N addition | (Xie et al., 2021) |
| *Pinus sylvestris* | N addition at 100 kg N $ha^{-1}$ $yr^{-1}$ | Lower EcM colonization rates | (Högberg et al., 2010) |

### 1.1.6 Common environmental multipliers

We apply the following common environmental multipliers when modelling the uptake/acquisition of all three pathways: soil temperature, soil moisture, and the plant's N limitation in the previous time step. The former two multipliers are soil layer specific. The soil temperature multiplier is a conventional $Q_{10}$ function, Eq. (S13). The soil moisture multiplier, from (Frolking et al., 2002), is selected because the formula lets both dry soil and excess moisture to inhibit nutrient uptake, Eq. (S14). The inhibition of waterlogging on nutrient uptake is supported by observational evidence (Struyf et al., 2011). The third multiplier is a feedback mechanism that makes the modelled PFTs ramp up

Deleted: (S12)

Deleted: (S13)

Deleted: (S14)

uptake/acquisition rates in a nutrient-poor environment while preventing them from infinitely accumulating nutrients when demands are already met, Eq. (S15). It is weakly supported by experimental observations that high tissue nutrient concentrations inhibit plant nutrient uptake (Glass et al., 2002). Figure S3 shows the form of Eq. (S15) under various $\alpha$-values. In the absence of suitable observational references and noting that the parameter does not have a large impact on model results in one-at-a-time sensitivity analysis (Figure S6), we chose $\alpha = 1.5$.

$$\mathcal{F}\left(T_{soi,i}\right) = q_{10}^{(T_{soi,i}-10)/10} \tag{S13}$$

$$\mathcal{F}\left(\Theta_{soi,i}\right) = \begin{cases} 1 - \left(\dfrac{\theta_{opt} - \Theta_{soi,i}}{\theta_{opt}}\right)^2 & \text{if } \Theta_{soi,i} \le \theta_{opt} \\ 1 - 0.5\left(\dfrac{\Theta_{soi,i} - \theta_{opt}}{1 - \theta_{opt}}\right) & \text{if } \Theta_{soi,i} > \theta_{opt} \end{cases} \tag{S14}$$

$$\mathcal{F}\left(F_{Nlimit,j}\right) = \frac{\alpha}{F_{Nlimit,j}^2 + \alpha - 1} \tag{S15}$$

$T_{soi,i}$ – soil temperature of layer $i$, °C

$q_{10}$ – $Q_{10}$ parameter for temperature sensitivity of nutrient uptake

$\Theta_{soi,i}$ – volumetric soil water content in soil layer $i$, $m^3\ m^{-3}$

$\theta_{opt}$ – optimal soil volumetric water content for nutrient uptake, $m^3\ m^{-3}$

$\alpha$ – parameter controlling the feedback of excessive nutrient uptake on uptake rates

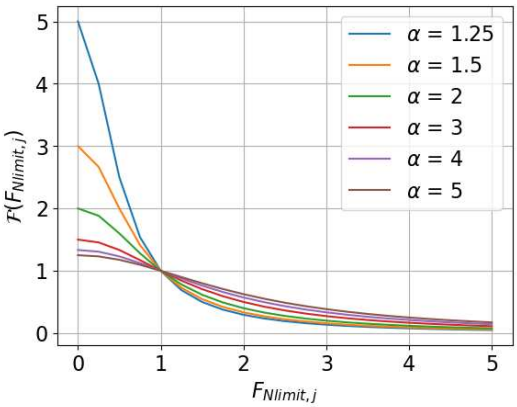


**Figure S3. Visualization of the N limitation multiplier, Eq. (S15), at different parameter values.**

### 1.1.7 Acquisition of nutrient from soil inorganic and organic sources via mycorrhizal roots

Mycorrhizal fungi growth, and hence their ability to obtain soil nutrients, depend partially on C transfer from the plants (He et al., 2018, 2021; Shao et al., 2023). In our implicit approach, we account for this phenomenon by applying a multiplier based on NSC availability (Eq. (S16)) and an upper bound based on the availability of new photosynthates (Sect. 1.1.8) on the acquisition rates of $PATH^{myc,inorg}$ and $PATH^{myc,org}$. In Eq. (S16), when a PFT has high NSC

compared to its structural biomass C in leaf and fine root, the multiplier approaches one, and in the opposite situation, zero.

$$\mathcal{F}(C_{ns,j}) = \frac{k_{nsc} C_{ns,j}}{k_{nsc} C_{ns,j} + C_{froot,j} + C_{leaf,j}} \quad \text{(S16)}$$

$k_{nsc}$ – unitless sensitivity parameter

$C_{ns,j}$ – nonstructural carbohydrates content, g C m$^{-2}$

$C_{froot,j}$ – displayed fine-root carbon biomass, g C m$^{-2}$

$C_{leaf,j}$ – displayed leaf-carbon biomass, g C m$^{-2}$

In each soil layer, the potential N acquisition rate via PATH$^{myc,org}$ is a function of the amount of ErM- or EcM-colonized fine-root biomass, $M_{myc,j} C_{froot,j} f_{froot,i,j}$, the environmental multipliers (Sect. 1.1.6), and the NSC multiplier, see Eq. (S17). The fraction of fine-root biomass in each soil layer, $f_{froot,i,j}$, is set using linear vertical rooting profiles, Eq. (S18), that are fitted on in situ minirhizotron data (Weber et al., 2025). The actual N acquisition rate via PATH$^{myc,org}$ in each soil layer is limited by the sizes of soil organic N pools and the fraction of those pools that can be accessed, Eq. (S19)-(S20), using the high bound 0.0001 in the CoupModel (He et al., 2018). The total actual N acquisition rate via PATH$^{myc,org}$ is calculated as the sum over all soil layers, Eq. (S21), followed by a final adjustment that prevents unnecessary uptake during nighttime and dormancy (see Sect. 1.1.8).

We restrict the mycorrhizal-available soil organic N pools to the three plant litter pools in the soil decomposition scheme (Sect. 1.1.3). This is because those three pools allow flexible C:N and C:P ratios, while the four SOM pools require fixed C:N and C:P ratios. To allow N and P acquisition from the SOM pools require considering how much C to release as fungal respiration. However, the current first-order decomposition processes in ELMv2-SPRUCE have no explicit microbial pools; as such, it is uncertain how much of the HR already reflects fungal respiration in the real world. There may also be difference between EcM and ErM in the fraction of released C (Clemmensen et al., 2021). Due to those difficulties, we leave the treatment of the SOM pools to future model development.

In the real world, ErM has limited ability to degrade lignin/lignin-like *Sphagnum* phenolics and other complex biopolymers (Ward et al., 2022). However, the lignin pool in ELMv2-SPRUCE is more of an abstract pool based on a decay rate than the real lignin compound (Oleson et al., 2013). Preventing the ErM-shrub association from accessing this pool will make its accessibility to organic N and P unrealistically low. Therefore, we allow the EcM-tree and ErM-shrub association to access all the litter pools.

$$N_{myc,pot,org,i,j} = u_{N,myc,j} M_{myc,j} C_{froot,j} F_{froot,i,j} \mathcal{F}(T_{soi,i}) \mathcal{F}(\Theta_{soi,i}) \mathcal{F}(F_{Nlimit,j}) F(C_{ns,j}) \quad \text{(S17)}$$

$$F_{froot,i,j} = \begin{cases} a_{root}(z_i - z_{i-1}) & \text{if } i > 1 \text{ or } b_{root} < 0 \\ a_{root} z_i + b_{root} & \text{if } i = 1 \text{ and } b_{root} > 0 \end{cases} \quad \text{(S18)}$$

$$N_{avail,org,i,j} = \frac{0.0001}{\Delta t}\left(O_{N,i,lab} + O_{N,i,cel} + O_{N,i,lig}\right) \quad \text{(S19)}$$

$$N_{pre,myc,org,i,j} = \min\left(N_{myc,pot,org,i,j}, N_{avail,org,i,j}\right) \quad \text{(S20)}$$

$$N_{pre,myc,org,j} = \sum_{i=1}^{10} N_{pre,myc,org,i,j} \quad \text{(S21)}$$

Deleted: (S17)
Formatted: Check spelling and grammar
Deleted: (S18)
Formatted: Check spelling and grammar
Deleted: (S19)
Deleted: (S20)
Formatted: Check spelling and grammar
Formatted: Check spelling and grammar
Deleted: (S21)
Formatted: Check spelling and grammar

$N_{myc,pot,org,i,j}$ – potential N acquisition from organic sources via mycorrhizal roots in one soil layer, g N $m^{-2}$

$u_{N,myc,j}$ – the maximum organic N acquisition rate per unit colonized fine-root biomass, gN g $C^{-1}$ $s^{-1}$

$F_{froot,i,j}$ – fraction of fine root in one soil layer, unitless

$a_{root}$ – slope parameter of cumulative fine-root distribution

$b_{root}$ – intercept parameter of cumulative fine-root distribution

$z_i$ – the bottom depth of the soil layer, m

$N_{avail,org,i,j}$ – soil organic N pool size available to the plant-fungi association, g N $m^{-2}$

$O_{N,i,lab}$ – soil organic N pool size in the labile litter pool in the soil layer, g N $m^{-2}$

$O_{N,i,cel}$ – soil organic N pool size in the cellulose litter pool in the soil layer, g N $m^{-2}$

$O_{N,i,lig}$ – soil organic N pool size in the lignin litter pool in the soil layer, g N $m^{-2}$

$N_{pre,myc,org,i,j}$ – the pre-adjustment actual acquired N from organic sources via mycorrhizal roots in one soil layer, g N $m^{-2}$

$N_{pre,myc,org,j}$ – the pre-adjustment actual acquired N from organic sources via mycorrhizal roots over all the soil layers, gN $m^{-2}$

Because inorganic N is much more scarce than organic N in peatland ecosystems, we limit the potential N acquisition rate by $PATH^{myc,inorg}$ by a Michaelis-Menten multiplier, Eq. (S22). The other terms in the calculation, Eq. (S23), are the same as those in the calculation of potential organic N acquisition rate, Eq. (S17). The potential acquisition rates are summed up over all the soil layers, Eq. (S24), and subject to a final adjustment (see Sect. 1.1.8).

Constraining the rate constant ($v_{N,fungi,j}$) and half-saturation point ($k_{N,j}$) in the Michaelis-Menten multiplier is difficult. Experimentally observed rate constants vary by three orders of magnitude ($10^{-12}$ to $10^{-9}$ g N $cm^{-2}$ $s^{-1}$ and $10^{-13}$ to $10^{-10}$ g P $cm^{-2}$ $s^{-1}$), and half-saturation points vary by one order of magnitude (0.25-3.338 g N $m^{-3}$ water, 0.049-0.17 g P $m^{-3}$ water) (Table S5, Table S6). Therefore, we first use hand-tuning to determine approximate guesses for those parameters. Then, during parameter optimization, we set the upper and lower bounds to be [0.1, 10] of the initial guesses of the rate constants, and [0.5, 2] of the initial guesses of the half-saturation points (Table S4).

We do not distinguish between $NH_4^+$ and $NO_3^-$ when calculating the N acquisition rate by $PATH^{myc,inorg}$. The concentration of $NO_3^-$ is near-zero compared to $NH_4^+$ in the SPRUCE ecosystem (main text Figure 2), and plants exhibit plasticity and acclimation in their N-form preference (Chalk and Smith, 2021; Daryanto et al., 2019). As such, we deem differentiating between these two chemical forms to be an unnecessary complexity.

$$\mathcal{F}_j\left(N_{conc,i}\right) = \frac{N_{conc,i}}{k_{N,j} + N_{conc,i}} \tag{S22}$$

$$N_{myc,pot,inorg,i,j} = v_{N,myc,j} M_{myc,j} C_{froot,j} F_{froot,i,j} \mathcal{F}_j\left(N_{conc,i}\right) \mathcal{F}\left(T_{soi,i}\right) \mathcal{F}\left(\Theta_{soi,i}\right) \mathcal{F}\left(F_{Nlimit,j}\right) F\left(C_{ns,j}\right) \tag{S23}$$

$$N_{pre,myc,inorg,j} = \sum_{i=1}^{10} N_{myc,pot,inorg,i,j} \tag{S24}$$

$N_{conc,j}$ – soil inorganic N concentration ($NH_4^+ + NO_3^-$; for P, $PO_4^{3-}$) in one soil layer, g N $m^{-3}$



Deleted: (S22)
Formatted: Do not check spelling or grammar
Deleted: (S23)
Deleted: (S17)
Formatted: Do not check spelling or grammar
Deleted: (S24)
Formatted: Do not check spelling or grammar
Deleted: Table S5
Deleted: Table S6
Formatted: Check spelling and grammar
Formatted: Check spelling and grammar
Deleted: Table S4
Formatted: Check spelling and grammar

$k_{N,j}$ – half-saturation point for inorganic N uptake/acquisition, including via mycorrhizal roots and uncolonized fine roots, g N $m^{-3}$

$N_{myc,pot,inorg,i,j}$ – potential inorganic N acquisition via mycorrhizal roots in one soil layer, g N $m^{-2}$ $s^{-1}$

$v_{N,myc,j}$ – maximum inorganic N acquisition rate per unit colonized fine-root biomass, g N g $C^{-1}$ $s^{-1}$

$N_{pre,myc,inorg,j}$ – pre-adjustment inorganic N acquisition via mycorrhizal roots over all the soil layers, g N $m^{-2}$ $s^{-1}$

### 1.1.8 Upper bound on the nonstructural carbohydrate cost of N acquisition via mycorrhizal roots

In addition to letting the plant's NSC abundance influence the acquisition rates of $PATH^{myc,inorg}$ and $PATH^{myc,org}$, Eq. (S16), we impose an upper bound on the total N acquisition from inorganic and organic sources via mycorrhizal associations due to their C cost to the plants. That is, the total acquired N from organic and inorganic sources, multiplied by a constant factor, $c_N$, must not exceed 50% of the net photosynthesis at each time step ($C_{net}$, defined in the beginning of Sect. 1.1.2), see Eq. (S25)-(S29). We choose the 50% threshold following the maximum value found in a previous meta-analysis (Hawkins et al., 2023). The use of net photosynthesis in the upper bound prevents nutrient acquisition during the night and during winter dormancy. The scaled-down inorganic N acquisition, combined with direct fine-root N uptake, undergo competition with soil decomposition, which is already described in Eq. (S9) and (S5). The total C cost to the plant is equal to the greater value between the total C cost of N acquisitions and the total C cost of P acquisitions via $PATH^{myc,inorg}$ and $PATH^{myc,org}$, Eq. (S30).

We subtract the C cost from the virtual XSMR pool (see Sect. 1.1.2) in this study, which has a damped negative effect on the NSC pool – if all other model terms are held constant, a more negative XSMR pool will incur more frequent replenishments from the NSC pool to the XSMR pool (Figure S2). We do not subtract from the NSC pool directly, because negative NSC pool sizes will cause numerical problems in ELMv2-SPRUCE, and because it is desirable to keep the model insensitive to $c_N$ and $c_P$ at this stage. The C cost of fungal nutrient uptake is not commonly reported in the literature and probably varies with environmental conditions. For example, (Hobbie and Högberg, 2012) found $c_N$ ranges from 0-180 g C g $N^{-1}$ based on isotopic theoretical calculations. They further suggest that as the environment becomes more N-abundant, the fungi allow a greater fraction of their assimilated N to be transferred to the plant, resulting in a decline in the C cost.

$$C_{pre,N,myc,j} = c_N\left(N_{pre,myc,org,i,j} + N_{pre,myc,inorg,j}\right) \quad \text{(S25)}$$

$$N_{myc,org,j} = N_{pre,myc,org,j} \min\left(\frac{C_{pre,N,myc,j}}{0.5C_{net,j}}, 1\right) \quad \text{(S26)}$$

$$N_{myc,org,i,j} = N_{pre,myc,org,i,j} \min\left(\frac{C_{pre,N,myc,j}}{0.5C_{net,j}}, 1\right) \quad \forall i \quad \text{(S27)}$$

$$N_{myc,inorg,j} = N_{pre,myc,inorg,j} \min\left(\frac{C_{pre,N,myc,j}}{0.5C_{net,j}}, 1\right) \quad \text{(S28)}$$

$$N_{myc,inorg,i,j} = N_{pre,myc,inorg,i,j} \min\left(\frac{C_{pre,N,myc,j}}{0.5C_{net,j}}, 1\right) \quad \forall j \quad \text{(S29)}$$

Deleted: (S16)

Deleted: (S25)

Deleted: (S29)

Deleted: (S9)

Deleted: (S5)

Deleted: (S30)

$$C_{myc,j} = \max\left(c_N\left(N_{myc,org,j} + F_{Nlimit}N_{myc,inorg,j}\right), c_P\left(P_{myc,org,j} + F_{Plimit}P_{myc,inorg,j}\right)\right) \quad \text{(S30)}$$

$C_{pre,N,myc,j}$ – pre-adjustment C cost of N acquisition from inorganic and organic sources via mycorrhizal roots to a PFT, g C m$^{-2}$ s$^{-1}$

$c_N$ – C cost per unit acquired N via mycorrhizal foots, g C g N$^{-1}$, $c_N = 20$; for P, $c_P = 200$

$N_{myc,org,j}$ – adjusted total rate of N acquisition from organic sources over all the soil layers via mycorrhizal roots, g N m$^{-2}$ s$^{-1}$

$N_{myc,org,i,j}$ – adjusted rate of N acquisition from organic sources in one soil layer via mycorrhizal roots, g N m$^{-2}$ s$^{-1}$

$N_{myc,inorg,j}$ – adjusted total rate of inorganic N acquisition over all the soil layers via mycorrhizal roots, g N m$^{-2}$ s$^{-1}$

$N_{myc,inorg,i,j}$ – adjusted rate of inorganic N acquisition from one soil layer via mycorrhizal roots, g N m$^{-2}$ s$^{-1}$

$C_{myc,j}$ – C cost of nutrient acquisition via mycorrhizal roots to a PFT, g C m$^{-2}$ s$^{-1}$

### 1.1.9 Reduction of soil organic N content due to the acquisition of mycorrhizal roots

To model the reduction in soil organic N content due to the acquisition by mycorrhizal roots, we distribute the final adjusted organic N acquisition, Eq. (S26), summed over all the vascular PFTs, across the three accessed litter pools proportional to pool size, see Eq. (S31). The organic C in those pools are not changed.

$$\Delta O_{N,i,h} = \begin{cases} -N_{myc,org,i,j}\dfrac{O_{N,i,h}}{O_{N,i,lab} + O_{N,i,cel} + O_{N,i,lig}}\Delta t & \forall h \in \{lab, cel, lig\} \\ & \text{if } j \in \{\text{spruce, tamarack}\} \\ -N_{myc,org,i,j}\dfrac{O_{N,i,h}}{O_{N,i,lab} + O_{N,i,cel}}\Delta t & \forall h \in \{lab, cel\} \\ & \text{if } j = \text{shrub} \end{cases} \quad \text{(S31)}$$

$\Delta O_{N,i,h}$ – change in the size of the plant litter pool in one soil layer in one time step, g N m$^{-2}$

### 1.1.10 Direct uptake of inorganic nutrients by uncolonized fine roots

In modelling direct fine-root uptake of inorganic nutrients, we included a root surface area term, Eq. (S32), from the PEATBOG model (Wu and Blodau, 2013). The term is related to measurable root economic traits, here radius and density (Bergmann et al., 2020), enabling distinction between the thinner shrub roots and the coarser tree roots at the SPRUCE site (Iversen et al., 2018). We parameterize the fine-root radius and density directly using the observed values at the SPRUCE site for first- and second-order fine roots, which are primarily responsible for the adsorptive function (Iversen et al., 2017; McCormack et al., 2015). The other multipliers in the uptake rate formula parallel those of inorganic N acquisition via mycorrhizal roots, except for the absence of the NSC multiplier, see Eq. (S33), and Eq. (S23). We use the same half-saturation point, $k_{N,j}$, for PATH$^{root}$ and PATH$^{myc,inorg}$ (Eq. (S22)), in order to limit model complexity in the presence of high observational uncertainty (Table S6). The uptake rates are modelled for each soil layer and summed up, Eq. (S34).

$$A_{froot,i,j} = \frac{0.01 C_{froot,j} F_{froot,i,j}}{r_j^2 \rho_j} \quad \text{(S32)}$$

Deleted: (S26)

Deleted: (S31)

Deleted: (S32)

Deleted: (S33)

Deleted: (S23)

Deleted: (S22)

Formatted: Do not check spelling or grammar

Deleted: (S34)

| | | |
|---|---|---|
| | $N_{froot,i,j} = v_{N,froot,j}(1 - M_{myc,j})A_{froot,i,j}\mathcal{F}_j(N_{conc,i})\mathcal{F}(T_{soi,i})\mathcal{F}(\Theta_{soi,i})\mathcal{F}(F_{Nlimit,j})$ | (S33) |
| | $N_{froot,j} = \sum_{i=1}^{10} N_{froot,i,j}$ | (S34) |

$A_{froot,i,j}$ – total surface area of fine roots in one soil layer, $cm^2$ $m^{-2}$

$r_j$ – fine-root radius of the PFT, cm

$\rho_j$ – fine-root density of the PFT, g C $cm^{-3}$

$v_{N,froot,j}$ – maximum fine-root inorganic N uptake rate per unit uncolonized root surface area, g N $cm^{-2}$ $s^{-1}$

### 1.2 Removal of pretreatment variability

For each variable among $AGNPP_{spruce}$, $AGNPP_{tamarack}$, annual maximum LAI of spruce, and annual maximum LAI of tamarack, we fit an ordinary least-squares regression:

| | | |
|---|---|---|
| | $X^{post} \sim I_{(CO_2)} + T_{air} + Year + X^{pre} + I_{(CO_2)} \times T_{air} + I_{(CO_2)} \times Year$ | (S35) |

, where $X^{post}$ is the post-treatment value in a year and enclosure, $I_{(CO_2)}$ indicates whether that enclosure is treated with elevated $CO_2$ ($I_{(CO_2)}$=1) or not ($I_{(CO_2)}$=0), $T_{air}$ is the annual mean air temperature in the year and enclosure, $X^{pre}$ is the observed year 2014 pre-treatment value in the enclosure. After fitting this initial formula, we drop all the insignificant terms using $p \leq 0.05$ criteria and re-fit a final regression. If the pretreatment term is still significant in the final regression, we remove its effect as $X^{adj} = X^{post} - b(X^{pre} - \bar{X}^{pre})$, where $b$ is the regression coefficient of $X^{pre}$, $\bar{X}^{pre}$ is the average pre-treatment value across all enclosure, and $X^{adj}$ is the adjusted observed value.

### 1.3 Upscaling of the NEE of the shrub-moss community

Automated chamber measurements of soil-air $CO_2$ exchanges were performed using two chambers per enclosure at the SPRUCE site during 2022 and 2023. The chambers are 50 cm in diameter and 25 cm high aboveground (15 cm inserted beneath soil) (Stelling et al., 2024). The 2022 data span only a couple of months in each enclosure, while the 2023 data span most of April to October. Therefore, we only upscaled the 2023 data to obtain a more reliable set of growing-season (2023-05-01 to 2023-10-31) average $NEE_{shrubmoss}$.

We gapfilled the chamber-level observed fluxes by using a $Q_{10}$ function to model the ecosystem respiration component and a rectangular hyperbolic function for the GPP component, following the conventional approach for NEE gapfilling (Lasslop et al., 2010). Previous work on the moss community at SPRUCE further found that water table depth ($W_h$) is an important covariate to include in those functions (Walker et al., 2017). Therefore, we tested multiple formulas and selected the best fit using the Akaike Information Criteria (AIC). For ecosystem respiration, we compared $Q_{10}$-only [Eq. (S36)] and $Q_{10}$+$W_h$ [Eq. (S37)] formulas (Walker et al., 2017). For GPP, we compared PAR-only [Eq. (S38)] and PAR+$W_h$ [Eq. (S39)] formulas (Walker et al., 2017), as well as a PAR+$W_h$+Tair [Eq. (S40)] formula that models the temperature effect on GPP as a unimodal function, $\mathcal{F}(T_{air})$. The temperature effect function is from the well-accepted Vegetation Photosynthesis Model (Glauch et al., 2025).

| | | |
|---|---|---|
| | $R_{eco} = r_{base} \cdot \left(Q_{10,eco}\right)^{\frac{T_{soil}-15}{10}}$ | (S36) |
| | $R_{eco} = \left(r_{base} + r_w W_h\right) \cdot \left(Q_{10,eco}\right)^{\frac{T_{soil}-15}{10}}$ | (S37) |
| | $GPP = \frac{\alpha \cdot PAR \cdot g_{max}}{\alpha \cdot PAR + g_{max}}$ | (S38) |
| | $GPP = \frac{\alpha \cdot PAR \cdot (g_{max} + g_w W_h)}{\alpha \cdot PAR + (g_{max} + g_w W_h)}$ | (S39) |
| | $GPP = \frac{\alpha \cdot PAR \cdot (g_{max} + g_w W_h)}{\alpha \cdot PAR + (g_{max} + g_w W_h)} \mathcal{F}(T_{air})$ | (S40) |
| | $\mathcal{F}(T_{air}) = \begin{cases} 0 & \text{if } T_{air} > t_{max} \text{ or } T_{air} < t_{min} \\ \frac{(T_{air} - t_{min}) \cdot (T_{air} - t_{max})}{(T_{air} - t_{min}) \cdot (T_{air} - t_{max}) - (T - t_{opt})^2} & \text{if } t_{max} < T_{air} < t_{min} \end{cases}$ | (S41) |

$R_{eco}$ – ecosystem respiration, µmol $CO_2$ $m^{-2}$ $s^{-1}$

$r_{base}$ – base rate of ecosystem respiration, µmol $CO_2$ $m^{-2}$ $s^{-1}$

$Q_{10,eco}$ – the Q10 parameter to be estimated

$T_{soil}$ – soil temperature at 5 cm depth, ºC

$r_{wt}$ – the sensitivity of base rate of ecosystem respiration to water table depth, µmol $CO_2$ $m^{-2}$ $s^{-1}$ $cm^{-1}$

$W_h$ – water table depth relative to the hollow surface, cm

$GPP$ – gross primary productivity, µmol $CO_2$ $m^{-2}$ $s^{-1}$

$\alpha$ – light use efficiency, µmol $CO_2$ $\mu mol^{-1}$ photons

$PAR$ – photosynthetically active radiation, $\mu$mol photons $m^{-2}$ $s^{-1}$

$g_{max}$ – maximum GPP at light saturation, µmol $CO_2$ $m^{-2}$ $s^{-1}$

$T_{air}$ – air temperature at 0.5 m height, matching the height of the collar measurements, ºC

$t_{min}$, $t_{max}$, $t_{opt}$ – maximum, minimum, and optimal temperature parameters for temperature response of GPP

The fitting was performed using nonlinear least squares (Levenberg-Marquardt algorithm via scipy.optimize.curve_fit in Python) separately for each plot. The two small chambers in each plot were pooled. The sign convention is NEE = $R_{eco}$ – GPP. The PAR covariate was measured inside the collars (Stelling et al., 2024). The other environmental covariates (5 cm soil temperature, 0.5 m air temperature, and water table depth) are from the SPRUCE environmental data (Hanson et al., 2016). We aggregated the flux measurements from 15-minute to 30-minute intervals because the water table depth covariate was only observed at 30-minute intervals. We used 0.5 m air temperature for the GPP fit because it is the lowest height at which air temperature was observed at SPRUCE and closest to the aboveground collar height (25 cm). The $R_{eco}$ fitting used nighttime $CO_2$ flux, defined as when PAR < 50 µmol $m^{-2}$ $s^{-1}$ and flux > 0. The $Q_{10}$+$W_h$ formula clearly outperformed the $Q_{10}$-only formula, with lower root mean squared error, lower AIC, and better seasonality (Figure S4). Therefore, we used the fitted $Q_{10}$+$W_h$ to gapfill a continuous $R_{eco}$ series spanning night- and day-time. We then subtracted the daytime $R_{eco}$ from the observed flux to obtain daytime GPP. The PAR-only formula on this GPP was clearly the worst, while the PAR+$W_h$ and PAR+$W_h$+$T_{air}$ formulas had similar performances, but PAR+$W_h$+$T_{air}$ had slightly lower root mean squared errors and AIC in all except two chambers with low GPP

Formatted: English (US)

Formatted: Font: Not Bold

Formatted: Font: Not Bold

(+0.00 ambient $CO_2$ and +2.25 elevated $CO_2$) (Figure S5). Therefore, we gapfilled the GPP values using the PAR+$W_h$+$T_{air}$. The observed $NEE_{shrubmoss}$ was then calculated from these gapfilled $R_{eco}$ and GPP and averaged between 2023-05-01 and 2023-10-31.

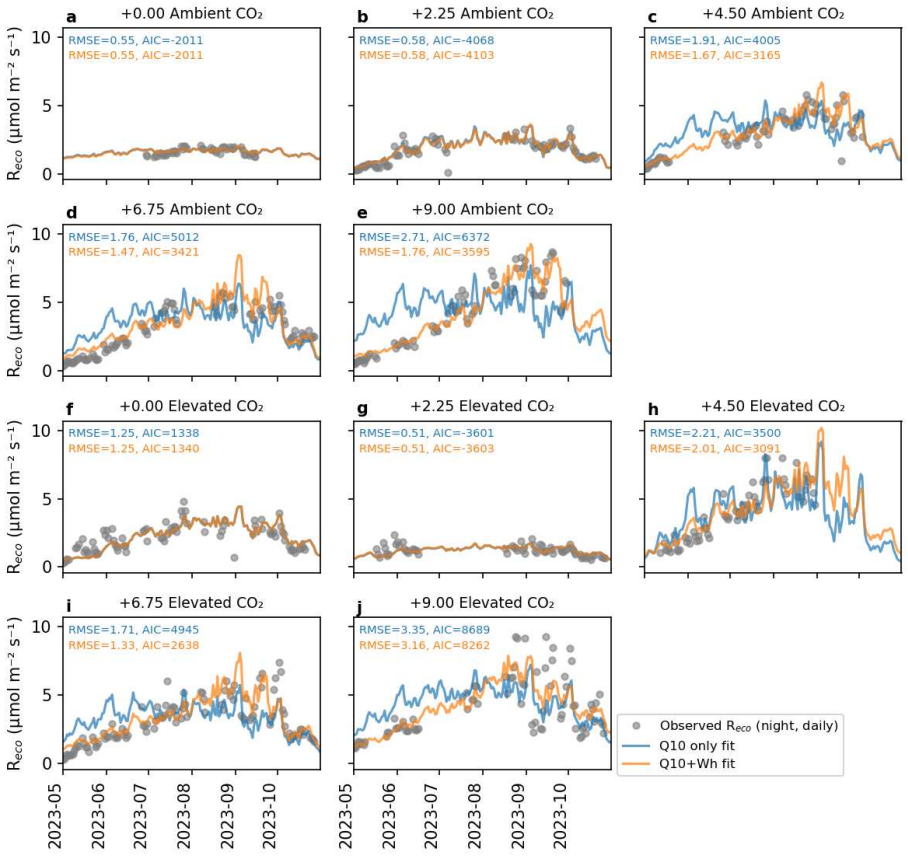


**Figure S4. Goodness-of-fit of the $Q_{10}$-only [Eq. (S36)] and $Q_{10}$+$W_h$ [Eq. (S37)] formulas on ecosystem respiration ($R_{eco}$). RMSE – root mean squared error. AIC – Akaike Information Criteria. Each plot was fitted individually.**

**Formatted:** Check spelling and grammar

**Formatted:** Check spelling and grammar

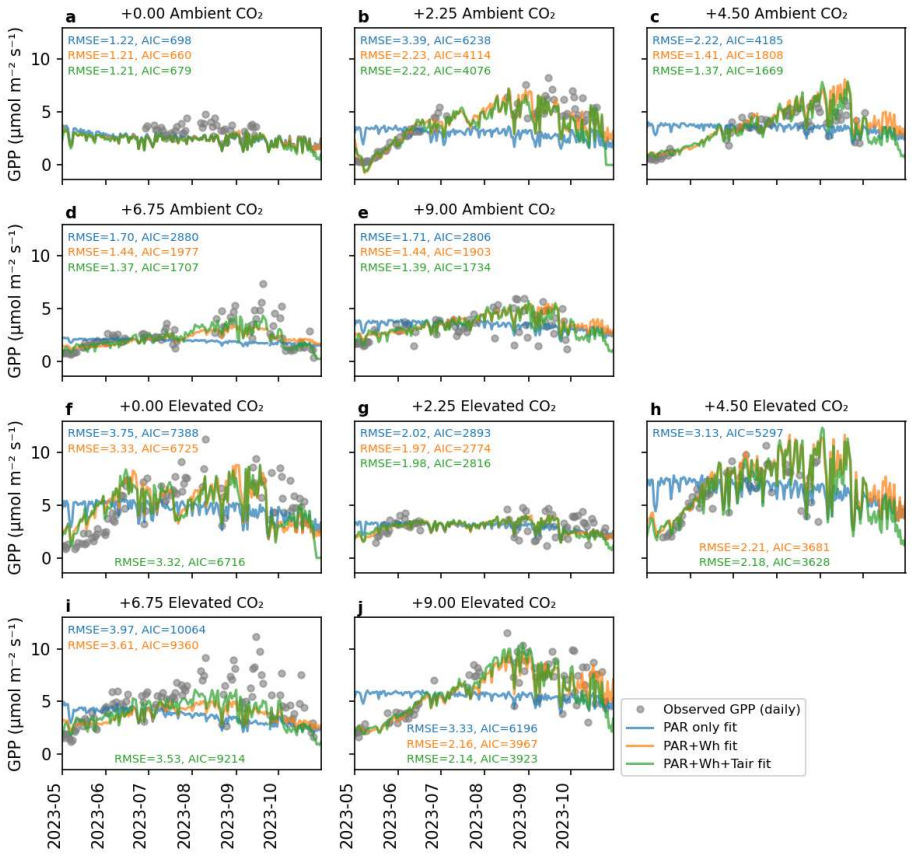


**Figure S5. Goodness-of-fit of the PAR-only [Eq. (S38)], PAR+$W_h$ [Eq. (S39)], and PAR+$W_h$+Tair [Eq. (S40)] formulas on gross primary productivity (GPP). RMSE – root mean squared error. AIC – Akaike Information Criteria. Each plot was fitted individually.**

## 2 Supplementary Tables

**Table S2. Biogeochemistry-related parameters in ELM-OLD that are updated in this study using observed or manually tuned values.**

| Parameter name (Unit) | Explanation | Plant functional type | Values | Source |
|---|---|---|---|---|
| leaf_long (year) | leaf longevity for evergreen leaves | Spruce | 5 | (Salmon et al., 2021) |
| froot_cn (gC $gN^{-1}$) | Fine root C:N ratio | Spruce | 35 | (Iversen et al., 2021) |
| | | Tamarack | 40 | |
| | | Shrub | 55 | |
| livewd_cn (gC $gN^{-1}$) | Live wood C:N ratio | Spruce | 90 | (Phillips et al., 2017) |
| | | Tamarack | 60 | |
| | | Shrub | 85 | |
| leaf_cp (gC $gP^{-1}$) | Leaf C:P ratio | Spruce | 655.78 | |
| | | Tamarack | 655.78 | |
| | | Shrub | 594.72 | |
| cn_s1 (gC $gN^{-1}$) | C:N ratio of the first SOM pool | - | 22 | (Griffiths et al., 2017) |
| cn_s2 (gC $gN^{-1}$) | C:N ratio of the second SOM matter pool | - | 22 | (Griffiths et al., 2017) |
| cn_s3 (gC $gN^{-1}$) | C:N ratio of the third SOM matter pool | - | 20 | (Griffiths et al., 2017) |
| cn_s4 (gC $gN^{-1}$) | C:N ratio of the fourth SOM pool | - | 20 | (Griffiths et al., 2017) |
| r_mort ($year^{-1}$) | Whole-plant turnover rate | Spruce | 0.2 | Manually tuned to match observed biomass magnitude |
| | | Tamarack | 0.2 | |
| | | Shrub | 0.12 | |

**Table S3. Biogeochemistry-related preexisting parameters in ELM-OLD that are optimized. The upper and lower bounds are determined based on previous ranges (Griffiths et al., 2017; Meng et al., 2021; Ricciuto et al., 2018).**

| Parameter name in ELMv2-SPRUCE (Unit) | Explanation | Plant functional type | Range | Optimized values in ELM-$OLD_{optim}$ |
|---|---|---|---|---|
| mbbopt (1) | Ball-Berry slope of conductance-photosynthesis relationship, unstressed | Spruce | [4.5, 13.5] | 10.26 |
| | | Tamarack | | 9.96 |
| | | Shrub | | 11.33 |
| vcmaxhd (J $mol^{-1}$) | Deactivation energy for Vcmax | Spruce | [191000, 210000] | 197844 |
| | | Tamarack | | 206246 |

| | | | | |
|---|---|---|---|---|
| | | Shrub | | 197588 |
| flnr (1) | Fraction of leaf N in in Rubisco enzyme | Spruce | [0.05, 0.30] | 0.08376 |
| | | Tamarack | | 0.19381 |
| | | Shrub | | 0.29826 |
| slatop ($m^2$ $gC^{-1}$) | Specific leaf area at top of canopy | Spruce | [0.0051, 0.0095] | 0.00909 |
| | | Tamarack | [0.01708, 0.02604] | 0.02572 |
| | | Shrub | [0.01666, 0.0308] | 0.01985 |
| br_mr_pft (gC $gN^{-1}$ $s^{-1}$) | Base rate of maintenance respiration | Spruce | [$10^{-6}$, 5*$10^{-6}$] | 3.283*$10^{-6}$ |
| | | Tamarack | | 1.319*$10^{-6}$ |
| | | Shrub | | 4.234*$10^{-6}$ |
| q10_mr_pft (1) | $Q_{10}$ of maintenance respiration | Spruce | [1.2, 3.8] | 2.322 |
| | | Tamarack | | 3.209 |
| | | Shrub | | 1.369 |
| froot_leaf (gC $gC^{-1}$) | Ratio of fine root to leaf allocation | Spruce | [0.3, 1.3] | 1.015 |
| | | Tamarack | | 1.085 |
| | | Shrub | | 0.628 |
| stem_leaf (n/a) | Parameter controlling stem-to-leaf allocation ratio | Spruce | [-0.5, -0.1] | -0.4796 |
| | | Tamarack | | -0.3084 |
| decomp_depth_efolding (m) | e-folding depth for reduction in decomposition | - | [0.3, 1.0] | 0.3039 |
| q10_hr (1) | $Q_{10}$ for heterotrophic respiration | - | [1.4, 2.5] | 1.922 |
| mino2lim (1) | Minimum anaerobic decomposition rate as a fraction of potential aerobic rate | - | [0.0001, 0.05] | 0.003131 |

**Table S4. Newly added parameters in ELM-MYCI that are manually tuned.**

| **Symbol (Unit)** | **Equation appeared in** | **Plant functional type** | **Value** | **Range in one-at-a-time sensitivity analysis** | **Source** |
|---|---|---|---|---|---|
| $a_j$ (1) | Eq. (S12) | Spruce | 0.7 | [0.2, 0.8] | Manually tuned based on observed ranges (Rossi et al., 2012; Xie et al., 2021) |
| | | Tamarack | 0.5 | | |

**Deleted:** (S12)

**Formatted:** (Asian) Chinese (China)

| | | | | | |
|---|---|---|---|---|---|
| $\theta_{opt}$ (1) | Eq. (S14) | - | 0.6 | [0.3, 0.9] | (Frolking et al., 2002) |
| $\alpha$ (1) | Eq. (S15) | - | 1.5 | [0.75, 2.25] | Selected based on comparing a range of values in Figure S3 |
| $k_{nsc}$ (1) | Eq. (S16) | - | 2 | [1, 3] | Manually tuned |
| $a_{root}$ (1) | Eq. (S18) | Spruce | 11.7605 | - | Fitted to observed fine root depth distribution at SPRUCE (Weber et al., 2025) |
| | | Tamarack | 11.7605 | - | |
| | | Shrub | 7.5535 | - | |
| $b_{root}$ (1) | Eq. (S18) | Spruce | -0.11713 | - | |
| | | Tamarack | -0.11713 | - | |
| | | Shrub | 0.04493 | - | |
| $u_{N,fungi,j}$ (gN gC$^{-1}$ s$^{-1}$) | Eq. (S17) | Tamarack | $1.0209*10^{-8}$ | [$1.0209*10^{-9}$, $1.0209*10^{-7}$] | Manually tuned to ensure all PFTs grow |
| | | Shrub | $3.5748*10^{-8}$ | [$3.5748*10^{-9}$, $3.5748*10^{-7}$] | |
| $k_{N,j}$ (gN m$^{-3}$) | Eq. (S22) | Spruce | 7 | [3.5, 14] | Manually tuned to approximately match annual average simulated soil inorganic N levels |
| | | Tamarack | 7 | | |
| | | Shrub | 7 | | |
| $k_{P,j}$ (gP m$^{-3}$) | Phosphorus counterpart of Eq. (S22) | Tamarack | 0.004955 | [0.002478, 0.009911] | Manually tuned to approximately match annual average simulated soil inorganic P levels |
| | | Shrub | 0.004955 | | |
| $v_{N,fungi,j}$ (gN gC$^{-1}$ s$^{-1}$) | Eq. (S23) | Spruce | $4.5977*10^{-9}$ | [$4.5977*10^{-10}$, $4.5977*10^{-8}$] | Manually tuned with reference to values in (He et al., 2021; Shao et al., 2023) |
| | | Shrub | $3.3289*10^{-9}$ | [$3.3289*10^{-10}$, $3.3289*10^{-8}$] | |
| $v_{P,fungi,j}$ (gP gC$^{-1}$ s$^{-1}$) | Phosphorus counterpart of Eq. (S23) | Tamarack | $2.7566*10^{-10}$ | [$2.7567*10^{-11}$, $2.7567*10^{-9}$] | |
| | | Shrub | $8.0369*10^{-10}$ | [$8.0369*10^{-11}$, $8.0369*10^{-9}$] | |
| $c_P$ (gC gP$^{-1}$) | Phosphorus counterpart of Eq. (S25), Eq. (S30) | - | 200 | [100, 1000] | Manually tuned in line with the typical order-of-magnitude N:P ratio (~10:1) in soil-plant systems |

Deleted: (S14)
Formatted: (Asian) Chinese (China)
Deleted: (S15)
Formatted: (Asian) Chinese (China)
Deleted: Figure S3
Formatted: (Asian) Chinese (China)
Deleted: (S16)
Formatted: (Asian) Chinese (China)
Deleted: (S18)
Formatted: Check spelling and grammar
Deleted: (S18)
Formatted: Check spelling and grammar
Formatted: Check spelling and grammar
Deleted: (S17)
Deleted: (S22)
Formatted: Check spelling and grammar
Deleted: (S22)
Formatted: Check spelling and grammar
Deleted: (S23)
Formatted: Check spelling and grammar
Deleted: (S23)
Formatted: Check spelling and grammar
Deleted: (S25)
Deleted: (S30)
Formatted: (Asian) Chinese (China)
Formatted: (Asian) Chinese (China)

| | | | | | |
|---|---|---|---|---|---|
| $r_j$ (cm) | Eq. (S32) | Spruce | 0.012 | - | Unpublished observed data (Iversen et al., 2018) |
| | | Tamarack | 0.018 | - | |
| | | Shrub | 0.0045 | - | |
| $\rho_j$ (gC cm$^{-3}$) | Eq. (S32) | Spruce | 0.16 | - | Unpublished observed data, assuming 46% C in biomass (Iversen et al., 2018) |
| | | Tamarack | 0.15 gC cm$^{-3}$ | - | |
| | | Shrub | 0.09 gC cm$^{-3}$ | - | |
| $v_{N,froot,j}$ (gN gC$^{-1}$ s$^{-1}$) | Eq. (S33) | Spruce | 4.2538*10$^{-12}$ | [4.2538*10$^{-13}$, 4.2538*10$^{-11}$] | Manually tuned with reference to values in (Shao et al., 2023; Wu and Blodau, 2013) |

**Table S5. Review of experimentally measured uptake rates by fungi-colonized and uncolonized fine roots. If the paper reported a maximum rate constant, that value is used here; otherwise, the fastest measured rate is used. The converted values in gN or gP cm$^{-2}$ s$^{-1}$ use Eq. (S32) to make the original values reported in different units comparable. The conversion used 0.015 cm radius and 0.155 gC cm$^{-3}$ density for trees, and 0.0045 cm radius and 0.09 gC cm$^{-3}$ density for shrub and herbs based on the SPRUCE-observed values in Table S4.**

| Plant species | Nutrient species | Value in original unit | Converted value (gN or gP cm$^{-2}$ s$^{-1}$) | Converted value (gN or gP gC$^{-1}$ s$^{-1}$) | Source |
|---|---|---|---|---|---|
| *Picea asperata*, uncolonized roots | $NH_4^+$ | 130 pmol cm$^{-2}$ s$^{-1}$ | 1.820*10$^{-9}$ | 2.401*10$^{-7}$ | (Xie et al., 2021) |
| | $NO_3^-$ | 90 pmol cm$^{-2}$ s$^{-1}$ | 1.260*10$^{-9}$ | 1.662*10$^{-7}$ | |
| *Picea asperata*, EcM colonized roots | $NH_4^+$ | 30 pmol cm$^{-2}$ s$^{-1}$ | 4.200*10$^{-10}$ | 5.540*10$^{-8}$ | |
| | $NO_3^-$ | 20 pmol cm$^{-2}$ s$^{-1}$ | 2.800*10$^{-10}$ | 3.693*10$^{-8}$ | |
| *Douglas fir*, uncolonized roots | $NH_4^+$ | 22 nmol m$^{-2}$ s$^{-1}$ | 3.080*10$^{-11}$ | 4.063*10$^{-9}$ | (Hawkins et al., 2008) |
| | $NO_3^-$ | 25 nmol m$^{-2}$ s$^{-1}$ | 3.500*10$^{-11}$ | 4.616*10$^{-9}$ | |
| *Lodgepole pine*, uncolonized roots | $NH_4^+$ | 14 nmol m$^{-2}$ s$^{-1}$ | 1.960*10$^{-11}$ | 2.585*10$^{-9}$ | |
| | $NO_3^-$ | 20 nmol m$^{-2}$ s$^{-1}$ | 2.800*10$^{-11}$ | 3.693*10$^{-9}$ | |
| Hardwood trees | $NH_4^+$ | 8 $\mu$mol g root$^{-1}$ hr$^{-1}$ | 2.359*10$^{-10}$ | 3.111*10$^{-8}$ | (Sanders-DeMott et al., 2018) |
| Hardwood trees | $NO_3^-$ | 0.25 $\mu$ mol g root$^{-1}$ hr$^{-1}$ | 7.371*10$^{-12}$ | 9.722*10$^{-10}$ | |
| *Eriophorum vaginatum* | $NH_4^+$ | 13.7 $\mu$mol g$^{-1}$ hr$^{-1}$ | 2.111*10$^{-11}$ | 5.328*10$^{-8}$ | (Chapin et al., 1993) |

Deleted: (S32)
Formatted: (Asian) Chinese (China)
Deleted: (S32)
Formatted: (Asian) Chinese (China)
Deleted: (S33)
Formatted: (Asian) Chinese (China)
Deleted: Table S5. Newly added parameters in ELM-MYCI that are optimized. ¶
Symbol
Symbol ... [1]
Deleted: estimated
Deleted: (S32)
Formatted: Check spelling and grammar
Deleted: with

| | | | | | |
|---|---|---|---|---|---|
| *Vaccinium macrocarpon*, uncolonized roots | $NO_3^-$ | 0.017 $\mu$ mol $g^{-1}$ DW $min^{-1}$ | $1.572*10^{-12}$ | $3.967*10^{-9}$ | (Kosola et al., 2007) |
| *Vaccinium macrocarpon*, ErM colonized roots | $NO_3^-$ | 0.16 $\mu$ mol $g^{-1}$ DW $min^{-1}$ | $1.479*10^{-11}$ | $3.733*10^{-8}$ | |
| *Pinus sylvestris*, uncolonized | $PO_4^{3-}$ | 0.2 nmol $s^{-1}$ $g^{-1}$ d. wt root | $4.701*10^{-11}$ | $6.200*10^{-9}$ | (Colpaert et al., 1999) |
| *Pinus sylvestris*, colonized whole plant | $PO_4^{3-}$ | 1 nmol $s^{-1}$ $g^{-1}$ d. wt root | $2.350*10^{-10}$ | $3.100*10^{-8}$ | |
| *Pinus sylvestris*, uncolonized | $PO_4^{3-}$ | 0.08 nmol $g^{-1}$ $s^{-1}$ | $1.880*10^{-11}$ | $2.480*10^{-9}$ | (Van Tichelen and Colpaert, 2000) |
| *Pinus sylvestris*, colonized whole plant | $PO_4^{3-}$ | 0.13-0.62 nmol $g^{-1}$ $s^{-1}$ | $3.055*10^{-11}$ - $1.457*10^{-10}$ | $4.030*10^{-9}$ - $1.922*10^{-8}$ | |
| *Calluna vulgaris*, colonized by endophytes and ErM | $PO_4^{3-}$ | 1500 pg mg root $FW^{-1}$ $hour^{-1}$ | $1.360*10^{-13}$ | $3.432*10^{-10}$ | (Arndal et al., 2013) |

**Table S6. Review of experimentally measured half-saturation point in uptake kinetics.**

| **Value in original unit** | **Converted value (gN $m^{-3}$ water)** | **Plant species** | **Nutrient species** | **Source** |
|---|---|---|---|---|
| 242 $\mu$mol $kg^{-1}$ | 3.338 | *Eriophorum vaginatum* | $NH_4^+$ | (Chapin et al., 1993) |
| Only linear relationship observed | - | *Vaccinium macrocarpon*, uncolonized roots | $NH_4^+$ | (Kosola et al., 2007) |
| Only linear relationship observed | - | *Vaccinium macrocarpon*, uncolonized roots | $NO_3^-$ | |
| 34.54 $\mu$mol $kg^{-1}$ | 0.48 | *Vaccinium macrocarpon*, colonized roots | $NH_4^+$ | |
| 17.75 $\mu$mol $kg^{-1}$ | 0.25 | *Vaccinium macrocarpon*, ErM colonized roots | $NO_3^-$ | |

| | | | | |
|---|---|---|---|---|
| 12.1 $\mu$mol kg$^{-1}$ | 0.17 | *Pinus sylvestris*, uncolonized | $PO_4^{3-}$ | (Van Tichelen and Colpaert, 2000) |
| 3.5-10.2 $\mu$mol kg$^{-1}$ | 0.049-0.143 | *Pinus sylvestris*, colonized whole plant | $PO_4^{3-}$ | |

**Table S7. Sphagnum cover (%) by year and treatment chamber (Norby et al., 2019; Weston D. 2020, 2021 unpublished data).**

| Treatment | 2016 | 2017 | 2018 | 2019 | 2020 | 2021 |
|---|---|---|---|---|---|---|
| +0.00 | 25 | 24.5 | 24.9 | 23.7 | 24.6 | 24.6 |
| +2.25 | 25 | 21.1 | 21.1 | 24 | 19 | 19 |
| +4.50 | 25 | 19.4 | 19.3 | 12.3 | 9.2 | 9.2 |
| +6.75 | 25 | 21.3 | 10.1 | 8.1 | 4 | 4 |
| +9.00 | 24 | 8.9 | 3.8 | 3.6 | 0.6 | 0.6 |
| +0.00 $CO_2$ | 25 | 25 | 24 | 23.3 | 23.3 | 23.3 |
| +2.25 $CO_2$ | 24.3 | 17.4 | 16.5 | 14.5 | 14.5 | 14.5 |
| +4.50 $CO_2$ | 25 | 4.8 | 5.7 | 3.7 | 1.2 | 1.2 |
| +6.75 $CO_2$ | 22 | 12.1 | 14 | 10.1 | 7.1 | 7.1 |
| +9.00 $CO_2$ | 23.1 | 11.2 | 4.2 | 3.7 | 1.7 | 1.7 |
| Ambient | 25 | 25 | 25 | 25 | 25 | 25 |

**Table S8. Measured *Sphagnum* or shrub aboveground biomass in the automated chambers divided by the measured *Sphagnum* or shrub aboveground biomass in the corresponding SPRUCE plot.**

| Treatment | *Sphagnum* ratio | Shrub ratio |
|---|---|---|
| +0.00 | 0.64 | 0.16 |
| +2.25 | 0.81 | 0.05 |
| +4.50 | 0.43 | 0.16 |
| +6.75 | 0.37 | 0.32 |
| +9.00 | 0.48 | 1.49 |
| +0.00 $CO_2$ | 1.04 | 0.18 |
| +2.25 $CO_2$ | 1.01 | 0.31 |
| +4.50 $CO_2$ | 0.58 | 2.36 |
| +6.75 $CO_2$ | 0.59 | 1.54 |
| +9.00 $CO_2$ | 0.96 | 0.78 |

## 3 Supplementary Figures

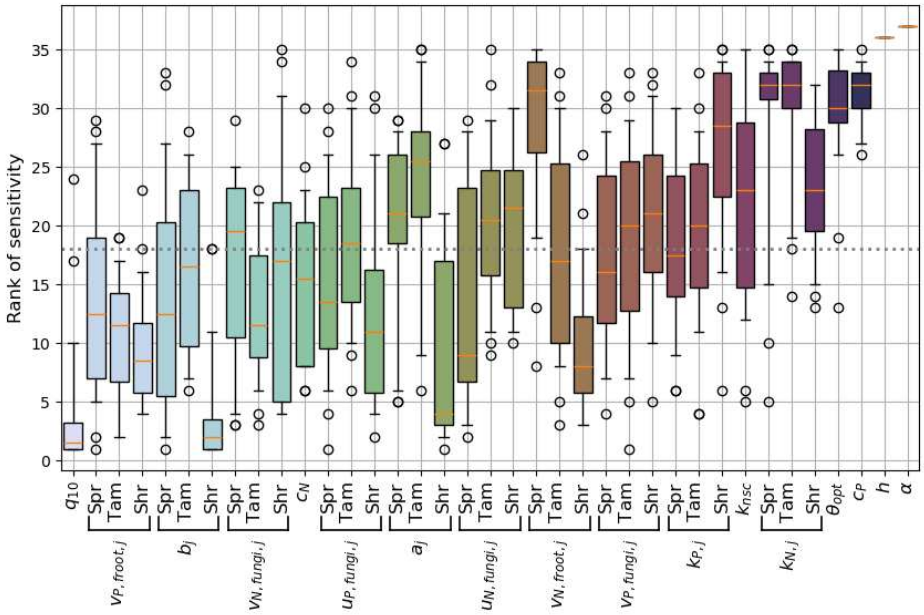


**Figure S6. Rank of the sensitivity of carbon fluxes to the newly added parameters in ELM-MYCI. A smaller rank means greater sensitivity. Parameters that have PFT-specific values are grouped together and labelled by Spr – spruce, Tam – tamarack, Shr – shrub. Boxplots show the [min, 5th percentile, 25th percentile, median, 75th percentile, 95th percentile, max] of the ranks across the means and slopes of all the independent carbon flux variables in ambient and elevated $CO_2$ enclosures. Parameters/PFT-specific values ranked below the threshold line (horizontal, dashed grey) are selected for ensemble simulation and optimization.**

**Deleted:** 4

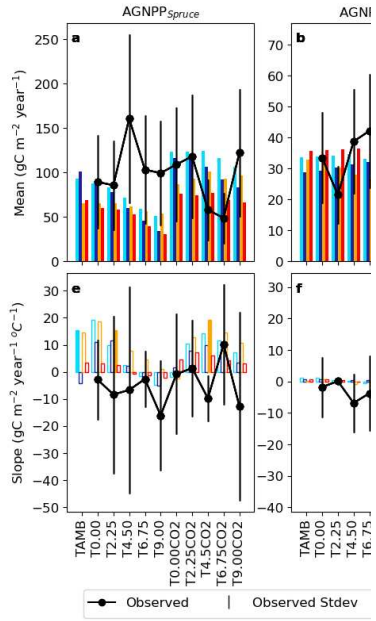


**Deleted:**

**Figure S5. Enclosure-by-enclosure mean and temperature sensitivity of selected C fluxes. The observational uncertainty intervals are estimated in the same manner as Fig. 1 (see main text Sect. 2.4). The modelled slopes have solid bars when they are significant at p≤0.05 (two-sided t-test), and otherwise hollow bars. The modelled values are from the best-performing ensemble members using RAE criteria (main text Eq. (1)).**

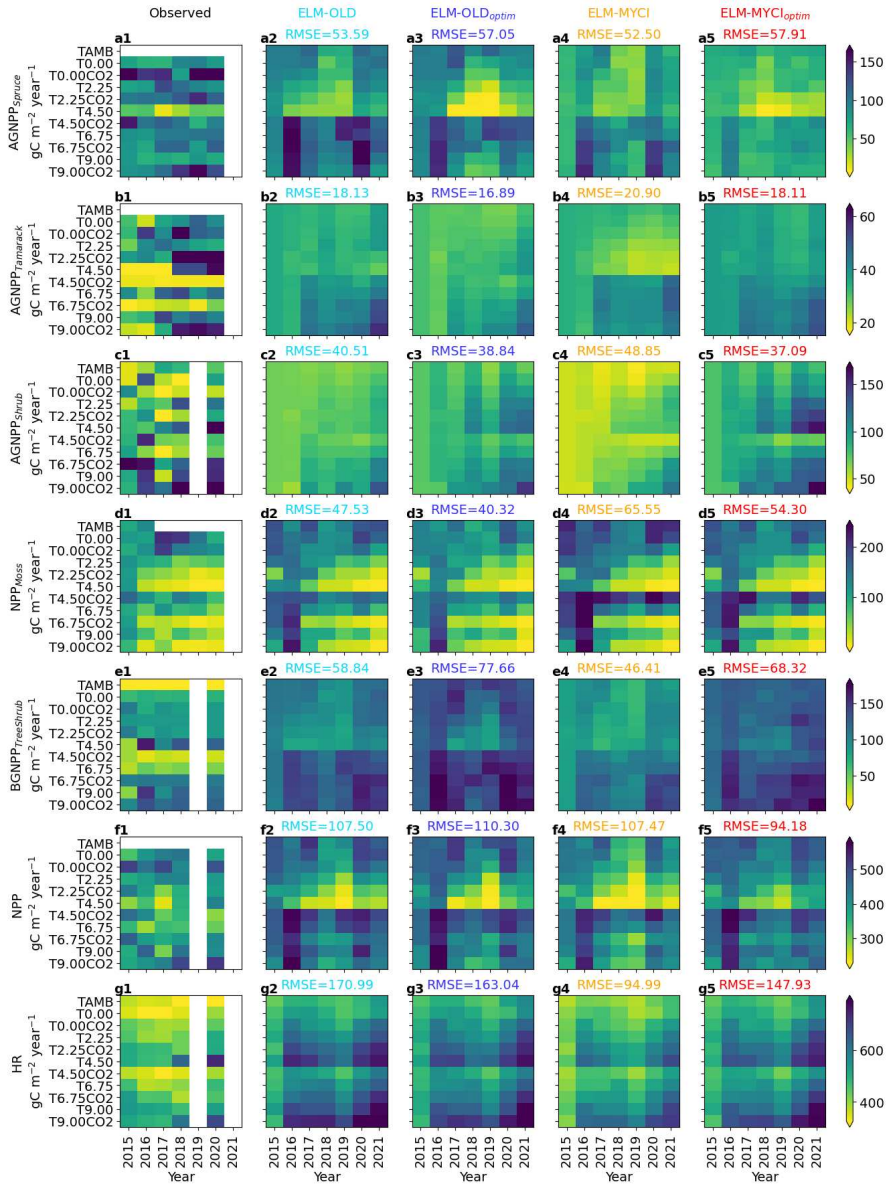


**Figure S7. Observed annual time series of selected C fluxes during the calibration period, and the corresponding simulated levels.** The root mean squared error (RMSE) values were calculated between each model setup and the observation, on all the data points displayed in one panel (i.e. across all the years and treatments).

Deleted: 5

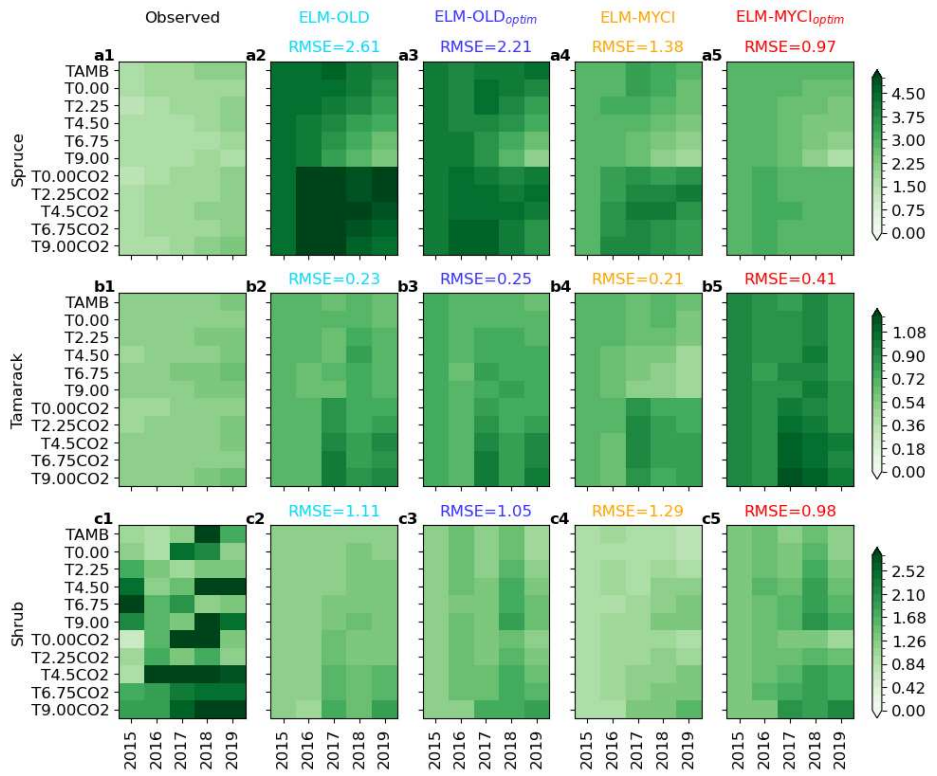


**Figure S8. Observed annual maximum leaf area index and the corresponding simulated levels by the four model setups ($m^2$ $m^{-2}$ ground area).**

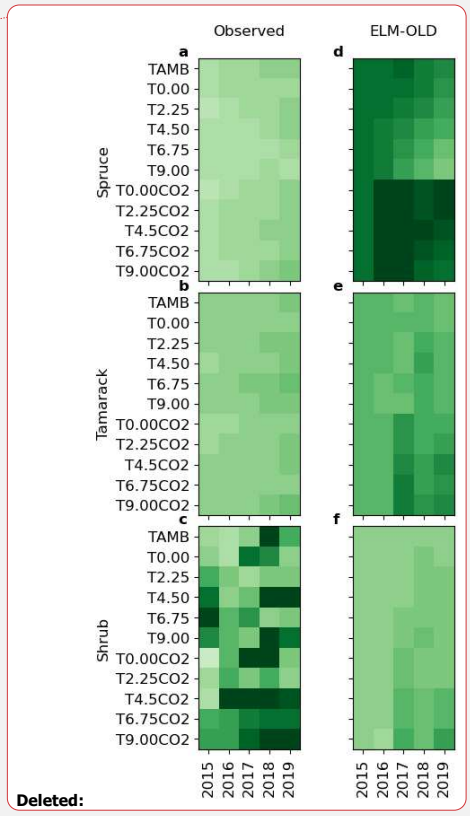


Deleted:

Deleted: 6

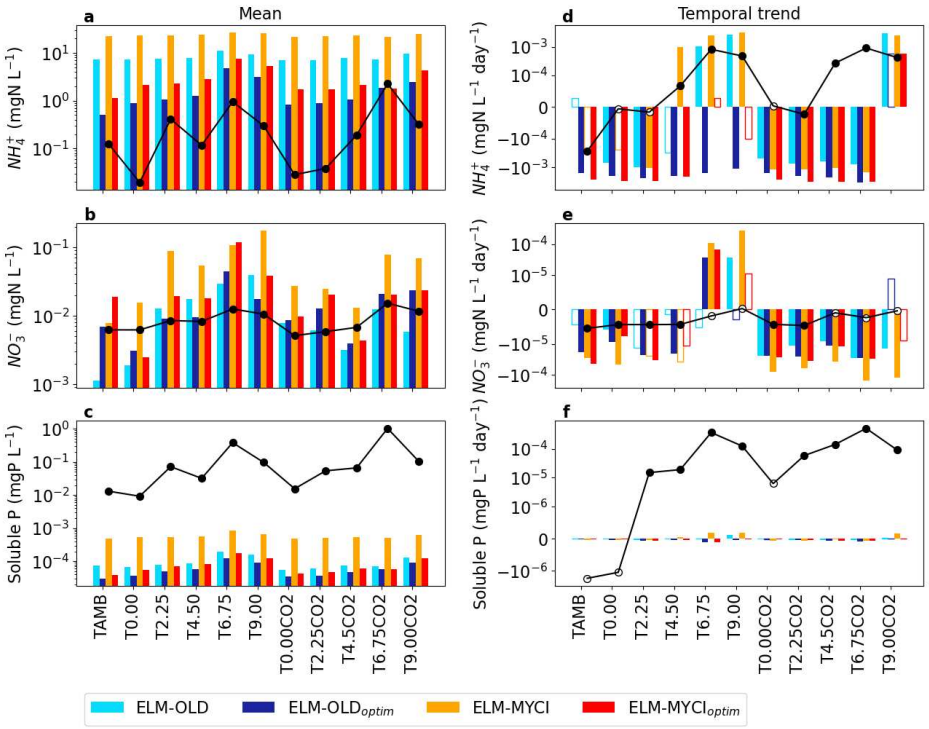


**Figure S9. Observed and simulated mean values and least squares linear temporal trends in hollow soil pore water nutrient concentrations at 30cm depth during 2015-2020. Logscale is used because the modeled and observed values differ by orders of magnitudes. For the temporal trends, solid bars mean the trend is significant at p≤0.05 (two-sided t-test) and empty bars means insignificant.**

Deleted: 7

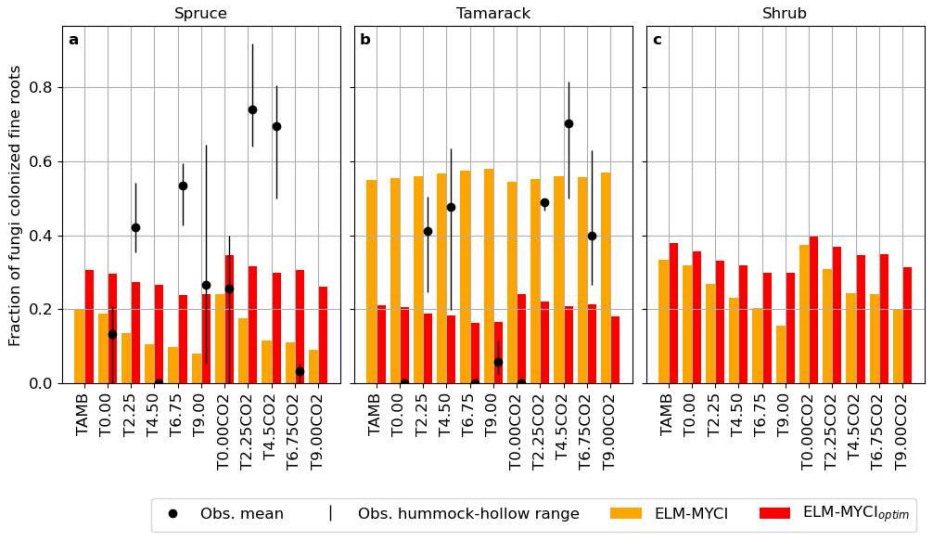


**Figure S10. Fraction of fungi-colonized fine roots observed for tamarack in selected enclosures and simulated by the two modified model setups for spruce, tamarack, and shrub in all the enclosures. The observations were made in summer 2017, with one data point from the hummock and one from the hollow (Duchesneau et al., 2024). The display shows their weighted mean (0.64 × hummock + 0.36 × hollow) and the range. The simulated values are averaged over 2015-2021 for each enclosure and use the same hummock-hollow average (0.64 x hummock + 0.36 x hollow) as all the other modelled variables.**

Deleted: 8

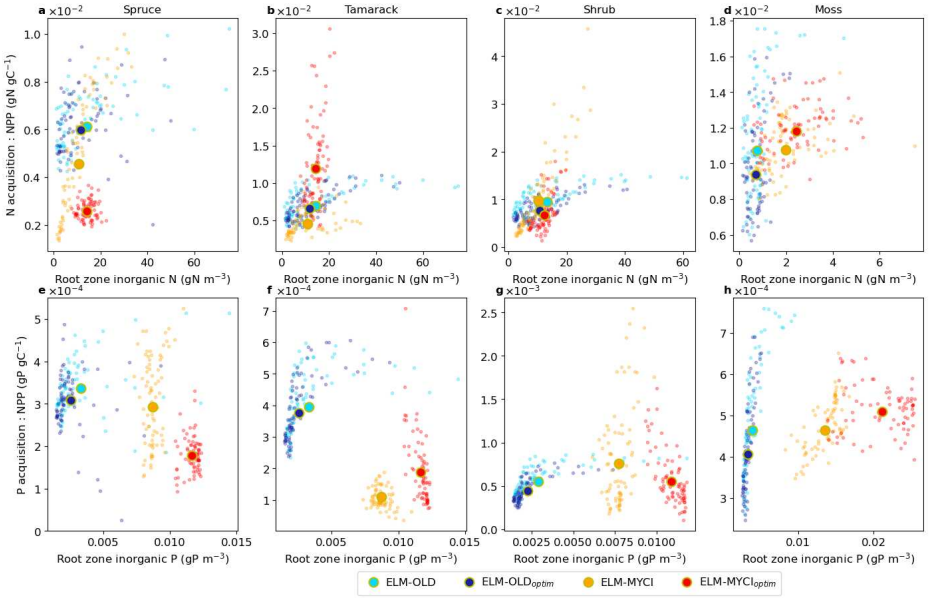


**Figure S11. Relationship between the annual total NP acquisition per unit net primary productivity (NPP) and the annual mean soil inorganic nutrient content in different model setups. The total acquisition is equal to inorganic nutrient uptake in ELM-OLD and ELM-OLD$_{optim}$, and equal to the sum of all three pathways (actual inorganic nutrient uptake by uncolonized fine roots, actual inorganic nutrient uptake by mycorrhizal roots, and actual organic nutrient uptake by mycorrhizal roots) in ELM-MYCI and ELM-MYCI$_{optim}$. We normalize the acquisition to per unit NPP to remove the influences from vegetation biomasses and highlight the differences in the shapes of the relationships. Each small dot represents a single enclosure-year combination, and all the dots together span all the enclosures and 2015-2021. The large dots represent averages over all the years and chambers. The soil inorganic nutrient contents are weighted averages over all the soil layers using the plant functional type's fine-root fractions in each soil layer.**

Deleted: 9

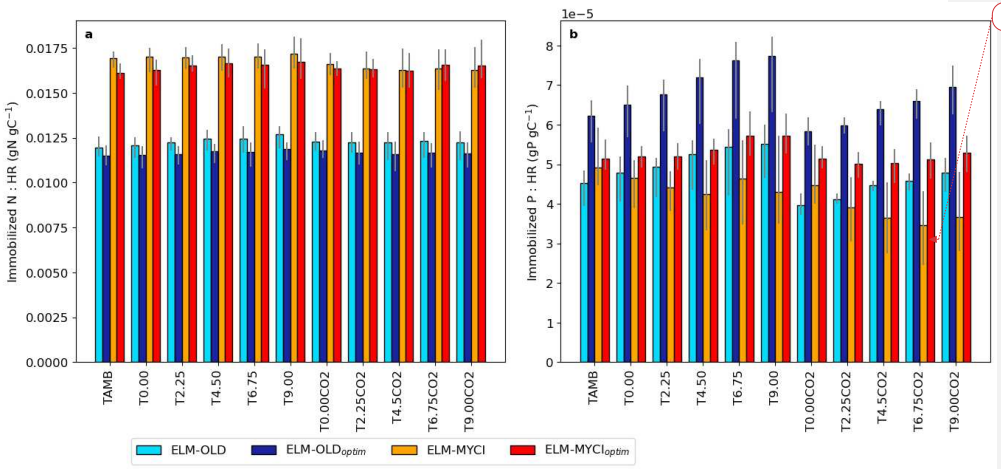


**Figure S12. Ratio of annual mean actual immobilized NP to annual mean heterotrophic respiration (HR) in the soil decomposition process, across the enclosures. The bars show the mean values during 2015-2021 and errorbars show the ranges.**

Formatted: Keep with next

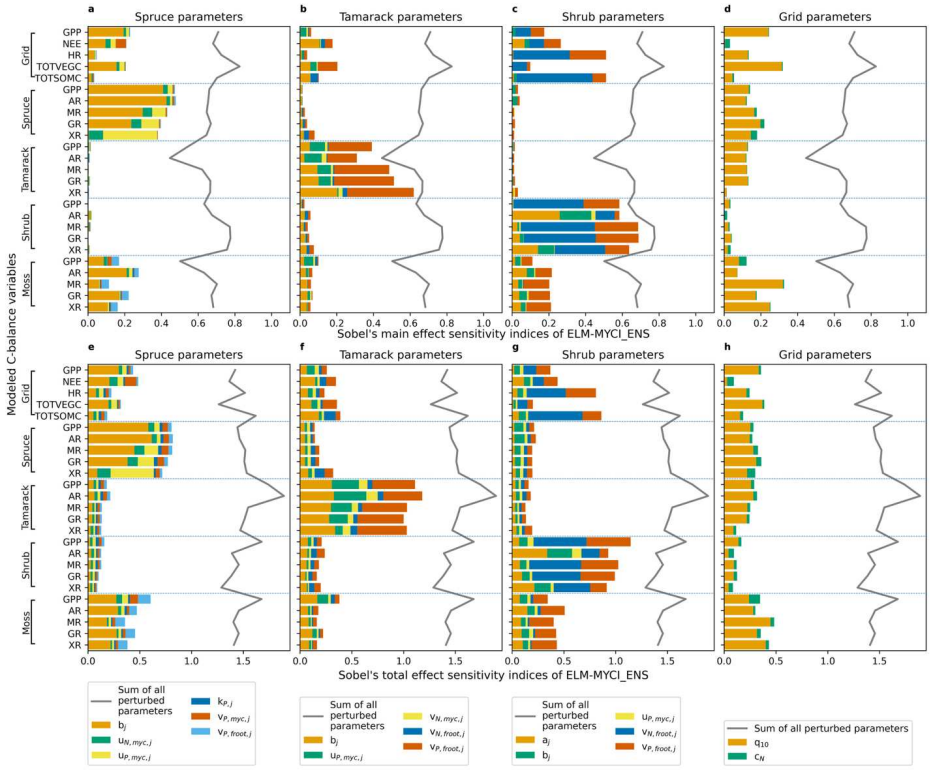


**Figure S13. Sobol's main-effect and total-effect sensitivity indices of selected C-balance variables to the newly added model parameters, calculated from ELM-MYCI_ENS. For better display, the indices are partitioned into subpanels according to whether it is a PFT-specific or column-level parameter. Stacking the bars across the four panels in each row gives the sum of the main or total effects over all the perturbed parameters, which are also displayed as a grey line for reference in each panel. The C-balance variables in each panel are grouped according to whether it is a column-level, spruce, tamarack, shrub, or moss variable. Parameter definitions can be found in  and equations referred therein.**

Deleted: 10

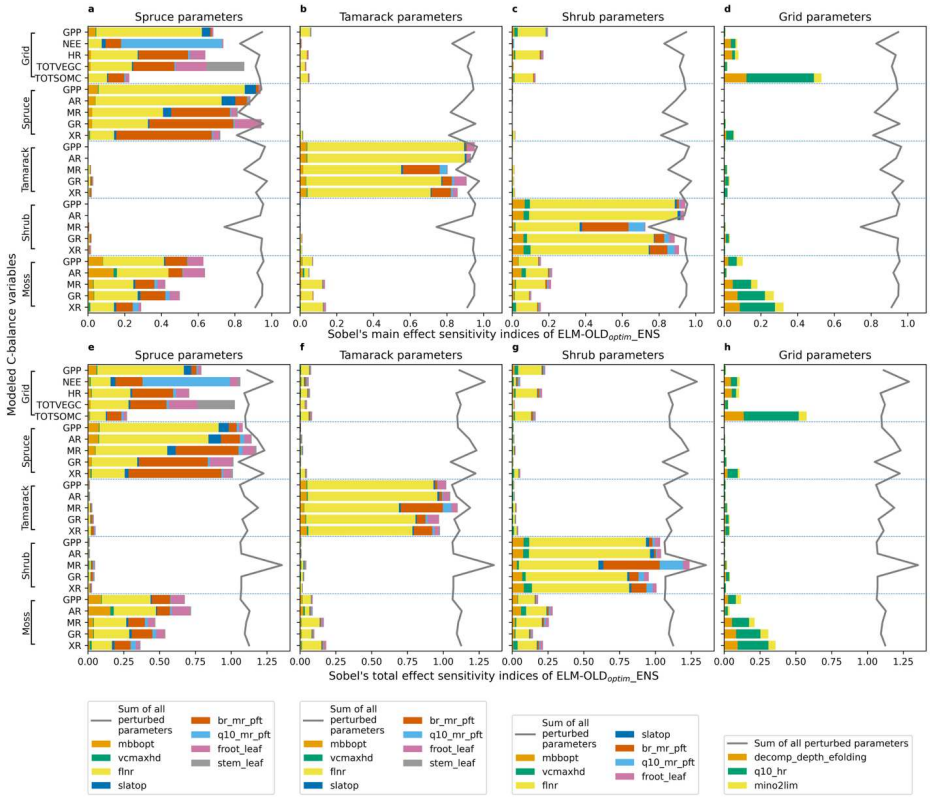


**Figure S14. Sobol's main-effect and total-effect sensitivity indices of selected C-balance variables to the preexisting model parameters, calculated from ELM-OLD$_{optim}$_ENS. For better display, the indices are partitioned into subpanels according to whether it is a PFT-specific or column-level parameter. Stacking the bars across the four panels in each column gives the sum of the main or total effects over all the perturbed parameters, which are also displayed as a grey line for reference in each panel. The C-balance variables in each panel are grouped according to whether it is a column-level, spruce, tamarack, shrub, or moss variable. Parameter definitions can be found in Table S3.**

Deleted: 11

## 4 References


Arndal, M. F., Merrild, M. P., Michelsen, A., Schmidt, I. K., Mikkelsen, T. N., and Beier, C.: Net root growth and nutrient acquisition in response to predicted climate change in two contrasting heathland species, Plant Soil, 369, 615–629, https://doi.org/10.1007/s11104-013-1601-8, 2013.

Bashian-Victoroff, C., Yanai, R. D., Horton, T. R., and Lamit, L. J.: Nitrogen and phosphorus additions affect fruiting of ectomycorrhizal fungi in a temperate hardwood forest, Fungal Ecology, 73, 101388, https://doi.org/10.1016/j.funeco.2024.101388, 2025.

Bergmann, J., Weigelt, A., van der Plas, F., Laughlin, D. C., Kuyper, T. W., Guerrero-Ramirez, N., Valverde-Barrantes, O. J., Bruelheide, H., Freschet, G. T., Iversen, C. M., Kattge, J., McCormack, M. L., Meier, I. C., Rillig, M. C., Roumet, C., Semchenko, M., Sweeney, C. J., van Ruijven, J., York, L. M., and Mommer, L.: The fungal collaboration gradient dominates the root economics space in plants, Sci. Adv., 6, eaba3756, https://doi.org/10.1126/sciadv.aba3756, 2020.

Burrows, S. M., Maltrud, M., Yang, X., Zhu, Q., Jeffery, N., Shi, X., Ricciuto, D., Wang, S., Bisht, G., Tang, J., Wolfe, J., Harrop, B. E., Singh, B., Brent, L., Baldwin, S., Zhou, T., Cameron-Smith, P., Keen, N., Collier, N., Xu, M., Hunke, E. C., Elliott, S. M., Turner, A. K., Li, H., Wang, H., Golaz, J. -C., Bond-Lamberty, B., Hoffman, F. M., Riley, W. J., Thornton, P. E., Calvin, K., and Leung, L. R.: The DOE E3SM v1.1 biogeochemistry configuration: Description and simulated ecosystem-climate responses to historical changes in forcing, J. Adv. Model Earth Syst., 12, https://doi.org/10.1029/2019MS001766, 2020.

Chalk, P. and Smith, C.: On inorganic N uptake by vascular plants: Can 15N tracer techniques resolve the NH4+ versus NO3− "preference" conundrum?, European Journal of Soil Science, 72, 1762–1779, https://doi.org/10.1111/ejss.13069, 2021.

Chapin, F. S., Moilanen, L., and Kielland, K.: Preferential use of organic nitrogen for growth by a non-mycorrhizal arctic sedge, Nature, 361, 150–153, https://doi.org/10.1038/361150a0, 1993.

Clemmensen, K. E., Durling, M. B., Michelsen, A., Hallin, S., Finlay, R. D., and Lindahl, B. D.: A tipping point in carbon storage when forest expands into tundra is related to mycorrhizal recycling of nitrogen, Ecology Letters, 24, 1193–1204, https://doi.org/10.1111/ele.13735, 2021.

Colpaert, J. V., Tichelen, K. K. V., Assche, J. a. V., and Laere, A. V.: Short-term phosphorus uptake rates in mycorrhizal and non-mycorrhizal roots of intact Pinus sylvestris seedlings, The New Phytologist, 143, 589–597, https://doi.org/10.1046/j.1469-8137.1999.00471.x, 1999.

Daryanto, S., Wang, L., Gilhooly, W. P., III, and Jacinthe, P.-A.: Nitrogen preference across generations under changing ammonium nitrate ratios, Journal of Plant Ecology, 12, 235–244, https://doi.org/10.1093/jpe/rty014, 2019.

Defrenne, C. E., Childs, J., Fernandez, C. W., Taggart, M., Nettles, W. R., Allen, M. F., Hanson, P. J., and Iversen, C. M.: High-resolution minirhizotrons advance our understanding of root-fungal dynamics in an experimentally warmed peatland, Plants, People, Planet, 3, 640–652, https://doi.org/10.1002/ppp3.10172, 2021.

Duchesneau, K., Defrenne, C., Petro, C., Malhotra, A., Moore, J., Childs, J., Hanson, P., Iversen, C., and Kostka, J.: SPRUCE Root Tip and Ectomycorrhizal Fungi Colonization Measurements from Ingrowth Cores, 2017, https://doi.org/10.25581/SPRUCE.119/2476173, 2024.

Forsmark, B., Nordin, A., Rosenstock, N. P., Wallander, H., and Gundale, M. J.: Anthropogenic nitrogen enrichment increased the efficiency of belowground biomass production in a boreal forest, Soil Biology and Biochemistry, 155, 108154, https://doi.org/10.1016/j.soilbio.2021.108154, 2021.

Frolking, S., Roulet, N. T., Moore, T. R., Lafleur, P. M., Bubier, J. L., and Crill, P. M.: Modeling seasonal to annual carbon balance of Mer Bleue Bog, Ontario, Canada, Global Biogeochemical Cycles, 16, 4-1-4–21, https://doi.org/10.1029/2001GB001457, 2002.

Glass, A. D. M., Britto, D. T., Kaiser, B. N., Kinghorn, J. R., Kronzucker, H. J., Kumar, A., Okamoto, M., Rawat, S., Siddiqi, M. Y., Unkles, S. E., and Vidmar, J. J.: The regulation of nitrate and ammonium transport systems in plants, Journal of Experimental Botany, 53, 855–864, https://doi.org/10.1093/jexbot/53.370.855, 2002.

Glauch, T., Marshall, J., Gerbig, C., Botía, S., Gałkowski, M., Vardag, S. N., and Butz, A.: *pyVPRM*: a next-generation vegetation photosynthesis and respiration model for the post-MODIS era, Geoscientific Model Development, 18, 4713–4742, https://doi.org/10.5194/gmd-18-4713-2025, 2025.

Griffiths, N. A., Hanson, P. J., Ricciuto, D. M., Iversen, C. M., Jensen, A. M., Malhotra, A., McFarlane, K. J., Norby, R. J., Sargsyan, K., Sebestyen, S. D., Shi, X., Walker, A. P., Ward, E. J., Warren, J. M., and Weston, D. J.: Temporal and Spatial Variation in Peatland Carbon Cycling and Implications for Interpreting Responses of an Ecosystem-Scale Warming Experiment, Soil Science Society of America Journal, 81, 1668–1688, https://doi.org/10.2136/sssaj2016.12.0422, 2017.

Hanson, P. J., Riggs, J. S., Nettles, W. R., Krassovski, M. B., and Hook, L. A.: SPRUCE whole ecosystems warming (WEW) environmental data beginning august 2015, Oak Ridge National Laboratory, TES SFA, U.S. Department of Energy, Oak Ridge, Tennessee, U.S.A., https://doi.org/10.3334/CDIAC/spruce.032, 2016.

Hawkins, B. J., Boukcim, H., and Plassard, C.: A comparison of ammonium, nitrate and proton net fluxes along seedling roots of Douglas-fir and lodgepole pine grown and measured with different inorganic nitrogen sources, Plant, Cell & Environment, 31, 278–287, https://doi.org/10.1111/j.1365-3040.2007.01760.x, 2008.

Hawkins, H.-J., Cargill, R. I. M., Van Nuland, M. E., Hagen, S. C., Field, K. J., Sheldrake, M., Soudzilovskaia, N. A., and Kiers, E. T.: Mycorrhizal mycelium as a global carbon pool, Current Biology, 33, R560–R573, https://doi.org/10.1016/j.cub.2023.02.027, 2023.

He, H., Meyer, A., Jansson, P.-E., Svensson, M., Rütting, T., and Klemedtsson, L.: Simulating ectomycorrhiza in boreal forests: implementing ectomycorrhizal fungi model MYCOFON in CoupModel (v5), Geoscientific Model Development, 11, 725–751, https://doi.org/10.5194/gmd-11-725-2018, 2018.

He, H., Jansson, P.-E., and Gärdenäs, A. I.: CoupModel (v6.0): an ecosystem model for coupled phosphorus, nitrogen, and carbon dynamics – evaluated against empirical data from a climatic and fertility gradient in Sweden, Geoscientific Model Development, 14, 735–761, https://doi.org/10.5194/gmd-14-735-2021, 2021.

Hobbie, E. A. and Högberg, P.: Nitrogen isotopes link mycorrhizal fungi and plants to nitrogen dynamics, New Phytologist, 196, 367–382, https://doi.org/10.1111/j.1469-8137.2012.04300.x, 2012.

Högberg, M. N., Briones, M. J. I., Keel, S. G., Metcalfe, D. B., Campbell, C., Midwood, A. J., Thornton, B., Hurry, V., Linder, S., Näsholm, T., and Högberg, P.: Quantification of effects of season and nitrogen supply on tree below-ground carbon transfer to ectomycorrhizal fungi and other soil organisms in a boreal pine forest, New Phytologist, 187, 485–493, https://doi.org/10.1111/j.1469-8137.2010.03274.x, 2010.

Iversen, C. M., McCormack, M. L., Powell, A. S., Blackwood, C. B., Freschet, G. T., Kattge, J., Roumet, C., Stover, D. B., Soudzilovskaia, N. A., Valverde-Barrantes, O. J., Van Bodegom, P. M., and Violle, C.: A global Fine-Root Ecology Database to address below-ground challenges in plant ecology, New Phytologist, 215, 15–26, https://doi.org/10.1111/nph.14486, 2017.

Iversen, C. M., Childs, J., Norby, R. J., Ontl, T. A., Kolka, R. K., Brice, D. J., McFarlane, K. J., and Hanson, P. J.: Fine-root growth in a forested bog is seasonally dynamic, but shallowly distributed in nutrient-poor peat, Plant Soil, 424, 123–143, https://doi.org/10.1007/s11104-017-3231-z, 2018.

Iversen, C. M., Brice, D. J., Childs, J., Vander Stel, H. M., and Salmon, V. G.: SPRUCE S1 bog production of newly-grown fine roots assessed using root ingrowth cores in 2013, , https://doi.org/10.25581/spruce.091/1782483, 2021.

Kosola, K. R., Workmaster, B. A. A., and Spada, P. A.: Inoculation of cranberry ( *Vaccinium macrocarpon* ) with the ericoid mycorrhizal fungus *Rhizoscyphus ericae* increases nitrate influx, New Phytologist, 176, 184–196, https://doi.org/10.1111/j.1469-8137.2007.02149.x, 2007.

Lasslop, G., Reichstein, M., Papale, D., Richardson, A. D., Arneth, A., Barr, A., Stoy, P., and Wohlfahrt, G.: Separation of net ecosystem exchange into assimilation and respiration using a light response curve approach: critical issues and global evaluation, Global Change Biology, 16, 187–208, https://doi.org/10.1111/j.1365-2486.2009.02041.x, 2010.

Malhotra, A., Brice, D. J., Childs, J., Graham, J. D., Hobbie, E. A., Vander Stel, H., Feron, S. C., Hanson, P. J., and Iversen, C. M.: Peatland warming strongly increases fine-root growth, Proc. Natl. Acad. Sci. U.S.A., 117, 17627–17634, https://doi.org/10.1073/pnas.2003361117, 2020.

McCormack, M. L., Dickie, I. A., Eissenstat, D. M., Fahey, T. J., Fernandez, C. W., Guo, D., Helmisaari, H., Hobbie, E. A., Iversen, C. M., Jackson, R. B., Leppälammi-Kujansuu, J., Norby, R. J., Phillips, R. P., Pregitzer, K. S., Pritchard, S. G., Rewald, B., and Zadworny, M.: Redefining fine roots improves understanding of below-ground contributions to terrestrial biosphere processes, New Phytologist, 207, 505–518, https://doi.org/10.1111/nph.13363, 2015.

Meng, L., Mao, J., Ricciuto, D. M., Shi, X., Richardson, A. D., Hanson, P. J., Warren, J. M., Zhou, Y., Li, X., Zhang, L., and Schädel, C.: Evaluation and modification of ELM seasonal deciduous phenology against observations in a southern boreal peatland forest, Agric. For. Meteorol., 308–309, 108556, https://doi.org/10.1016/j.agrformet.2021.108556, 2021.

Norby, R. J., Childs, J., Hanson, P. J., and Warren, J. M.: Rapid loss of an ecosystem engineer: *Sphagnum* decline in an experimentally warmed bog, Ecology and Evolution, 9, 12571–12585, https://doi.org/10.1002/ece3.5722, 2019.

Oleson, K. W., Lawrence, D. M., Bonan, G. B., Drewniak, B., Huang, M., Levis, S., Li, F., Riley, W. J., Swenson, S. C., Thornton, P. E., Bozbiyik, A., Fisher, R., Heald, C. L., Kluzek, E., Lamarque, F., Lawrence, P. J., Leung, L. R., Muszala, S., Ricciuto, D. M., Sacks, W., Sun, Y., Tang, J., and Yang, Z.-L.: Technical Description of version 4.5 of the Community Land Model (CLM), National Center for Atmospheric Research, Boulder, CO, USA, 2013.

Phillips, J. R., Brice, D. J., Hanson, P. J., Childs, J., Iversen, C. M., Norby, R. J., and Warren, J. M.: SPRUCE pretreatment plant tissue analyses, 2009 through 2013, , https://doi.org/10.3334/CDIAC/spruce.038, 2017.

Renaudin, M., Khlifa, R., Legault, S., Kembel, S. W., Kneeshaw, D., Moore, J.-D., and Houle, D.: Long-Term Simulated Nitrogen Deposition Has Moderate Impacts on Soil Microbial Communities across Three Bioclimatic Domains of the Eastern Canadian Forest, Forests, 14, 1124, https://doi.org/10.3390/f14061124, 2023.

Ricciuto, D., Sargsyan, K., and Thornton, P.: The impact of parametric uncertainties on biogeochemistry in the E3SM Land Model, J. Adv. Model. Earth Syst., 10, 297–319, https://doi.org/10.1002/2017MS000962, 2018.

Rossi, S., Bordeleau, A., Houle, D., and Morin, H.: Effect of chronic ammonium nitrate addition on the ectomycorrhizal community in a black spruce stand, Can. J. For. Res., 42, 1204–1212, https://doi.org/10.1139/x11-176, 2012.

Salmon, V. G., Brice, D. J., Bridgham, S., Childs, J., Graham, J., Griffiths, N. A., Hofmockel, K., Iversen, C. M., Jicha, T. M., Kolka, R. K., Kostka, J. E., Malhotra, A., Norby, R. J., Phillips, J. R., Ricciuto, D., Schadt, C. W., Sebestyen, S. D., Shi, X., Walker, A. P., Warren, J. M., Weston, D. J., Yang, X., and Hanson, P. J.: Nitrogen and phosphorus cycling in an ombrotrophic peatland: a benchmark for assessing change, Plant Soil, 466, 649–674, https://doi.org/10.1007/s11104-021-05065-x, 2021.

Sanders-DeMott, R., Sorensen, P. O., Reinmann, A. B., and Templer, P. H.: Growing season warming and winter freeze–thaw cycles reduce root nitrogen uptake capacity and increase soil solution nitrogen in a northern forest ecosystem, Biogeochemistry, 137, 337–349, https://doi.org/10.1007/s10533-018-0422-5, 2018.

Shao, S., Wu, J., He, H., Moore, T. R., Bubier, J., Larmola, T., Juutinen, S., and Roulet, N. T.: Ericoid mycorrhizal fungi mediate the response of ombrotrophic peatlands to fertilization: a modeling study, New Phytol., 238, 80–95, https://doi.org/10.1111/nph.18555, 2023.

Stelling, J. M., Mayes, M. A., Hanson, P. J., and Krassovski, M.: SPRUCE: Carbon Dioxide and Methane Soil Flux Measurements at High Temporal Resolution, Beginning in 2022, , https://doi.org/10.25581/spruce.104/1922635, 2024.

Struyf, E., Kotowski, W., Jacobs, S., Van Damme, S., Bal, K., Opdekamp, W., Backx, H., Van Pelt, D., and Meire, P.: Tracing Si–N–P ecosystem-pathways: is relative uptake in riparian vegetation influenced by soil waterlogging, mowing management and species diversity?, Hydrobiologia, 674, 41–50, https://doi.org/10.1007/s10750-011-0737-x, 2011.

Thornton, P. E. and Rosenbloom, N. A.: Ecosystem model spin-up: Estimating steady state conditions in a coupled terrestrial carbon and nitrogen cycle model, Ecological Modelling, 189, 25–48, https://doi.org/10.1016/j.ecolmodel.2005.04.008, 2005.

Van Tichelen, K. K. and Colpaert, J. V.: Kinetics of phosphate absorption by mycorrhizal and non-mycorrhizal Scots pine seedlings, Physiologia Plantarum, 110, 96–103, https://doi.org/10.1034/j.1399-3054.2000.110113.x, 2000.

Vesala, R., Kiheri, H., Hobbie, E. A., Van Dijk, N., Dise, N., and Larmola, T.: Atmospheric nitrogen enrichment changes nutrient stoichiometry and reduces fungal N supply to peatland ericoid mycorrhizal shrubs, Science of The Total Environment, 794, 148737, https://doi.org/10.1016/j.scitotenv.2021.148737, 2021.

Walker, A. P., Carter, K. R., Gu, L., Hanson, P. J., Malhotra, A., Norby, R. J., Sebestyen, S. D., Wullschleger, S. D., and Weston, D. J.: Biophysical drivers of seasonal variability in *Sphagnum* gross primary production in a northern temperate bog, JGR Biogeosciences, 122, 1078–1097, https://doi.org/10.1002/2016JG003711, 2017.

Ward, E. B., Duguid, M. C., Kuebbing, S. E., Lendemer, J. C., and Bradford, M. A.: The functional role of ericoid mycorrhizal plants and fungi on carbon and nitrogen dynamics in forests, New Phytol., 235, 1701–1718, https://doi.org/10.1111/nph.18307, 2022.

Weber, S. E., Childs, J., Latimer, J., Hanson, P. J., Salmon, V. G., Schwaner, G., and Iversen, C. M.: Warming and elevated CO2 cause greater and deeper root growth by shrubs in a boreal bog, https://doi.org/10.1101/2025.06.26.661811, 30 June 2025.

Wu, Y. and Blodau, C.: PEATBOG: a biogeochemical model for analyzing coupled carbon and nitrogen dynamics in northern peatlands, Geosci. Model Dev., 6, 1173–1207, https://doi.org/10.5194/gmd-6-1173-2013, 2013.

Xie, L., Zhou, X., Liu, Q., Zhao, C., and Yin, C.: Inorganic nitrogen uptake rate of *Picea asperata* curtailed by fine root acclimation to water and nitrogen supply and further by ectomycorrhizae, Physiologia Plantarum, 173, 2130–2141, https://doi.org/10.1111/ppl.13562, 2021.

**Page 21: [1] Deleted** **Wang, Yaoping** **3/24/26 11:36:00 AM**